

**DESIGN AND EXPERIMENTAL INVESTIGATION OF  
A MICROCHANNEL HEAT EXCHANGER**

**A THESIS SUBMITTED TO  
THE GRADUATE SCHOOL OF NATURAL AND APPLIED SCIENCES  
OF  
MIDDLE EAST TECHNICAL UNIVERSITY**

**BY**

**MURAT ÇETİN**

**IN PARTIAL FULFILLMENT OF THE REQUIREMENTS  
FOR  
THE DEGREE OF MASTER OF SCIENCE  
IN  
MECHANICAL ENGINEERING**

**APRIL 2010**

Approval of the thesis:

**DESIGN AND EXPERIMENTAL INVESTIGATION OF  
A MICROCHANNEL HEAT EXCHANGER**

submitted by **MURAT ÇETİN** in partial fulfillment of the requirements for the degree of **Master of Science in Mechanical Engineering Department, Middle East Technical University** by,

Prof. Dr. Canan ÖZGEN  
Dean, Graduate School of **Natural and Applied Sciences**

Prof. Dr. Suha ORAL  
Head of Department, **Mechanical Engineering, METU**

Asst. Prof. Dr. Almila Güvenç YAZICIOĞLU  
Supervisor, **Mechanical Engineering Department, METU**

**Examining Committee Members:**

Asst. Prof. Dr. İlker TARI  
Mechanical Engineering Dept., METU

Asst. Prof. Dr. Almila Güvenç YAZICIOĞLU  
Mechanical Engineering Dept., METU

Asst. Prof. Dr. Ahmet YOZGATLIGİL  
Mechanical Engineering Dept., METU

Asst. Prof. Dr. Cüneyt SERT  
Mechanical Engineering Dept., METU

Prof. Dr. Sadık KAKAÇ  
Mechanical Engineering Dept., TOBB ETU

**Date: 30.04.2010**

**I hereby declare that all information in this document has been obtained and presented in accordance with academic rules and ethical conduct. I also declare that, as required by these rules and conduct, I have fully cited and referenced all material and results that are not original to this work.**

Name, Surname: Murat ÇETİN

Signature :

## **ABSTRACT**

### **DESIGN AND EXPERIMENTAL INVESTIGATION OF A MICROCHANNEL HEAT EXCHANGER**

Çetin, Murat

M.Sc., Department of Mechanical Engineering

Supervisor: Asst. Prof. Dr. Almıla Güvenç YAZICIOĞLU

April 2010, 175 pages

Due to the high performance of electronic components, the heat generation is increasing dramatically. Heat dissipation becomes a significant issue in efficiency promotion and stable operation. Microchannels are of current interest for use in heat exchangers where very high heat transfer performance is desired. Microchannels provide high heat transfer coefficients because of their small hydraulic diameters. In this study, the design and experimental investigation of fluid flow and heat transfer in a microchannel heat exchanger is conducted. Water and air are used as the working fluids and flowed through microchannels. The heat exchanger has been designed with 6 rows of microchannels for water flow and 7 rows of microchannels for forced flow of air. The heights of the microchannels are 4 mm and 10 mm respectively for water and air flows. Microchannels are brazed to form the heat exchanger. For forced convection cooling with air, a military fan is used. A constant heat source has been specifically designed for experiments. Water flow and heat transfer experiments are conducted on the aluminum microchannel heat exchanger. An experimental method of imposing a constant heat flux to water prior to the entrance to the microchannel heat exchanger, to adjust the inlet temperatures is used.

From the data obtained, the rate of heat transfer, effectiveness and various other parameters have been computed and the results have been compared with those from an available commercial heat exchanger. The results indicate that the heat exchanger performs well and provides 681 W of cooling in a volume 677.6 cm<sup>3</sup> while the commercial heat exchanger provides 702.5 W of cooling in a volume 2507.5 cm<sup>3</sup>. In addition, air-side Colburn modulus has been obtained with respect to Reynolds number.

**Keywords:** Microchannel, Heat Exchanger, Brazing

## ÖZ

### **BİR MİKROKANAL ISI DEĞİŞTİRİCİSİNİN TASARIMI VE PERFORMANSININ DENEYSEL OLARAK İNCELENMESİ**

Çetin, Murat

Yüksek Lisans, Makina Mühendisliği Bölümü

Tez Yöneticisi : Yrd. Doç. Almıla Güvenç YAZICIOĞLU

Nisan 2010, 175 sayfa

Yüksek performanslı elektronik komponentler ısı üretimini çok fazla arttırmaktadır. Verimli ve stabil uygulamalarda ısı dağıtımı önemli bir sorun olmaktadır. Yüksek ısı transfer performansı istenildiğinde mikrokanallar ısı değiştiricilerinde kullanılmaktadır. Düşük hidrolik parametreleri sayesinde mikrokanallar yüksek ısı transfer katsayıları sağlamaktadır. Bu çalışmada, alüminyumdan yapılmış mikrokanallı bir ısı değiştiricisi tasarlandı ve sıvı akışı ve zorlanmış konveksiyonla ısı transferi deneyleri yapıldı. Mikrokanallardan akan sıvı olarak su ve hava kullanıldı. Isı değiştiricisi su akışı için 6 ve hava akışı için 7 sıralık mikrokanallı olarak tasarlandı. Su akışı için 4 mm, hava akışı için 10 mm yüksekliğindeki mikrokanallar kullanıldı. Mikrokanallar sert lehimle yapılarak ısı değiştiricisi oluşturuldu. Zorlanmış konveksiyonla soğutma için askeri bir fan kullanıldı. Isı değiştiricisine girmeden önce, sabit ısı akışı sağlayan bir ısıtma tankında şartlandırarak suyun giriş sıcaklığı ayarlandı.

Elde edilen verilerden ısı transfer hızı, verimlilik ve çeşitli diğer değişkenler hesaplandı ve sonuçlar mevcut ticari bir ısı değiştiricisinin sonuçları ile karşılaştırıldı. Sonuçlar göstermekte ki ısı değiştiricisi iyi çalışmakta ve 677.6 cm<sup>3</sup>'lük hacimde 681 W'lık soğuma sağlayabilmektedir. Oysa ticari ısı

deęiřtiricisi 702.5 W'lık soęumayı 2507.5 cm<sup>3</sup>'lük hacimde yapmaktadır. İlaveten, hava tarafi için Reynold sayısına göre Colburn katsayısı elde edildi.

**Anahtar Kelimeler:** Mikrokanal, Isı Deęiřtiricisi, Sert Lehimleme

## ACKNOWLEDGMENTS

I would like to express my sincere thanks to my supervisor, Asst. Prof. Dr. Almıla G. YAZICIOĞLU, for her continuous guidance, support throughout the course of this thesis. I would also like to thank my committee members, Prof. Dr. Sadık KAKAÇ, Asst. Prof. Dr. İlker TARI, Asst. Prof. Dr. Ahmet YOZGATGİL, Asst. Prof. Dr. Cüneyt SERT for their valuable comments and suggestions on the contents of this thesis.

I would like to thank my colleagues at ASELSAN, specifically Mr. Uğur ETİZ and Mr. Murat PARLAK for their substantial role in this thesis in inspiring me to work in the field of microchannel heat exchangers. Their contributions are greatly appreciated and are respectfully acknowledged. I would like to express my sincere appreciation to Mr. Muharrem KAYNAKÖZ, Mr. Atakan KABUKCU, Mr. Emrah ALPSAN for their crucial advices during the preparation of this thesis.

I would like to thank ASELSAN Inc. for providing financial and hardware support and facilities to research literature. The help, encouragement and patience of all my colleagues throughout experiments are particularly appreciated. I would like to also thank EMD Inc. and Mr. Mustafa ATAYAKULOL for their support during the preliminary production of the heat exchanger.

I would like to express my deepest thanks to my family for their endless support, love and faith. The help and encouragement of my brother Suat ÇETİN throughout the research are particularly appreciated. My gratitude is endless for my wife Semra ÇETİN, without her presence this thesis would not have been possible.

# TABLE OF CONTENTS

ABSTRACT.....	iv
ÖZ .....	vi
ACKNOWLEDGMENTS .....	viii
TABLE OF CONTENTS.....	ix
LIST OF TABLES .....	xii
LIST OF FIGURES .....	xvi
LIST OF SYMBOLS .....	xix
CHAPTERS	
1.INTRODUCTION .....	1
1.1 Heat Exchanger .....	1
1.2 Miniaturization and Microchannel Concepts.....	6
1.3 Electronics Cooling Technologies .....	9
1.4 Motivation.....	14
1.5 Present Study .....	16
2.LITERATURE SURVEY .....	18
3.THEORY OF HEAT EXCHANGERS.....	27
3.1 Heat Transfer Analysis .....	27
3.2 Overall Thermal Coefficient, UA .....	30
3.3 Fin Efficiency.....	32
3.4 Heat Exchanger Effectiveness and NTU .....	33
3.5 Pressure Drop.....	34
3.6 Heat Transfer Coefficient .....	35
3.7 Geometrical Properties.....	37
4.EXPERIMENTAL PROCEDURES AND RESULTS .....	41
4.1 Design of the Microchannel Heat Exchanger .....	41
4.2 Manufacturing of the Microchannel Heat Exchanger.....	45
4.3 The Preliminary Heat Exchangers .....	53
4.4 The Test Heat Exchanger.....	58
4.5 Test Setup.....	61
4.6 Experiments .....	66
4.7 Experimental Results .....	69

5.DISCUSSION AND COMPARISON OF RESULTS.....	73
5.1 Outlet Temperatures of Water .....	73
5.2 Pressure Drop of Water.....	74
5.4 Number of Transfer Units.....	75
5.5 Effectiveness .....	78
5.6 Colburn Factor of Air.....	79
5.6 Comparison The Microchannel Heat Exchanger with a Commercial Heat Exchanger .....	80
5.7 Critic of Experimental Setup .....	82
6.CONCLUSION.....	84
6.1 Future Work.....	85
REFERENCES .....	87
APPENDICES	
A.SAMPLE CALCULATIONS .....	94
A.1 Geometrical Parameters .....	95
A.2 Surface Geometrical Properties .....	98
A.3 Mean Temperatures and Fluid Properties .....	102
A.4 Compactness of the Heat Exchanger .....	104
A.4 Mass Flow Rates .....	105
A.5 Reynolds Number .....	107
A.6 Nusselt Number.....	107
A.7 Convection Heat Transfer Coefficient, h .....	108
A.7 Stanton Number .....	108
A.8 Colburn Factor .....	109
A.9 Fin Efficiency.....	109
A.10 The Overall Surface Efficiency.....	111
A.11 The Convection Resistance of Water Side.....	111
A.12 The Fouling Resistance of Water Side.....	112
A.13 The Wall Resistance.....	112
A.14 The Convection Resistance of Air Side .....	112
A.15 The Fouling Resistance of Air Side .....	113
A.16 The Total Thermal Resistance .....	113
A.17 Experimental Heat Transfer from Water .....	113
A.18 Experimental Heat Transfer to Air.....	114
A.19 Maximum Heat Transfer.....	114
A.20 Experimental Overall Thermal Coefficient.....	114
A.21 Heat Capacity Rates .....	115
A.22 Number of Transfer Unit.....	115
A.23 Effectiveness .....	116
A.24 Experimental Effectiveness.....	116
A.25 Experimental Heat Transfer Coefficient of Air .....	116
A.26 Pressure Drop of Water.....	116

B.THEORETICAL AND EXPERIMENTAL CALCULATION RESULTS .....	118
C.DRAWINGS OF THE MICROCHANNEL HEAT EXCHANGER .....	134
D.TEST COMPONENTS .....	156
D1. Data Logger.....	156
D2. Flowmeter .....	157
D3. Temperature / Pressure Transducer.....	159
D4. Axial Fan.....	162
D5. Pump .....	164
D6. Expansion Unit.....	165
D7. Heating Tank.....	166
D8. Air Velocity Meter .....	168
E.MATERIAL PROPERTIES .....	169

## LIST OF TABLES

<b>Table 4.1:</b> Measurement instruments of experimental setup.....	62
<b>Table 4.2:</b> Input variables of the experiments.....	68
<b>Table 4.3:</b> Measured parameters of water for all experiments.....	70
<b>Table 4.4:</b> Pressure drop of water for all experiments.....	71
<b>Table 4.5:</b> Measured parameters of air for all experiments.....	72
<b>Table 5.1:</b> Experimental overall thermal coefficient $(U \cdot A)_{exp}$ , number of transfer units $NTU_{exp}$ where $\dot{m}_h = 0.009 \text{ kg/s}$ and air mass flow rate is changing.....	76
<b>Table 5.2:</b> Experimental overall thermal coefficient $(U \cdot A)_{exp}$ , number of transfer units $NTU_{exp}$ where $\dot{m}_h = 0.013 \text{ kg/s}$ and air mass flow rate is changing.....	76
<b>Table 5.3:</b> Experimental overall thermal coefficient $(U \cdot A)_{exp}$ , number of transfer units $NTU_{exp}$ where $\dot{m}_h = 0.019 \text{ kg/s}$ and air mass flow rate is changing.....	77
<b>Table 5.4:</b> Experimental overall thermal coefficient $(U \cdot A)_{exp}$ , number of transfer units $NTU_{exp}$ where $\dot{m}_h = 0.024 \text{ kg/s}$ and air mass flow rate is changing.....	77
<b>Table A.1:</b> Water thermophysical properties.....	103
<b>Table A.2:</b> Water properties at $T = 54.35 \text{ }^\circ\text{C}$ for experiment 1.....	103
<b>Table A.3:</b> Air thermophysical properties.....	104
<b>Table A.4:</b> Air properties at $T = 34.2 \text{ }^\circ\text{C}$ for experiment 1.....	104
<b>Table B.1:</b> Mass flow rates and Reynolds numbers of water and air side for each experiment.....	118
<b>Table B.2:</b> Dimensionless numbers and convection heat transfer coefficient, h of water side where $\dot{m}_h = 0.009 \text{ kg/s}$ and air mass flow rate is changing.....	119

<b>Table B.3:</b> Dimensionless numbers and convection heat transfer coefficient, $h$ of water side where $\dot{m}_h = 0.013$ kg/s and air mass flow rate is changing.....	119
<b>Table B.4:</b> Dimensionless numbers and convection heat transfer coefficient, $h$ of water side where $\dot{m}_h = 0.019$ kg/s and air mass flow rate is changing.....	120
<b>Table B.5:</b> Dimensionless numbers and convection heat transfer coefficient, $h$ of water side where $\dot{m}_h = 0.024$ kg/s and air mass flow rate is changing.....	120
<b>Table B.6:</b> Overall surface efficiency, convection and fouling resistance of water side where $\dot{m}_h = 0.009$ kg/s and air mass flow rate is changing.....	121
<b>Table B.7:</b> Overall surface efficiency, convection and fouling resistance of water side where $\dot{m}_h = 0.013$ kg/s and air mass flow rate is changing.....	121
<b>Table B.8:</b> Overall surface efficiency, convection and fouling resistance of water side where $\dot{m}_h = 0.019$ kg/s and air mass flow rate is changing.....	122
<b>Table B.9:</b> Overall surface efficiency, convection and fouling resistance of water side where $\dot{m}_h = 0.024$ kg/s and air mass flow rate is changing.....	122
<b>Table B.10:</b> Dimensionless numbers and convection heat transfer coefficient, $h$ of air side where $\dot{m}_h = 0.009$ kg/s and air mass flow rate is changing.....	123
<b>Table B.11:</b> Dimensionless numbers and convection heat transfer coefficient, $h$ of air side where $\dot{m}_h = 0.013$ kg/s and air mass flow rate is changing.....	123
<b>Table B.12:</b> Dimensionless numbers and convection heat transfer coefficient, $h$ of air side where $\dot{m}_h = 0.019$ kg/s and air mass flow rate is changing.....	124
<b>Table B.13:</b> Dimensionless numbers and convection heat transfer coefficient, $h$ of air side where $\dot{m}_h = 0.024$ kg/s and air mass flow rate is changing.....	124
<b>Table B.14:</b> Overall surface efficiency, convection and fouling resistance of air side where $\dot{m}_h = 0.009$ kg/s and air mass flow rate is changing...	125

<b>Table B.15:</b> Overall surface efficiency, convection and fouling resistance of air side where $\dot{m}_h = 0.013$ kg/s and air mass flow rate is changing...	125
<b>Table B.16:</b> Overall surface efficiency, convection and fouling resistance of air side where $\dot{m}_h = 0.019$ kg/s and air mass flow rate is changing...	126
<b>Table B.17:</b> Overall surface efficiency, convection and fouling resistance of air side where $\dot{m}_h = 0.024$ kg/s and air mass flow rate is changing...	126
<b>Table B.18:</b> Heat capacity rates.....	127
<b>Table B.19:</b> Heat transfer rates.....	128
<b>Table B.20:</b> Experimental overall thermal coefficients.....	129
<b>Table B.21:</b> Total thermal resistance $R_t$ , experimental overall surface coefficient $(U \cdot A)_{exp}$ , number of transfer units $NTU_{exp}$ where $\dot{m}_h = 0.009$ kg/s and air mass flow rate is changing.....	130
<b>Table B.22:</b> Total thermal resistance $R_t$ , experimental overall surface coefficient $(U \cdot A)_{exp}$ , number of transfer units $NTU_{exp}$ where $\dot{m}_h = 0.013$ kg/s and air mass flow rate is changing.....	130
<b>Table B.23:</b> Total thermal resistance $R_t$ , experimental overall surface coefficient $(U \cdot A)_{exp}$ , number of transfer units $NTU_{exp}$ where $\dot{m}_h = 0.019$ kg/s and air mass flow rate is changing.....	131
<b>Table B.24:</b> Total thermal resistance $R_t$ , experimental overall surface coefficient $(U \cdot A)_{exp}$ , number of transfer units $NTU_{exp}$ where $\dot{m}_h = 0.024$ kg/s and air mass flow rate is changing.....	131
<b>Table B.25:</b> Experimental convection heat transfer coefficient $h_{exp}$ , Stanton number $St_{exp}$ and Colburn factor $j_{exp}$ of air side where $\dot{m}_h = 0.009$ kg/s and air mass flow rate is changing.....	132
<b>Table B.26:</b> Experimental convection heat transfer coefficient $h_{exp}$ , Stanton number $St_{exp}$ and Colburn factor $j_{exp}$ of air side where $\dot{m}_h = 0.013$ kg/s and air mass flow rate is changing.....	132
<b>Table B.27:</b> Experimental convection heat transfer coefficient $h_{exp}$ , Stanton number $St_{exp}$ and colburn factor $j_{exp}$ of air side where $\dot{m}_h = 0.019$ kg/s and air mass flow rate is changing.....	133

<b>Table B.28:</b> Experimental convection heat transfer coefficient $h_{exp}$ , Stanton number $St_{exp}$ and Colburn factor $j_{exp}$ of air side where $\dot{m}_h = 0.024\text{kg/s}$ and air mass flow rate is changing.....	133
<b>Table E.1:</b> Air properties at atmospheric pressure [38].....	169
<b>Table E.2:</b> Calculated air properties at atmospheric pressure for each experimental average temperature of air.....	170
<b>Table E.3:</b> Water (saturated) thermal properties [38].....	171
<b>Table E.4:</b> Calculated water thermal properties for each experimental average temperature of water.....	172
<b>Table E.5:</b> Calculated water and air viscosity for each experimental at wall temperature.....	173

## LIST OF FIGURES

<b>Figure 1.1:</b> A plate-fin unmixed-unmixed crossflow heat exchanger [3].....	2
<b>Figure 1.2:</b> Temperature distribution in an unmixed-unmixed crossflow heat exchanger [2].....	3
<b>Figure 1.3:</b> Plain, wavy and interrupted fin geometries for plate fin heat exchangers [3].....	4
<b>Figure 1.4:</b> Plate fin heat exchangers [2].....	5
<b>Figure 1.5:</b> Trends in increasing power density and categorization of cooling methods employed by INTEL [7].....	10
<b>Figure 1.6:</b> A heat sink-fan assembly (left) and various heat pipe configurations (right) [7].....	11
<b>Figure 1.7:</b> Liquid cooling system schematics (left) and example of a liquid cooled heat sink mounted on a PCB [7].....	12
<b>Figure 1.8:</b> Schematics of liquid heat sink (left), minichannel heat sink (center), and microchannel heat sink (right) [6].....	12
<b>Figure 1.9:</b> Localized spray cooling (left) and system level spray cooling (right) [7].....	13
<b>Figure 1.10:</b> Schematic representation of thermoelectric cooling (left), thermoelectric modules (right) [18].....	14
<b>Figure 3.1:</b> LMTD correction factor F for a single pass crossflow heat exchanger with both fluids unmixed [2].....	30
<b>Figure 3.2:</b> Cross flow plain fin heat exchanger [1].....	37
<b>Figure 3.3:</b> Idealized plain rectangular fin [1].....	38
<b>Figure 4.1:</b> A view of the sandwich construction design of the microchannel heat exchanger.....	44
<b>Figure 4.2:</b> The preliminary design of the microchannel heat exchanger.....	45

<b>Figure 4.3:</b> A view of the sandwich construction of the air side plain fins for the preliminary heat exchanger before dip brazing .....	54
<b>Figure 4.4:</b> A view of the assembly step of the preliminary heat exchanger before dip brazing.....	55
<b>Figure 4.5:</b> Secondary heat exchanger in dip brazing.....	56
<b>Figure 4.6:</b> A view of the first quarter specimen of the preliminary microchannel heat exchanger produced in dip brazing, after being sliced into four specimens.....	57
<b>Figure 4.7:</b> A view of the second quarter specimen of the preliminary microchannel heat exchanger produced in dip brazing, after sliced into four specimens.....	57
<b>Figure 4.8:</b> A view of the microchannel heat exchanger assembled vertically.....	58
<b>Figure 4.9:</b> The test specimen produced in vacuum brazing.....	59
<b>Figure 4.10:</b> All parts require to assemble the microchannel heat exchanger in vacuum brazing.....	59
<b>Figure 4.11:</b> The jig and fixture of the microchannel heat exchanger in vacuum brazing.....	60
<b>Figure 4.12:</b> The test microchannel heat exchanger.....	60
<b>Figure 4.13:</b> A view of experimental setup.....	61
<b>Figure 4.14:</b> Heating tank.....	64
<b>Figure 4.15:</b> The finger protector part of the fan.....	65
<b>Figure 4.16:</b> A view of air velocity meter assembled to the microchannel heat exchanger.....	66
<b>Figure 4.17:</b> Data logger and the power supplier used in experiments.....	67
<b>Figure 4.18:</b> Inlet and outlet temperatures of the water & time step for experiment 5.....	69
<b>Figure 5.1:</b> Outlet temperatures of water.....	73
<b>Figure 5.2:</b> Pressure drop of water.....	75
<b>Figure 5.3:</b> Effectiveness of the microchannel heat exchanger.....	78
<b>Figure 5.4:</b> Experimental Colburn factor of air.....	79

<b>Figure 5.5:</b> Temperature differences of water for the microchannel heat exchanger and the commercial heat exchanger where mass flow rate of air decreasing.....	81
<b>Figure 6.1:</b> A thermal view of the microchannel heat exchanger.....	85
<b>Figure A.1:</b> Section view of the heat exchanger.....	95
<b>Figure A.2:</b> Detailed section view of water side of the heat exchanger.....	95
<b>Figure A.3:</b> Detailed section view of air side of the heat exchanger.....	96
<b>Figure A.4:</b> Detailed view of plain fin of both sides of the heat exchanger.....	96
<b>Figure D.1:</b> The data logger.....	156
<b>Figure D.2:</b> The flowmeter output & flow rate graph.....	157
<b>Figure D.3:</b> The flowmeter dimensions.....	158
<b>Figure D.4:</b> The temperature / pressure transducer's dimensions [inch].....	160
<b>Figure D.5:</b> The temperature / pressure transducer.....	161
<b>Figure D.6:</b> The fan dimensions [inch].....	162
<b>Figure D.7:</b> Detailed dimensions of the fan.....	163
<b>Figure D.8:</b> The performance curve of the fan.....	163
<b>Figure D.9:</b> Performance curve of the pump.....	164
<b>Figure D.10:</b> Detailed drawings of the expansion unit.....	165
<b>Figure D.11:</b> Isometric view of the heating tank.....	166
<b>Figure D.12:</b> Top view of the heating tank.....	166
<b>Figure D.13:</b> Bottom side view of the heating tank.....	167
<b>Figure D.14:</b> Air velocity meter.....	168

## LIST OF SYMBOLS

$a$	Short length of a rectangular profile
$A$	Heat transfer area
$A_c$	Total heat transfer area of cold side or net free flow area
$A_f$	Fin (secondary) area
$A_h$	Total heat transfer area of hot side
$A_p$	Primary area of fluid
$A_T$	Total area of heat exchanger
$A_w$	Total heat transfer area of wall
$A_0$	Free flow area of cross section
$A_1$	Total surface area on fluid 1 side
$b$	Long length of a rectangular profile or distance between two plates in the heat exchanger (fin height)
$C^*$	Heat capacity rate ratio
$C$	Heat capacity rate
$C_{min}$	Minimum of heat capacity rate ratios
$C_{max}$	Maximum of heat capacity rate ratios
$c_p$	Specific heat
$D_h$	Hydraulic diameter
$F$	Correction factor of cross flow arrangement
$G$	Mass velocity of fluid
$h$	Convection heat transfer coefficient
$I_0$	Zeroth order modified Bessel function
$I_1$	First order modified Bessel function
$I_n$	$n^{\text{th}}$ order modified Bessel function
$j$	Colburn Factor

$k$	Thermal conductivity of fluid
$L_f$	Fin flow length
$l_1$	Adiabatic fin height
$L_1$	Length of heat exchanger in horizontal plane
$L_2$	Length of heat exchanger normal to $L_1$ direction in horizontal plane
$L_3$	Length of heat exchanger normal to horizontal plane
$m$	Fin efficiency parameter
$\dot{m}$	Mass flow rate
$n_f$	Total number of fins in the core
$N_f$	Number of fins per unit length
$N_p$	Total number of fluid passages
$Nu$	Nusselt number
$NTU$	Number of transfer units
$p$	Wetted perimeter of cross section
$P$	Temperature effectiveness of the heat exchanger
$p_{c1}$	Inlet pressure of cold fluid
$p_{c2}$	Outlet pressure of cold fluid
$p_f$	One fin width
$p_{h1}$	Inlet pressure of hot fluid
$p_{h2}$	Outlet pressure of hot fluid
$Pr$	Prandtl number
$\Delta p_c$	Pressure drop of cold fluid
$\Delta p_h$	Pressure drop of hot fluid
$Q$	Total heat transfer
$Q_{max}$	Maximum heat transfer
$R$	Ratio of the heat capacity rate
$R_c$	Convection resistance of hot fluid
$R_{fc}$	Fouling resistance factor of cold side
$R_{fh}$	Fouling resistance factor of hot side

$R_{f,c}$	Fouling resistance of hot side
$R_{f,h}$	Fouling resistance of hot side
$Re$	Reynolds number
$R_h$	Convection resistance of hot fluid
$R_t$	Total thermal resistance
$R_w$	Wall resistance
$St$	Stanton number
$T_{c1}$	Inlet temperature of cold fluid
$T_{c2}$	Outlet temperature of cold fluid
$\Delta T_c$	Temperature difference of inlet and outlet temperatures of cold fluid
$T_{h1}$	Inlet temperature of hot fluid
$T_{h2}$	Outlet temperature of hot fluid
$\Delta T_h$	Temperature difference of inlet and outlet temperatures of hot fluid
$T_i$	Inlet temperature of hot fluid
$t_i$	Inlet temperature of cold fluid
$\Delta T_{max}$	Maximum temperature difference between fluids
$\Delta T_{lm}$	Effective mean temperature difference
$\Delta T_{lm,cf}$	Log mean temperature difference (LMTD) for a counterflow arrangement
$T_o$	Outlet temperature of cold fluid
$t_o$	Outlet temperature of cold fluid
$u$	Velocity
$U$	Overall heat transfer coefficient
$U \cdot A$	Overall heat transfer coefficient
$V_T$	Total volume
 <i>Greek symbols</i>	
$\alpha$	Thermal diffusivity

$\alpha_c$	Aspect ratio of rectangular cross section
$\beta$	Surface density
$\delta$	Fin thickness
$\delta_w$	Wall thickness
$\varepsilon$	Effectiveness of heat exchanger
$\eta_f$	Fin efficiency
$\eta_o$	Overall surface efficiency
$\eta_{o,c}$	Overall surface efficiency of cold side
$\eta_{o,h}$	Overall surface efficiency of hot side
$\mu$	Viscosity of fluid evaluated at mean temperature
$\rho$	Density of fluid
$\nu$	Dynamic viscosity of fluid

### *Subscripts*

ave	Average value
b	Bulk temperature or mean temperature
c	Cold fluid property
cf	Counterflow arrangement
exp	Experimental
f	Fin property
h	Hot fluid property
lm	Log mean
w	Wall property
T	Total
1	Fluid 1 or hot fluid property
2	Fluid 2 or cold fluid property

# CHAPTER 1

## INTRODUCTION

This introductory chapter aims at presenting the need of understanding heat exchangers with microchannel flow and heat transfer from an electronics cooling point of view, in conjunction with the global trends in cooling technologies and the requirements of the national defense industry.

### 1.1 Heat Exchanger

A heat exchanger is a device that is used to transfer thermal energy between two or more fluids, between a solid surface and a fluid, or between solid particles and a fluid, at different temperatures and in thermal contact. Typical applications include heating or cooling of a fluid stream of concern and evaporation or condensation of single or multi component fluid stream [1].

Heat exchangers are used in a wide variety of applications. These involve power production, process, chemical and food industries, electronics, environmental production engineering, waste heat recovery, manufacturing industry, air conditioning, refrigeration and space applications. Over the past quarter century the importance of heat exchanger has increased immensely from the viewpoint of energy conservation, conversion, recovery and successful implementation of new energy sources. Heat exchangers constitute a multibillion dollar industry in the United States alone and there are over 300 companies engaged in the manufacture of a wide array of heat exchangers [2].

Heat exchangers can be classified in many different ways; for example, according to transfer processes, number of fluids and heat transfer mechanism,

construction type and flow arrangements. Another arbitrary classification can be made, based on the heat transfer surface area/volume ratio into compact and noncompact heat exchangers [2].

A crossflow exchanger is a heat exchanger in which the two fluids flow in directions normal to each other. This is one of the most common flow arrangements used for extended surface heat exchangers because it greatly simplifies the header design at the entrance and exit of each fluid. Thermodynamically, the effectiveness for the crossflow exchanger falls in between that for the counterflow and parallel flow arrangements [1].

A fluid stream is considered unmixed when it passes through individual flow channels or tubes with no fluid mixing between adjacent flow channels [1]. Fig. 1.1 shows a typical plate-fin unmixed-unmixed crossflow heat exchanger. As seen in Fig. 1.2, outlet temperatures of the fluids in a plate-fin unmixed-unmixed crossflow heat exchanger are not constant and show variations from one corner to the other of heat exchanger.

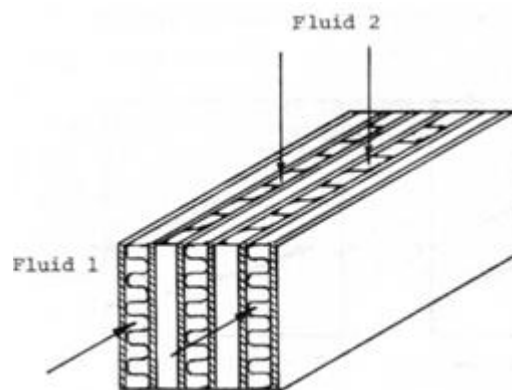


**Figure 1.1:** A plate-fin unmixed-unmixed crossflow heat exchanger [3]

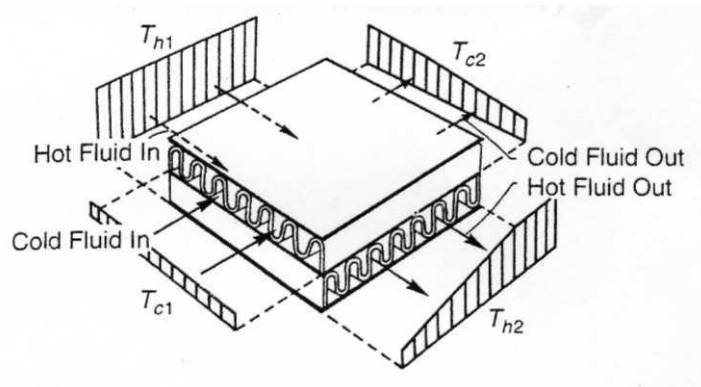


**Figure 1.2:** Temperature distribution in an unmixed-unmixed crossflow heat exchanger [2]

The heat transfer surface is a surface of the exchanger core that is in direct contact with fluids and through which heat is transferred by conduction. That portion of the surface that is in direct contact with both the hot and cold fluids and transfer heat between them is referred to as the primary or direct surface. To increase the heat transfer area, appendages may be intimately connected to the primary surface to provide an extended, secondary or indirect surface. These extended surface elements are referred to as fins. Thus, heat is conducted through the fin and convected from the fin to the surrounding fluid, or vice versa, depending on whether the fin is being cooled or heated. As a result, the addition of fins to the primary surface reduces the thermal resistances on that side and thereby increases the total heat transfer from the surface for the same temperature difference. Fins may form flow passages for the individual fluids, but do not separate the two fluids of the exchanger. These secondary surface or fins may also be introduced primarily for structural strength purpose or to provide thorough mixing of a highly viscous liquid [2].

Fins are die or roll formed and are attached to the plates by brazing, soldering, adhesive bonding, welding, mechanical fit or extrusion. Plate fins are categorized as (1) plain and straight fins, such as plain triangular and rectangular fins, (2) plain but wavy fins (wavy in the main fluid flow direction) and (3)

interrupted fins, such as offset strip, louver, perforated and pin fins [4]. Fin geometries for plate-fin heat exchangers are presented in Fig. 1.3.

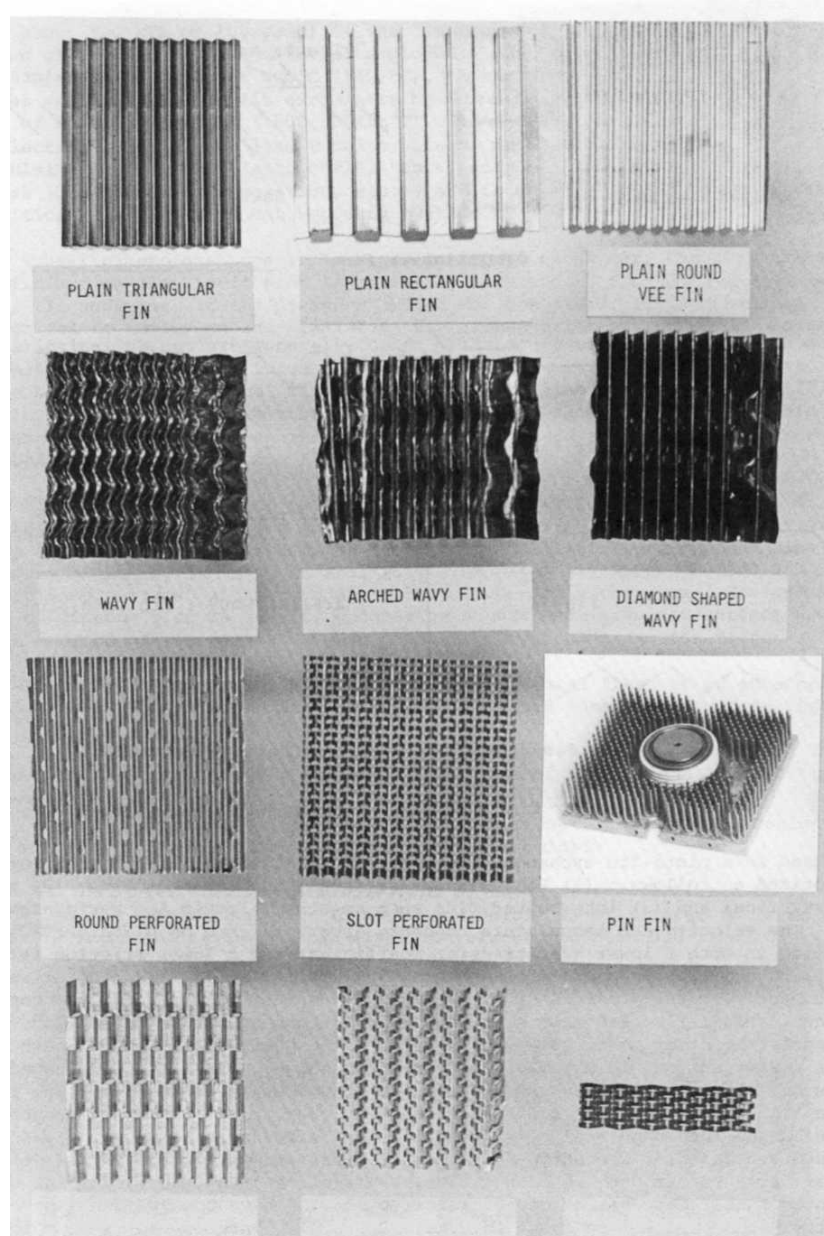


**Figure 1.3:** Plain, wavy and interrupted fin geometries for plate fin heat exchangers [3]

Plate fin heat exchangers are designed to pack a high heat transfer capacity into a small volume. They consist of a series of flat plates employing a sandwich-

type construction. The space between the parting sheets is filled with fins that are stamped and folded in an accordion pattern. The fins are usually bended to the parting sheets by brazing [4]. Some typical construction examples of plate-fin heat exchangers are shown in Fig. 1.4.

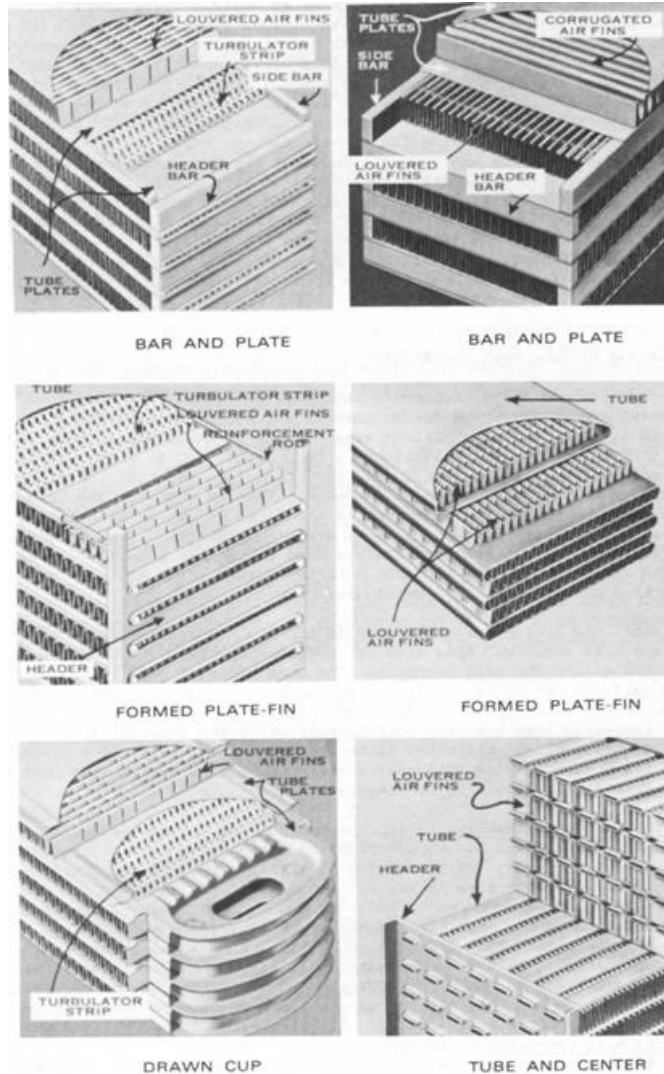


**Figure 1.4:** Plate fin heat exchangers [2]

## 1.2 Miniaturization and Microchannel Concepts

The concept of miniaturization may be said to form the basis of a relatively young field of technology, *MicroElectroMechanical Systems* (MEMS). When Richard P. Feynman referred to his anticipation of a trend towards miniaturization in his talk titled “There’s Plenty of Room at the Bottom”, delivered at the annual meeting of the American Physical Society in 1959, he made a striking remark: “In the year 2000, when they look back at this age, they will wonder why it was not until the year 1960 that anybody began to seriously move in this direction.” [5].

It was not until two decades after Feynman’s famous speech that Tuckerman and Pease first made use of miniaturization for the purposes of heat removal, within the scope of a Ph.D. study in 1981. Their publication titled “High Performance Heat Sinking for VLSI” [6] is credited as the first study on microchannel heat transfer. Their pioneering work has motivated many researchers to focus on the topic and microchannel flow has been recognized as a high performance heat removal tool ever since. Presently, modeling and experimental investigation of microchannel flow and heat transfer are rapidly maturing, although conflicts among researchers as to how microscale flows should be modeled and discrepancies between experimental results remain [7].

As is evident from the diversity of application areas, the study of flow and heat transfer in microchannels is very important for the technology of today and the near future, as developments are following the trend of miniaturization in all fields.

Before proceeding with microchannel flow and heat transfer, it is appropriate to introduce a definition for the term “microchannel”. The scope of the term is among the topics of debate between researchers in the field. Mehendale et al. [8] used the following classification based on manufacturing techniques

required to obtain various ranges of channel dimensions, “ $C_D$ ”, being the smallest channel dimension:

$1 \mu\text{m} < C_D < 100 \mu\text{m}$	: Microchannels
$100 \mu\text{m} < C_D < 1 \text{ mm}$	: Minichannels
$1 \text{ mm} < C_D < 6 \text{ mm}$	: Compact passages
$6 \text{ mm} < C_D$	: Conventional passages

Kandlikar and Grande [9] adopted a different classification based on the rarefaction effect of gases in various ranges of channel dimensions, “ $C_D$ ” being the smallest channel dimension:

$1 \mu\text{m} < C_D < 10 \mu\text{m}$	: Transitional Microchannels
$10 \mu\text{m} < C_D < 200 \mu\text{m}$	: Microchannels
$200 \mu\text{m} < C_D < 3 \text{ mm}$	: Minichannels
$3 \text{ mm} < C_D$	: Conventional passages

A simpler classification was proposed by Obot [10] based on the hydraulic diameter rather than the smallest channel dimension. Obot classified channels of hydraulic diameter under 1 mm ( $D_h < 1 \text{ mm}$ ) as microchannels, which was also adopted by many other researchers such as Bahrami [11, 12] and Bayraktar [13]. This definition is considered to be more appropriate for the purposes of this thesis as the classification proposed by Kandlikar and Grande is based on the behavior of gas flows, which is partially outside the scope of this study, and the classification proposed by Mehendale is based on manufacturing processes which are expected to change and/or improve in the future. The definition adopted by Obot is more convenient as it is based on the channel geometry alone and that it makes use of the hydraulic diameter concept, which is the primary representative dimension for internal flow geometry of the heat exchanger [7].

In the last few decades, new frontiers have been opened up by advances in our ability to produce microscale devices and systems. The numerous advantages that can be realized by constructing devices with microscale features have, in many cases, been exploited without a complete understanding of the way the miniaturized geometry alters the physical processes. Microchannels are used in a variety of devices incorporating single-phase liquid flow [14]. Their extremely high heat transfer capability is the primary point of interest of microchannels for this thesis. Besides heat related applications, microscale fluid flow also finds important applications in MEMS. Microducts are used in infrared detectors, diode lasers, and miniature gas chromatographs; micropumps are used for inkjet printing, environmental testing, and electronics cooling; microturbines are being developed as miniature energy generators and microvalves [15]. Chemical and biological applications such as microreactors and lab-on-a-chip devices are also many.

Microelectronic devices, which include a variety of applications such as PCs, servers, laser diodes and Rf devices are constantly pushing the heat flux density requirements to higher levels. What seemed to be an impossibly high limit of  $200 \text{ W/cm}^2$  of heat dissipation in 1993 now seems to be a feasible target. The new challenge for the coming decade is on the order of  $600\text{-}1000 \text{ W/cm}^2$ . The available temperature differences are becoming smaller, and in some cases as low as only a few  $^{\circ}\text{C}$ . These high levels of heat dissipation require a dramatic reduction in the channel dimensions, matched with suitable coolant loop systems to facilitate the fluid movement away from the heat source [14].

The higher volumetric heat transfer densities require advanced manufacturing techniques and lead to more complex manifold designs [14]. During the past two decades dramatic advances have been made in microfabrication techniques. Many of the same manufacturing techniques developed for the fabrication of electronic circuits are being used for the fabrication of compact heat exchangers. A systems perspective will be taken,

which involves transferring the heat generated in the electronic components through a path involving multiple media, leading to its ultimate rejection. Since this rejection is to ambient air for most ground based electronic equipment, liquid cooling schemes require a remote liquid to air heat exchanger, whose size and efficiency ultimately determine the size of the overall cooling systems. Capabilities and characteristics of micro fabrication play a key role in the development of such devices. [15].

### **1.3 Electronics Cooling Technologies**

Following the invention of the chip, methods for cooling of electronics have improved and sophisticated at an ever increasing pace in conjunction with the rapid development of the electronics industry. The importance of cooling for electronic components is that high temperatures not only decrease their lifetime by accelerating failure mechanisms in materials, but they also reduce the overall reliability of the assembly by accelerating failure mechanisms in connections and interfaces [16]. The evident trend in the development of integrated circuits is that the sizes are getting smaller while the heat dissipation quantities are getting larger. To meet the rapidly rising heat densities, methods of thermal engineering applied to the cooling of electronics have evolved from primitive, passive structures to advanced systems. The power dissipation trend of INTEL processor chips, shown in Fig. 1.5, is representative of the silicon industry in general [17].

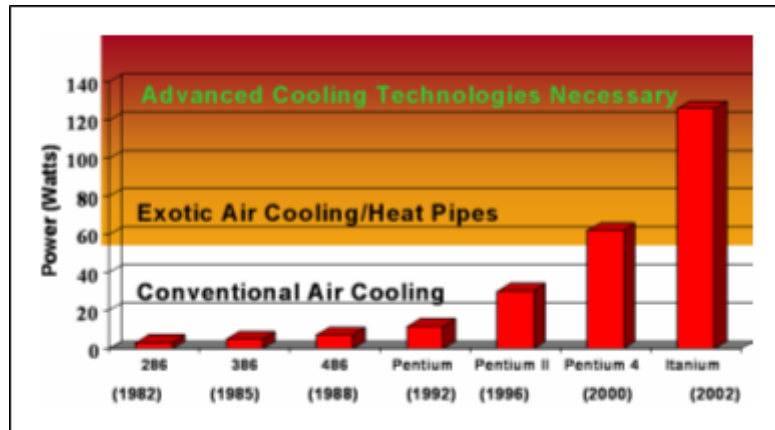


**Figure 1.5:** Trends in increasing power density and categorization of cooling methods employed by INTEL [7]

The categorization of cooling methods employed by INTEL given in the figure above shows that conventional cooling methods have become insufficient by the year 2000. Conventional air cooling methods refer to making use of natural or forced convection together with heat spreaders or heat sinks. As long as the heat dissipation of the chips to be cooled is moderate, it is preferable to use a simple heat sink design that can provide adequate cooling with natural convection. For higher heat fluxes, natural convection is not sufficient and fans must be used to obtain higher heat removal rates associated with forced convection.

When conventional air cooling methods do not suffice, enhanced cooling tools such as fan-heat sink assemblies or heat pipes must be used. Fan-heat sink assemblies are commonly used in personal computers to cool high performance processors, while heat pipes are commonly used in laptop computers where space is a major limitation. Fan-heat sink assemblies are, in fact, an extension of forced cooling methods where the heat sink is designed to achieve maximum cooling performance with the air flow due to the fan attached to it. Heat pipes, on the other hand, are structures that attain extraordinarily high thermal conductivity, enabling the heat dissipated by the chips to be carried effectively to an appropriate location for cooling [7]. Fig. 1.6 shows a heat-sink assembly and various heat pipe configurations.

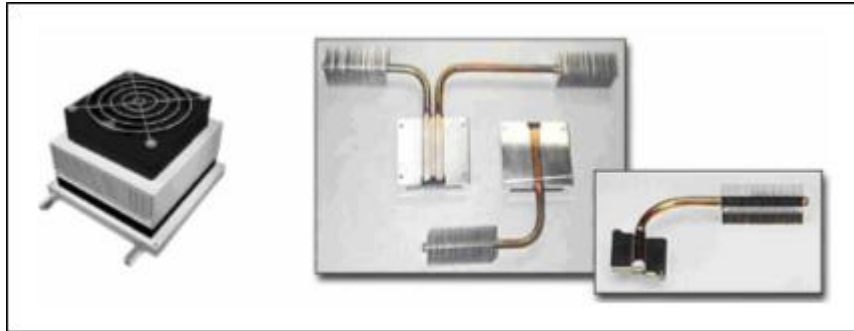


**Figure 1.6:** A heat sink-fan assembly (left) and various heat pipe configurations (right) [7]

When the limits of extended air cooling methods fall short of accommodating the rising heat densities to be cooled, advanced cooling technologies must be employed to achieve the high cooling performance required. The first milestone in advanced cooling is to utilize a coolant liquid instead of air. The heat removal capacity of liquids (e.g. water) is much higher compared to that of air; however, use of a liquid cooling system involves major changes in design compared to air cooling. To avoid damage to the electronics, the coolant must be totally isolated. A heat exchanger must be employed to serve as a medium of heat exchange between the coolant and the surrounding atmosphere. A pump must be used in place of the fan, heat sinks must be replaced by cold plates, or liquid cooled heat sinks, to generate a heat path between the chip and the coolant [7]. A schematic representative of liquid cooling system is given in Fig. 1.7.

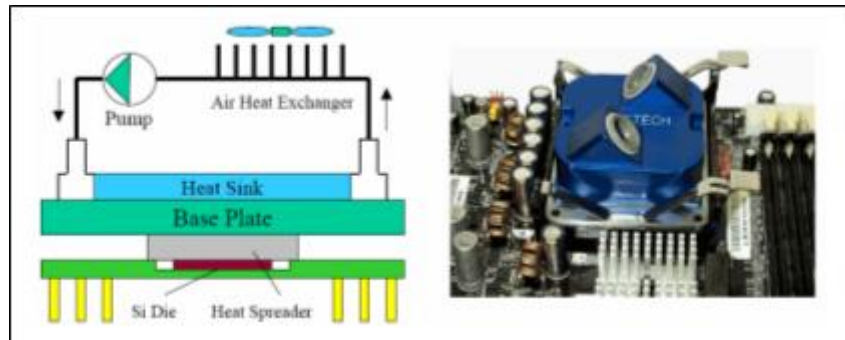


**Figure 1.7:** Liquid cooling system schematics (left) and example of a liquid cooled heat sink mounted on a PCB [7]

The cooling capabilities of liquid systems are wide ranging, depending on the coolant used, the performance of the heat exchanger, the pumping power, and the thermal interface between the heat source and the coolant. Conventional liquid cooling utilizes simple liquid heat sink geometries, commonly of rectangular cross section. The cooling method is characterized by the geometry of the heat sink. The cooling capacity of the system increases as the channel size decreases, leading to the categorization of "conventional liquid cooling", "minichannel liquid cooling", and "microchannel liquid cooling" [7]. A schematic view of a liquid heat sink is shown in Fig.1.8 and also in same figure minichannel and microchannel heat sink are presented.



**Figure 1.8:** Schematics of liquid heat sink (left), minichannel heat sink (center), and microchannel heat sink (right) [6]

Liquid cooling by means of conventional, minichannel, or microchannel liquid heat sinks is appropriate for the cooling of most high heat flux applications.

Many supercomputers of recent years employ microchannel liquid cooling, while microchannel liquid cooling is used most commonly in military radar applications.

In certain applications, where highly localized heat sources cannot be cooled sufficiently by channel cooling, spray cooling is employed. In this method, an atomizer (or nozzle) converts the liquid flow into a spray that impinges directly on the surface to be cooled. Dielectric coolants are used to avoid damage to the electronics. Because the coolant and heat source are brought into direct contact, the thermal path is more effective and higher cooling capacities may be achieved. Spray cooling may be designed to cool local hot spots in a system using a few nozzles, or to cool larger areas using a set of nozzles [7]. Fig. 1.9 shows good examples of localized spray cooling and system level spray cooling.

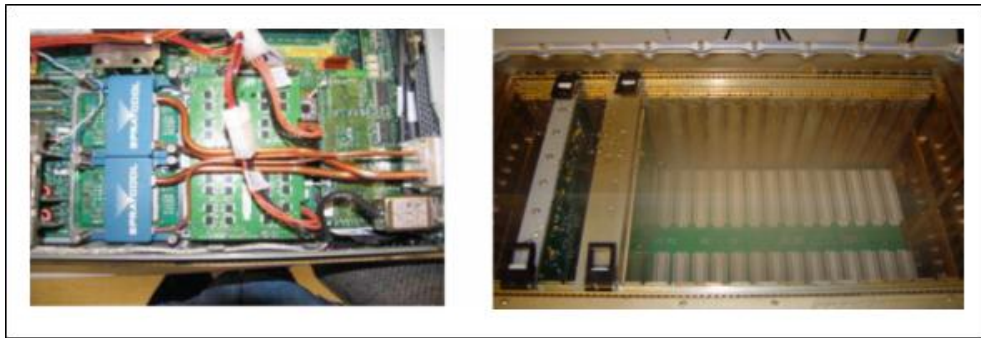


**Figure 1.9:** Localized spray cooling (left) and system level spray cooling (right) [7]

A final method worth mentioning among advanced cooling technologies is thermoelectric cooling. The Peltier effect, achieved by using a series of P and N type semiconductors, causes a finite temperature difference between the two surfaces of a thermoelectric cooler when a voltage is applied. The cold side of the thermoelectric cooler is attached to the surface to be cooled, while the hot side must be cooled by another cooling system (such as a heat sink and a fan) to achieve as low a temperature as possible at the heat source. The temperature difference between the cold side and hot side of high performance thermoelectric

coolers may exceed 100°C. In this way, very low temperatures at the heat source may be obtained. The drawback of this technique is that yet another cooling method must be employed for the hot side, and the electric power requirements of thermoelectric modules are high [7]. Thermoelectric cooling and modules are schematically shown in Fig.1.10.

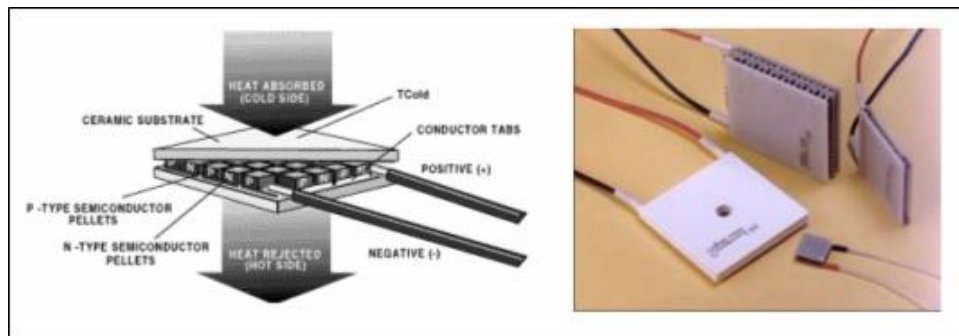


**Figure 1.10:** Schematic representation of thermoelectric cooling (left), thermoelectric modules (right) [18]

## 1.4 Motivation

The requirements of electronics cooling are much more critical in military electronic applications when compared to commercial applications such as personal computers, laptops and communication equipments. This is due to two reasons in conjunction. Firstly, the heat dissipation rates in military applications are usually higher; and secondly, military electronics is required to function reliably in harsh environments. The typical operating temperature specification for military equipment is the  $-30\text{ }^{\circ}\text{C} / +55\text{ }^{\circ}\text{C}$  range and this range is being extended nowadays, i.e the lower bound is approaching to  $-40\text{ }^{\circ}\text{C}$  and the upper bound is becoming  $+60\text{ }^{\circ}\text{C}$ . Usually, the lower bound causes no problems in terms of functionality or reliability. There are, however, occasional cases in which the system must be heated to a particular temperature before beginning operation. In such instances, a heater must be employed, which is a relatively simple design consideration. It is the upper bound of  $+55\text{ }^{\circ}\text{C}$  that challenges the thermal engineer

in the design of thermal management systems for military electronics. Although upper limits given by manufacturers for the operating temperature of some electronic components rate as high as +150 °C, it is desirable to keep the surfaces of most components under the +85 °C level. For integrated circuits, and many other electronic components, the heat dissipated by the component causes a significant temperature rise. When heat fluxes are large, that is, when large amounts of heat are dissipated by small components, such as in high performance chips, the temperature rise of the component may be as high as 20 °C or higher.

Cooling strategies for electronic components that are to comply with military operational specifications must be designed to keep the temperature rise of the component very small. The methods of cooling required at the component level may vary from conventional air cooling to advanced cooling methods such as microchannel liquid cooling and spray cooling. The selection of the cooling method is primarily based on the maximum heat flux associated with the device or component of interest. For military applications, it is common practice to employ conventional liquid cooling for heat fluxes in the order of tens of  $\text{W}/\text{cm}^2$ . When the maximum heat flux to be cooled approaches or exceeds  $100 \text{ W}/\text{cm}^2$ , microchannel liquid cooling becomes necessary. Such high heat fluxes are frequently encountered in the microwave modules of phased array radars in military applications. A systems perspective will be taken, which involves transferring the heat generated in the electronic components through a path involving multiple media, leading to its ultimate rejection. Since this rejection is to ambient air for most ground based electronic equipment, liquid cooling schemes require a remote liquid to air heat exchanger, whose size and efficiency ultimately determine the size of the overall cooling systems. Capabilities and characteristics of the heat exchanger play a key role in cooling of electronic equipments. Employing smaller channel dimensions in the heat exchanger results in higher heat transfer performance, although it is accompanied by a higher volumetric pressure drop per unit length. The higher volumetric heat transfer densities require advanced manufacturing techniques such as brazing and lead to more complex

designs. Because of above mentioned reasons, a brazed microchannel heat exchanger becomes the most suitable solution for military applications, which necessitate high heat removal capabilities.

### **1.5 Present Study**

This study focuses on the experimental investigation of a microchannel heat exchanger designed for liquid cooling systems in high performance radar cooling applications. The primary aim of the work is to determine the limits of the heat removal capability of the microchannel heat exchanger, which will be used in liquid cooling systems of radar applications. The goal is to be able to cool the liquid used in systems (e.g. water).

The secondary aim of this work is to design a national microchannel heat exchanger and to manufacture with national sources. In military applications one of the most critical aims is to lessen the dependence of our country to foreign countries. By means of this study one product will not to be need importing.

The other aim of this work is to gain the capability of flexibility in geometrical dimensions of the heat exchanger. Importing the product on the shelf restricts the designer and also the system in geometrical shape, dimensions, construction type, fluid type and etc. which are defined by the firms. After this study, we are able to determine the fin heights or length of the dimension and the other dimensions which the national system necessitates. In general, the ready-made product is either larger in volume or less efficient for the systems. This experience in design, and production of a microchannel heat exchanger will result in smaller and lighter liquid cooling systems in aerospace and defense industries. This experimental study will ensure that in spite of the rising heat fluxes, heat removal capacity of the system can be adjusted by altering the fin dimensions or fin type. By means of designing and producing an original microchannel heat exchanger, mounting

details of the heat exchanger will not be criteria for choosing or designing the systems. Moreover, time consumed to import a heat exchanger will decrease dramatically and also the response time to the change of design which is in nature of military projects will fall down and all these drops and flexibility result in saving money.

The starting point of this study is that if a design of the liquid cooling systems in military projects is possible, the product, the microchannel heat exchanger, to be used in this system can be also designed and national microchannel heat exchanger can be produced.

In this study, the literature survey is given in Chapter 2. Chapter 3 provides the theoretical background of the heat exchanger. Design and production steps of the heat exchanger are given in Chapter 4. Experimental setup, parameters of the experiment and experimental results are also discussed in the same chapter. Chapter 5 is devoted to the comparison of the results obtained from the experiments among each other, and to the discussion of possible reasons for the particular trends observed. In the last chapter, conclusions and suggestions for future work are provided. All detailed theoretical calculations according to Chapter 3 are given in Appendix A. Appendix B provides all theoretical and experimental calculations results of the heat exchanger. Technical drawings of the heat exchanger are given in Appendix C. Appendix D is devoted to detailed information about experimental setup. Thermophysical properties of materials used in this study are given in Appendix E.

## CHAPTER 2

### LITERATURE SURVEY

The following is a review of the research that has been completed especially on microchannel heat exchangers ( $\mu$ HEX) over the last decade. The literature survey is arranged according to similarity to the work done in this thesis.

In one of the recent studies by Al-Nmir et al. [19], an investigation of the hydrodynamic and thermal behavior of the flow in parallel plate  $\mu$ HEX is performed numerically, by adopting a combination of both the continuum approach and the possibility of slip at the boundaries. In their work, both viscous dissipation and internal heat generation were neglected. Fluent analysis was made based on solving continuum and slip boundary condition equations. The flows were assumed as laminar, two dimensional, steady and incompressible with constant thermo-physical properties and without a heat source/sink. Effects of different parameters; such as, Knudsen number (Kn), heat capacity ratio (Cr), effectiveness ( $\epsilon$ ), and number of transfer units (NTU) were examined. The study showed that both the velocity slip and the temperature jump at the walls increase with increasing Kn due to the flow not being completely aware of the presence of the wall as a result of the relatively low number of collisions between the fluid molecules. The increase of the slip conditions reduce the frictional resistance of the wall against the flow, and under the same pressure gradient, pumping force leads to that the fluid flows much more in the heat exchanger. It was reported that increasing Kn leads to an increase in the temperature at the heat exchanger wall. On the other hand, at low values of Kn, the NTU increases with increasing Cr, but at high values of Kn the NTU decreases with increasing Cr. With regard to the

effect of  $Cr$  on  $\varepsilon$ , it was found that increasing  $Cr$  leads to a reduction in  $\varepsilon$  for all  $Kn$ .

Very recently, Mathew and Hegab theoretically analyzed the thermal performance of parallel flow  $\mu$ HEX subjected to constant external heat transfer [20]. The equations for predicting the axial temperatures as well as the effectiveness of the fluids of the  $\mu$ HEX operating under laminar flow conditions were developed. In addition, an equation for determining the heat transfer between the fluids was formulated. Mathew and Hegab developed this particular model in such a way that it can be used for a parallel flow [20] with either balanced or unbalanced flow (i.e. heat capacities of two fluids are equal or not) and also it enables to calculate the temperature of the fluids at any axial location. Moreover, the model can be used when the individual fluids are subjected to either equal or unequal amounts of external heat transfer. On the other hand, the model is limited to microchannel flow applications in which the working fluids are incompressible, single phase, maintaining no-slip wall conditions, and do not exhibit any rarefaction effects. The last restriction results in a restriction on the lower limit of the microchannel diameter. For example, if air is used, the minimum hydraulic diameter must be 68 nm which is the mean free path of air. In this paper, under unbalanced flow conditions, it was stated that the effectiveness of the fluids depend on the fluid with the lowest heat capacity, it is greatest when the hot fluid has the lowest heat capacity. At a given NTU, the reduction in heat capacity ratio improved the effectiveness of the fluids. Under certain operating conditions temperature cross over was observed in the heat exchanger.

In another recent work, characteristics of the flow in Chevron plate heat exchangers were examined through visualization tests of channels where Chevron angles are  $28^\circ$  and  $65^\circ$  [21]. The correlations derived with the friction factor,  $f$  and Nusselt number,  $Nu$  for flow in channels of arbitrary geometry were used to evaluate thermal and hydraulic characteristics of the entrance. Then, experimental results were utilized to adjust the derived correlations. This paper is useful to

understand the mechanisms determining heat transfer and pressure drop in Chevron plate channels and the corresponding influence of the flow conditions and geometrical parameters. This study can be thought of as a continuation of Dović's thesis [22]. In this study [21], the model focuses on the single cell, which is the smallest repeating unit of the channel composed of two crossing ducts with (close to) sinusoidal cross sections. In the experiments, injections of dye to the transparent wall or the central part of the single cell were used to visualize the flow in the channel. Solutions for the prediction of heat transfer and pressure drop in parallel heat exchanger channels have been provided to give results which are consistent with the experiments for a wide range of flow conditions and geometrical parameters. These solutions can be useful when no experimental data are available for a particular flow regime and geometry. This study can be improved with more experimental data for plates of various geometries.

Tsuzuki et al. proposed a new flow configuration, named S-shaped fin configuration to reduce the  $\mu$ HEX pressure drop [23]. A numerical study using a 3D-CFD code, FLUENT, was performed to find Nusselt number correlations for the  $\mu$ HEX. A method to evaluate the heat transfer performance of the whole heat exchanger from the two correlations was proposed. The copper heat exchanger, whose dimensions are  $1240 \times 68 \times 4.75 \text{ mm}^3$ , comprises cold water channels and hot  $\text{CO}_2$  channels. For both hot and cold sides, simulations were done to attain accurate empirical correlations for different temperatures. PROPATH, a database for thermo-physical properties of the fluids was used to for  $\text{CO}_2$ . The results were in the neighborhood of 3% error when a comparison was made with other numerical studies. On the other hand, the difference between experimental results and the correlations was approximately 5%. Although the Reynolds number on the  $\text{CO}_2$  side is sufficiently large to be regarded as turbulent flow, it was small for the water side. However water flow showed rather more turbulent behavior than laminar, with Reynolds number less than 1500. The results indicate that the pressure drop of the S-shaped fin configuration was about one-seventh of that of

the conventional zigzag configuration while the heat transfer rate was almost identical.

One of the comprehensive studies in counter flow  $\mu$ HEX area was done last year [24]. In this work, numerical simulations were made to study the effect of the size and shape of channels; such as circular, square, rectangular, iso-triangular, and trapezoidal, in counter flow  $\mu$ HEX. The results show that for the same volume of heat exchanger, increasing the number of channels leads to an increase in both effectiveness and pressure drop. Moreover circular channels give the best overall performance (thermal and hydraulic) among various channel shapes. The second best overall performance is provided by square channels. New correlations are developed to predict the value of heat exchanger effectiveness and performance index as a function of the relative size of the channels with overall heat exchanger volume, Reynolds number, and thermal conductivity ratio.

Recently, an experimental analysis of two designed  $\mu$ HEX, whose cross sectional areas are  $100 \times 100$  and  $200 \times 200 \mu\text{m}^2$ , was performed to compare with the predictions of the classical viscous flow and heat transfer theory [25]. The working fluid was deionized water. The minimum Reynolds number of each current was defined by the minimum flow rate that could steadily be controlled by the pump. The maximum Reynolds number was restricted by the maximum flow rate of the pump, which was 1 L/min, and occasionally the pressure drop, which cannot be larger than 4 bars, to avoid leaks. The results showed good agreement with the general theory and no special effect related to the small dimensions of the channels was observed. On the other hand, the author mentioned that the plate conduction thermal resistance is a major restriction for  $\mu$ HEX performance. For the current thesis, the plate thickness and plate material are critical in the design of the  $\mu$ HEX.

In another work, Schgulla et al. investigated a heat exchanger made of plastic with heat fluxes up to  $500 \text{ W/cm}^2$ , a pressure drop of 0.16 MPa, and mass

flow of water 200 kg/h per passage [8]. The use of plastic results in higher temperature resistance, higher stability, higher water throughputs and higher flow velocities. The specific fluid data of deionised water have been assumed to be constant in the temperature range between 10°C and 95°C.

Kang and Tseng theoretically modeled thermal and fluidic characteristics of a cross-flow  $\mu$ HEX assuming that flows in rectangular channels, where fin height and width are 32  $\mu\text{m}$  and 200  $\mu\text{m}$  respectively, are incompressible, steady, and laminar [27]. They compared the theoretical solutions with the experimental data from the available literature and validated the theoretical model. The interactive effect between the effectiveness and pressure drop in the  $\mu$ HEX was analyzed. Besides, they showed that the heat transfer rate and the pressure drop at the same effectiveness value are significantly affected by the average temperature of the hot and cold side flow. The results were confirmed by Kang and Tseng as they indicated that different effectiveness values influence heat transfer and pressure drop considerably. The effect of the change of the  $\mu$ HEX material from silicon to copper and dimensions were also investigated. A small volume of the heat exchanger (i.e. 9 x 9 x 10.2 mm) enables almost the same temperature distribution. In their study, the surface temperature on the wall of the heat exchanger was assumed as constant. Steady heat transfer rate and constant solid and fluid properties were used. Pressure drop, flow rates, inlet and outlet temperatures from both sides of the heat exchanger were measured in experiments. The temperatures difference between cold and hot fluids' inlets and outlets were measured to be 10°C under same effectiveness value ( $\epsilon=0.333$ ). Kang and Tseng could achieve a heat transfer rate larger than 2700W for different average temperatures. Their study shows that under the same effectiveness value, a small rise in the temperatures of working fluids results in an increase of the heat transfer rate, but a decrease in pressure drop occurs. An increase in effectiveness causes a decrease if both the heat transfer rate and pressure drop. The experiments showed that a better heat transfer rate can be achieved by small effectiveness values. Kang and Tseng claimed that enlarging the dimensions of the heat exchanger has some

advantages and disadvantages regarding the pressure drop and the heat transfer rate; an optimization must be done according to design criteria [27]. For example, by only doubling the size of the heat exchanger without changing fin parameters, the heat transfer rate increases from 2700 W to 22000 W; however, the pressure drop also increases about three-to-four times.

Vamadevan and Kraft used aluminum brazing to produce a microchannel tube heat exchanger [28]. They investigated the effect of processing on the mechanical behavior of aluminum brazing on the microchannel tube heat exchanger. Commercially extruded and processed AA3102 microchannel tube was exposed to a brazing thermal cycle. A special apparatus was developed to provide pressure test capabilities up to 69 MPa (10,000 psi), and simultaneous sample heating up to 180°C for microchannel tube samples. This paper is useful to understand the behavior of microchannels after brazing process.

Wen et al. used CFD simulation, FLUENT, and PIV (Particle Image Velocymeter) to determine the turbulent flow structure inside the entrance of a plate fin heat exchanger [29]. PIV is an instantaneous whole-field measurement technique, which uses a pulsed light-sheet to illuminate a gas flow seeded with tracer particles. By means of PIV, a series of velocity vectors and streamline graphs of different cross sections are obtained. The turbulence flow was calculated by the Semi-implicit SIMPLER Algorithm method in the velocity and pressure conjugated problem, and a second order upwind differential scheme was applied for the approximation of the convective terms. The computation and experiment were performed under the similar inlet Reynolds number ( $Re = 6.0 \times 10^4$ ). CFD results and PIV data were in good agreement with each other. The authors conclude that PIV and CFD are well suitable to analyze complex flow patterns.

A few years ago, Foli et al. introduced multi-objective genetic algorithms for determining the optimal geometric parameters of the microchannels in  $\mu$ HEX to maximize the heat transfer rate under specified design constraints [30]. CFD

analysis with an analytical method of calculating the optimal geometric parameters was also performed. This paper is important and a good work, because there is limited published literature on attempts at designing  $\mu$ HEX for optimal performance. This work is different from the other studies in that a commercial CFD analysis program, CFD-ACE+ has been used.

Nika et al. introduced new techniques to analyze heat exchangers [31]. The scope of their work was thermoacoustic phenomena in multi-channel heat exchangers, without phase change of the fluid. In this study, microchannels were made of silicon by means of LIGA (Lithographie Galvano Abformung) technique. The authors listed three factors, which are thermal characteristic time, aerodynamic matrix of transfer, and thermal efficiency, to analyze the aerodynamic and thermal performance of a  $\mu$ HEX. This work concerns only situations where the displacement of the fluid is considerably smaller than the length of the heat exchanger itself, and abrupt changes of the wall temperature or of the section are also prohibited.

Kanlayasairi and Paul worked on a fabrication procedure for NiAl microchannel arrays [32]. For leakage tests, they made a similar work as the current work. This paper introduced a microlamination procedure for producing high-aspect-ratio NiAl microchannel arrays. Several 28:1 aspect ratio NiAl microchannel arrays were produced. Metallography was conducted to evaluate the geometry of the microchannels. Reactive diffusion bonding was introduced as a joining technique for NiAl lamina. Laser micromachining was applied to cut the NiAl lamina without thermal cracking.

Jiang et al. performed an experimental comparison of  $\mu$ HEX with microchannel and porous media [33]. The effect of the dimensions on heat transfer was analyzed numerically. It was emphasized that the heat transfer performance of the  $\mu$ HEX using porous media is better than that of the  $\mu$ HEX using microchannels, but the pressure drop of the former is much larger.

As mentioned before there is a substantial research on microchannels and heat sinks. Recently, Alpsan performed a research on microchannel heat sinks for phased array radar cooling applications [7]. In this research, experimental measurements and numerical simulations were performed on copper and aluminum microchannel heat sinks of 300, 420, 500, and 900  $\mu\text{m}$  channel widths. Alpsan designed the heat sinks specifically for use with T/R (transmit/receive) module cooling applications of military phased array radars. An analytical calculation was also performed to aid in the design methodology. Alpsan used a chip carrier mounted with attenuators to simulate the localized head load of actual transmit/receive modules. Distilled water was used as the coolant with flow rates ranging from 0.50 lpm (liters per minute) to 1.00 lpm. Local heat fluxes as high as  $100 \text{ W/cm}^2$  were tested. Temperature measurements were taken by thermistors on the heat load surface and by J-type thermocouples in the water and air regions. Pressure measurements were taken by pressure transducers at the heat sink inlet and outlet regions. A digital output flow meter was used to record the coolant flow rate. In his study, experimental results showed that copper specimens were significantly superior to aluminum specimens in terms of cooling performance, as expected, due to their difference in thermal conductivity. The thermally best performing specimen, the 300  $\mu\text{m}$  copper specimen, yielded a maximum temperature rise of  $26.1 \text{ }^\circ\text{C}$  between the heat load and coolant inlet, at a coolant flow rate of 1.00 lpm and local heat flux of  $100 \text{ W/cm}^2$ , leading to a thermal resistance of  $0.63 \text{ }^\circ\text{C/W}$ . The pressure drop measured across the heat sink under these conditions was 0.030 bars. The experimental results regarding thermal performance were observed to be consistent when compared to similar studies in the literature. Results for pressure drop, however, showed significant departure. This was attributed to the geometrical differences in the heat sinks between studies compared. Alpsan also carried out numerical simulations using the commercial Computational Fluid Dynamics (CFD) software FLUENT<sup>®</sup>. Effects of thermal interface layers and heat spreading due to the localized heat load were investigated. Simulation results for temperature were seen to agree fairly well with experimental data as long as thermal interface layers were accounted for. The

simple analytical calculation for temperature, based on the classical fin approach, deviated greatly from experimental results due to the thermal interface and heat spreading effects not being included in the calculation. The analytical calculation for pressure drop, based on conventional theory for developing flow, coincided perfectly with the numerical results. This study showed that the T/R modules of military phased array radars, dissipating as high as  $100 \text{ W/cm}^2$  locally, could be cooled within the limits of the harsh environmental conditions required of military applications with moderate pressure drops.

Philips investigated fluid flow and heat transfer in microchannels experimentally and numerically [34]. Fluid flow and heat transfer experiments were conducted on a copper  $\mu$ HEX. An experimental method of imposing a constant surface temperature to the  $\mu$ HEX was used. In this study, the friction factor results from the experiments agreed fairly well with theoretical correlations and moreover the experimental Nusselt number results agreed with theory very well in the transition/turbulent regime, but the results show a higher Nusselt number in the laminar regime than predicted by theoretical correlations. Philips created a CFD model to simulate the fluid in the inlet plenum and the microchannels. The results from these simulations showed good agreement with the experimental data in the transition/turbulent regime as well as with theoretical correlations for laminar and turbulent flow.

Literature shows that the microchannels and microchannels heat sinks were studied extensively, but there is limited research related to the performance of two fluid microchannel heat exchangers and there is not much comprehensive investigations to study the effect of channels shape on the performance of two fluid cross flow  $\mu$ HEX. However, there has been an increase on this subject in the past few years.

## CHAPTER 3

### THEORY OF HEAT EXCHANGERS

In this chapter, basic heat transfer equations will be outlined for the thermal analysis of a  $\mu$ HEX. Performance calculations of the heat exchanger (rating problem) will be carried out. First, heat transfer from the hot fluid to the cold fluid will be determined. Then effective mean temperature difference of the fluids inlet and outlet temperatures will be investigated to determine the heat transfer. The overall heat transfer coefficients will be introduced in this analysis. Next, fin efficiency and overall surface efficiency will be explained. Heat transfer effectiveness, heat capacity rate ratios and number of transfer unit will be determined. To determine the convective heat transfer coefficient some dimensionless numbers will be introduced. Finally geometrical properties will be analyzed to find the hydraulic diameter of both sides.

#### 3.1 Heat Transfer Analysis

Under steady state conditions with negligible potential and kinetic energy changes, if the fluids do not undergo a phase change and have constant specific heats,  $c_p$  and there is negligible heat transfer between the exchanger and its surroundings, for hot and cold fluids, heat transfer rate may be expressed as below

$$Q = (\dot{m} \cdot c_p)_h \cdot (T_{h1} - T_{h2}) \quad (1)$$

and

$$Q = (\dot{m} \cdot c_p)_c \cdot (T_{c2} - T_{c1}) \quad (2)$$

where  $\dot{m}$  is the rate of mass flow. The subscripts h and c refer to the hot and cold fluids, respectively and the numbers 1 and 2 designate the fluid inlet and outlet conditions, respectively. As cold fluid enthalpy increases and hot fluid enthalpy decreases, heat will be transferred from the hot fluid to the cold fluid.

The temperature difference between the hot and cold fluids varies with position in the heat exchanger. Therefore, in the heat transfer analysis of heat exchangers, it is convenient to establish an appropriate mean value of the temperature difference between the hot and cold fluids such that the total heat transfer rate  $Q$  between the fluids can be determined from the following equation:

$$Q = U \cdot A \cdot \Delta T_{lm} \quad (3)$$

Here,  $A$  is the total hot side or cold side heat transfer area and  $U$  is the overall heat transfer coefficient based on that area.  $\Delta T_{lm}$  is the effective mean temperature difference and is a complex function of  $T_{h1}$ ,  $T_{h2}$ ,  $T_{c1}$ ,  $T_{c2}$ .  $\Delta T_{lm}$  can be determined analytically in terms of the following quantities:

$$\Delta T_{lm,cf} = \frac{(T_{h2}-T_{c1})-(T_{h1}-T_{c2})}{\ln \left[ \frac{T_{h2}-T_{c1}}{T_{h1}-T_{c2}} \right]} \quad (4)$$

$$P = \frac{T_{c2}-T_{c1}}{T_{h1}-T_{c1}} = \frac{\Delta T_c}{\Delta T_{max}} \quad (5)$$

$$R = \frac{C_c}{C_h} = \frac{T_{h1}-T_{h2}}{T_{c2}-T_{c1}} = \frac{\Delta T_h}{\Delta T_c} \quad (6)$$

Here,  $\Delta T_{lm,cf}$  is the log mean temperature difference (LMTD) for a counterflow arrangement with the same fluid inlet and outlet temperatures.  $P$  is a measure of the ratio of the heat actually transferred to the heat which would be transferred if the same cold fluid temperature was raised to the hot fluid temperature; therefore  $P$  is the temperature effectiveness of the heat exchanger on the cold fluid side.  $R$  is the ratio of the heat capacity rate ( $\dot{m}c_p$ ) of the cold fluid to that of the hot fluid and it is called the heat capacity rate ratio [2].

$\Delta T_{lm}$  may also be used for multipass and crossflow heat exchangers by multiplying it with a correction factor F

$$Q = U \cdot A \cdot \Delta T_{lm} = U \cdot A \cdot F \cdot \Delta T_{lm,cf} \quad (7)$$

F is nondimensional and depends on the temperature effectiveness P, the heat capacity ratio R and the flow arrangement

$$F = \Phi (P, R, \text{flow arrangement}) \quad (8)$$

The correction factor F is less than unity for crossflow and multipass arrangements. The correction factor for crossflow and multipass arrangement is available in graphical form in Ref [2]. For a crossflow heat exchanger with both fluids unmixed Fig. 3.1 is used.

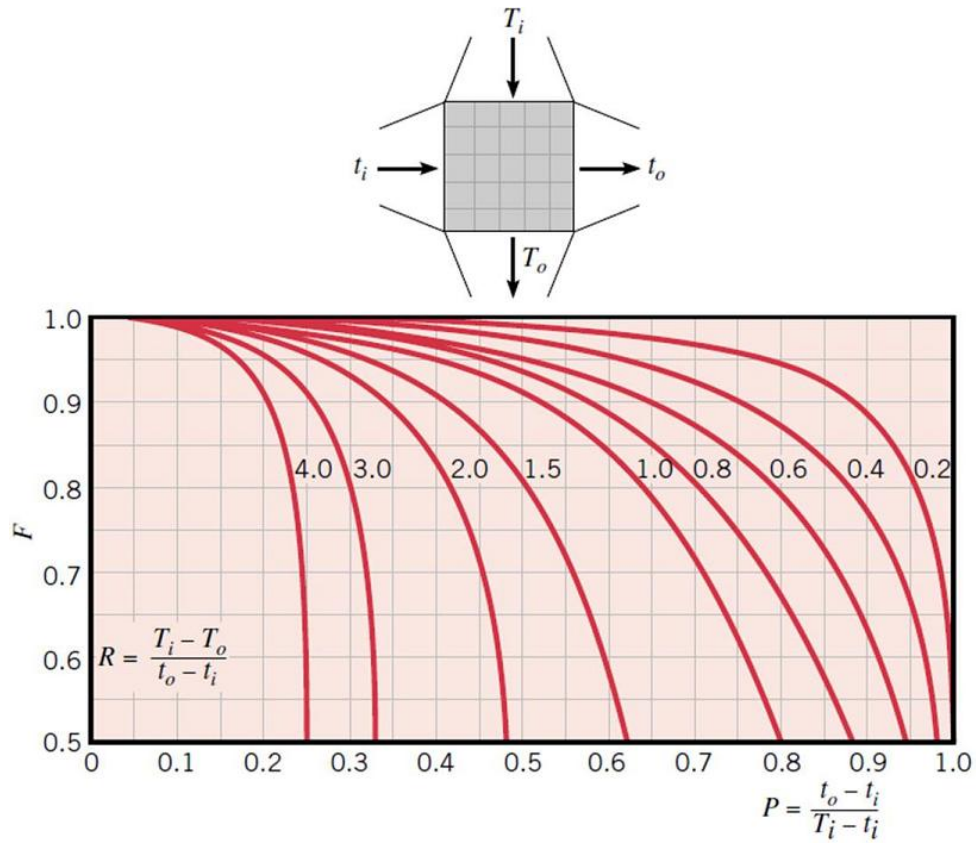


**Figure 3.1:** LMTD correction factor  $F$  for a single pass crossflow heat exchanger with both fluids unmixed [2]

### 3.2 Overall Thermal Coefficient, $UA$

At steady state, heat is transferred from the hot fluid to the cold fluid with the following processes: convection to the hot fluid wall, conduction through the wall and subsequent convection from the wall to the cold fluid. In many heat exchangers, a fouling film is formed as a result of accumulation of scale or rust formation, deposits from fluid, chemical reaction products between the fluid and the wall material or biological growth. Fouling results in an additional insulating layer to the heat transfer surface. As a result, the total thermal resistance includes the thermal convection resistances of both sides, the wall resistance and fouling resistances of both sides [1].

$$R_t = R_h + R_{f,h} + R_w + R_{f,c} + R_c \quad (9)$$

where

$$R_h = \frac{1}{(\eta_{0,h} \cdot h \cdot A)_h} \quad (10)$$

$$R_{f,h} = \frac{R_{fh}}{\eta_{0,h} \cdot A_h} \quad (11)$$

$$R_w = \frac{\delta_w}{k_w \cdot A_w} \quad (12)$$

$$R_{f,c} = \frac{R_{fc}}{\eta_{0,c} \cdot A_c} \quad (13)$$

$$R_c = \frac{1}{(\eta_{0,c} \cdot h \cdot A)_c} \quad (14)$$

In Eqs. (15-20),  $R_h$  and  $R_c$  represent the convection resistances of hot and cold fluids with finned surfaces, respectively. The separating wall resistance is shown as  $R_w$ .  $R_{fh}$  and  $R_{fc}$  represent the fouling resistances of hot and cold sides respectively. It is extremely difficult to predict a specific fouling behavior for most cases since a large number of variables can materially alter the type fouling and its rate of formation. Sources of fouling resistance in the literature are rather limited. The most referenced source of fouling factors is in the standards of the Tubular Exchanger Manufacturers Association, available in Ref [2].

The total thermal resistance is also expressed as the inverse of overall thermal coefficient.

$$R_t = \frac{1}{U \cdot A} \quad (15)$$

The overall thermal coefficient  $UA$  may be defined optionally in terms of the surface area of the hot surface or the cold surface or the wall conduction wall areas.

$$UA = U_h \cdot A_h = U_c \cdot A_c = U_w \cdot A_w \quad (16)$$

$$UA = \left( \frac{1}{(\eta_{0,h} \cdot h \cdot A)_h} + \frac{R_{fh}}{\eta_{0,h} \cdot A_h} + \frac{\delta_w}{k_w \cdot A_w} + \frac{R_{fc}}{\eta_{0,c} \cdot A_c} + \frac{1}{(\eta_{0,c} \cdot h \cdot A)_c} \right)^{-1} \quad (17)$$

### 3.3 Fin Efficiency

The  $\eta$  in thermal resistances represents fin efficiency. In most two-fluid plate fin heat exchangers, fins are used to increase the surface area and consequently, to increase the total rate of heat transfer. Assuming there is no heat transfer through the center of the fin and it is treated as adiabatic, the fin efficiency of a plain fin is:

$$\eta_f = \frac{\tanh(m \cdot l_1)}{m \cdot l_1} \quad (18)$$

where

$$m = \left[ \frac{2 \cdot h}{k_f \cdot \delta} \left( 1 + \frac{\delta}{L_f} \right) \right]^{1/2} \quad (19)$$

$$l_1 = \frac{b}{2} - \delta \quad (20)$$

where  $b$  is the fin height (the distance between two plates in the heat exchanger),  $\delta$  is the fin thickness,  $l_1$  is the adiabatic fin height,  $L_f$  is the fin length and  $k_f$  is thermal conductivity of fin and  $h$  is the convection heat transfer coefficient [1].

The overall surface efficiency is expressed as:

$$\eta_0 = \left[ 1 - (1 - \eta_f) \cdot \frac{A_f}{A} \right] \quad (21)$$

### 3.4 Heat Exchanger Effectiveness and NTU

Heat capacity rate ratio,  $C^*$  is the ratio of the smaller to the larger heat capacity rate of hot and cold fluids.

$$C^* = \frac{C_{min}}{C_{max}} \quad (22)$$

where

$$C_{min} = \min(C_c, C_h) \quad (23)$$

$$C_{max} = \max(C_c, C_h) \quad (24)$$

$$C_c = (\dot{m} \cdot c_p)_c \quad (25)$$

$$C_h = (\dot{m} \cdot c_p)_h \quad (26)$$

The fluid that might undergo the maximum temperature difference is the fluid with the minimum heat capacity rate. The maximum heat transfer is expressed as:

$$Q_{max} = (\dot{m} \cdot c_p)_c \cdot (T_{h1} - T_{c1}) \quad \text{if } C_c < C_h \quad (27)$$

$$Q_{max} = (\dot{m} \cdot c_p)_h \cdot (T_{h1} - T_{c1}) \quad \text{if } C_h < C_c \quad (28)$$

Effectiveness  $\varepsilon$  is a measure of the thermal performance of a heat exchanger and can be defined as the ratio of the actual heat transfer rate to the thermodynamically limited maximum possible heat transfer rate.

$$\varepsilon = \frac{Q}{Q_{max}} = \frac{C_h \cdot (T_{h1} - T_{h2})}{C_{min} \cdot (T_{h1} - T_{c1})} = \frac{C_c \cdot (T_{c2} - T_{c1})}{C_{min} \cdot (T_{h1} - T_{c1})} \quad (29)$$

The number of transfer units,  $NTU$ , designates the nondimensional heat transfer size of the heat exchanger and is defined as a ratio of the overall thermal conductance to the minimum heat capacity rate:

$$NTU = \frac{U \cdot A}{C_{min}} \quad (30)$$

Effectiveness  $\varepsilon$  can be expressed as function of  $NTU$  and  $C^*$ . The derivation of  $\varepsilon - NTU$  expressions is complicated. In Ref [3] for a cross-flow and unmixed flow arrangement, an equation is available.

$$\begin{aligned} \varepsilon = 1 - e^{-(1+C^*) \cdot NTU} \cdot [ & I_0(2 \cdot NTU \cdot \sqrt{C^*}) \\ & + \sqrt{C^*} \cdot I_1(2 \cdot NTU \cdot \sqrt{C^*}) \\ & - \frac{1-C^*}{C^*} \cdot \sum_{n=2}^{\infty} C^{*\frac{n}{2}} \cdot I_n(2 \cdot NTU \cdot \sqrt{C^*})] \end{aligned} \quad (31)$$

Here,  $I_0, I_1, I_n$  are the modified Bessel functions. Moreover  $\varepsilon$  vs.  $NTU$  is available in Ref [3].

### 3.5 Pressure Drop

The amount of pressure drop of both fluids is an important part of performance analysis. It is difficult to predict the pressure drop in a non-standard heat exchanger. Therefore, in this work, pressure drop will be determined using the measured difference in pressure at the inlet and outlet of the heat exchanger for both fluids.

$$\Delta p_h = p_{h1} - p_{h2} \quad (32)$$

$$\Delta p_c = p_{c1} - p_{c2} \quad (33)$$

where  $p_{h1}, p_{c1}$  are inlet pressure of hot and cold fluids respectively and outlet pressures are,  $p_{h2}$  and  $p_{c2}$ .

### 3.6 Heat Transfer Coefficient

For the determination of convection heat transfer coefficient  $h$ , some dimensionless numbers will be introduced.

The Reynolds number,  $Re$ , is interpreted as a flow characteristic proportional to the ratio of flow momentum rate to viscous force for a specified geometry.  $Re$  is also called as flow modulus and defined for internal flow as

$$Re = \frac{G \cdot D_h}{\mu} \quad (34)$$

and

$$G = \frac{\dot{m}}{A_0} = \rho \cdot u_m \quad (35)$$

where  $A_0$  is the cross sectional area,  $\rho$  is the density,  $\mu$  is the viscosity of fluid and  $u_m$  is the mean fluid velocity. For internal flows, if  $Re < 2300$  then the flow is laminar.  $D_h$  is defined for noncircular ducts and is expressed as:

$$D_h = 4 \cdot \frac{A_c}{p} = \frac{4 \cdot (\text{net free flow area})}{\text{wetted perimeter}} \quad (36)$$

The Nusselt number,  $Nu$ , is one of the dimensionless representations of the heat transfer coefficient.  $Nu$  is a ratio of the convective conductance to pure molecular thermal conductance over the hydraulic diameter. It is defined as:

$$Nu = \frac{h \cdot D_h}{k} \quad (37)$$

Here,  $k$  is the thermal conductivity of the fluid.

The Stanton number,  $St$ , is the ratio of convection heat transfer to the enthalpy rate change of the fluid reaching the wall temperature.  $St$  does not depend on any geometrical characteristic dimension. It is defined as:

$$St = \frac{h}{G \cdot c_p} \quad (38)$$

The Prandtl number,  $Pr$ , is the fluid property modulus representing the ratio of momentum diffusivity to thermal diffusivity of the fluid.  $Pr$  is expressed as:

$$Pr = \frac{\nu}{\alpha} = \frac{\mu \cdot c_p}{k} \quad (39)$$

The Colburn factor,  $j$ , is the modified Stanton number to take into account the moderate variations in the fluid Prandtl number. It is defined as:

$$j = St \cdot Pr^{2/3} = \frac{Nu \cdot Pr^{-1/3}}{Re} \quad (40)$$

For a rectangular channel,  $Nu$  depends on the channel aspect ratio  $\alpha_c = \frac{a}{b}$  (where  $a$  is the short length of a rectangular profile and  $b$  is the long length of rectangular profile) and the wall boundary conditions. For liquid flow in rectangular microchannel, fully developed laminar flow and taking into account temperature variations of liquid,  $Nu$  can be expressed as below [38]:

$$Nu = [8.235 \cdot (1 - 1.883 \cdot \alpha_c + 3.767 \cdot \alpha_c^2 - 5.814 \cdot \alpha_c^3 + 5.361 \cdot \alpha_c^4 - 2 \cdot \alpha_c^5)] \cdot \left(\frac{\mu_b}{\mu_w}\right)^{-0.14} \quad (41)$$

The subscripts  $b$  and  $w$  designate properties evaluated at the bulk mean temperature and wall temperature respectively.

### 3.7 Geometrical Properties

The determination of geometrical characteristics for finned cross flow heat exchangers is somewhat complicated due to the presence of plain fins. The plain fin used can be assumed as rectangular. However, in reality the rectangular fin geometry has rounded corners instead of the sharp corners as shown in Fig. 3.2. The primary surface area and secondary (fin) surface area associated with a rectangular fin are also shown in Figs. 3.2 and 3.3. These sketches represent a good approximation due to the braze fillet and radius.

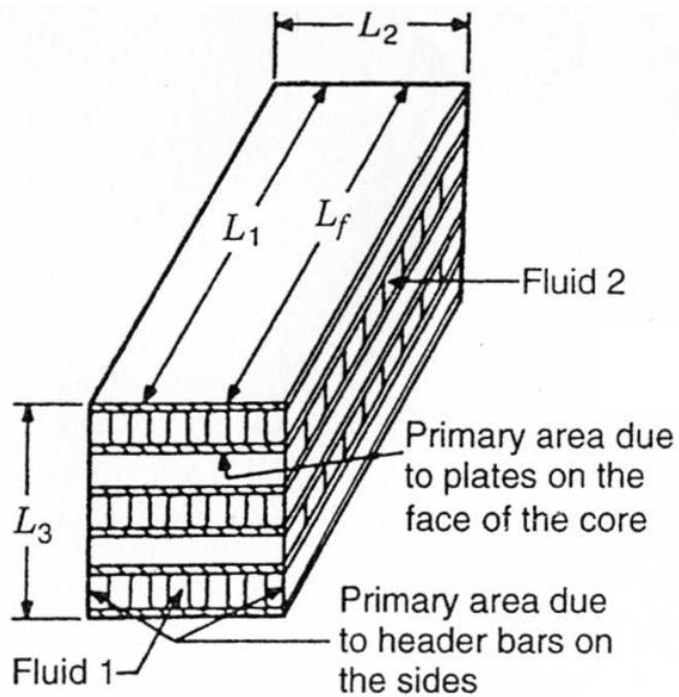


**Figure 3.2:** Cross flow plain fin heat exchanger [1]

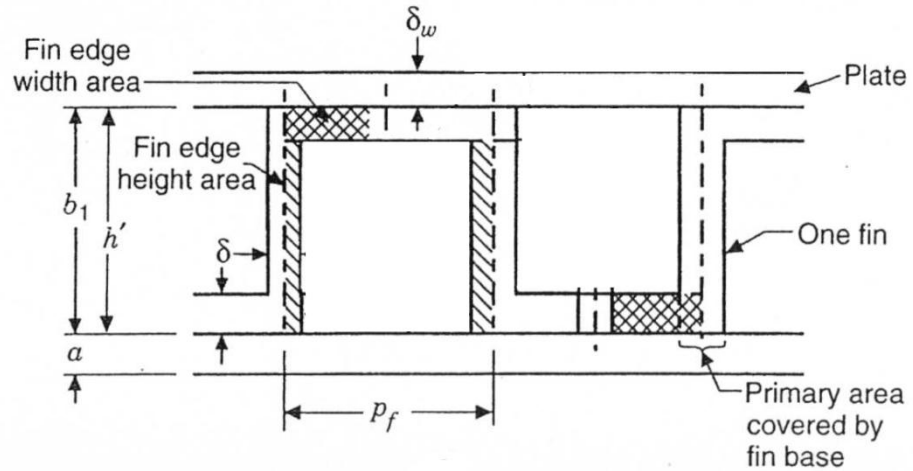


**Figure 3.3:** Idealized plain rectangular fin [1]

The total heat transfer area  $A$  for fluid 1 consists of primary,  $A_p$  and secondary (fin),  $A_f$  surface area swept by fluid 1, and is identical for fluid 2 due to the symmetrical conditions of the heat exchanger. The following four components are needed for calculating the primary surface area:

- (1) plate area,
- (2) fin base area that covers the plate,
- (3) header bar area on the sides for fluid 1 near the ends of fins in the  $L_2$  direction
- (4) header bars and plates exposed area of the blocked fluid 2 passage at fluid 1 core inlet and outlet faces.

The secondary (fin) area consists of

- (1) fin height area,
- (2) fin edge height area
- (3) fin edge width area.

The primary surface area is then the sum of components 1, 3 and 4 minus component 2. These four components of the primary surface area are now derived as:

$$\text{total plate area} = 2 \cdot L_1 \cdot L_2 \cdot N_p \quad (42)$$

where  $N_p$  is the total number of fluid 1 passages in the  $L_3$  direction.

$$\text{fin base area covering plates} = 2 \cdot \delta \cdot L_f \cdot n_f \quad (43)$$

$$= 2 \cdot \delta \cdot L_f \cdot N_f \cdot L_2 \cdot N_p \quad (44)$$

where  $L_f$  is the fin flow length,  $n_f = N_f L_2 N_p$  is the total number of fins in the core and  $N_f$  is the number of fins per unit length in the  $L_2$  direction. The fin flow length is slightly shorter than the core flow length  $L_1$  in an actual core.

$$\text{area of header bars on the side for fluid 1} = 2 \cdot b_1 \cdot L_1 \cdot N_p \quad (45)$$

$$\text{area of header bars and plates of fluid 2 at fluid 1 core inlet and outlet faces} = 2 \cdot (b_2 + 2 \cdot \delta_w) \cdot (N_p + 1) \cdot L_2 \quad (46)$$

The total primary surface area on the fluid 1 side is then

$$A_{p,1} = 2 \cdot L_1 \cdot L_2 \cdot N_p - 2 \cdot \delta \cdot L_f \cdot N_f \cdot L_2 \cdot N_p + 2 \cdot b_1 \cdot L_1 \cdot N_p + 2 \cdot (b_2 + 2 \cdot \delta_w) \cdot (N_p + 1) \cdot L_2 \quad (47)$$

The three components of the secondary (fin) area are:

$$\text{fin height area} = 2 \cdot (b_1 - \delta) \cdot L_f \cdot n_f \quad (48)$$

$$\text{fin edge height area} = 2 \cdot (b_1 - \delta) \cdot \delta \cdot n_f \quad (49)$$

$$\text{fin edge width area} = 2 \cdot p_f \cdot \delta \cdot n_f \quad (50)$$

The total secondary area on fluid 1 side is:

$$A_{f,1} = 2 \cdot (b_1 - \delta) \cdot L_f \cdot n_f + 2 \cdot (b_1 - \delta) \cdot \delta \cdot n_f + 2 \cdot p_f \cdot \delta \cdot n_f \quad (51)$$

Finally, the total surface area on fluid 1 side is:

$$A_1 = A_{p,1} + A_{f,1} \quad (52)$$

The free flow area on fluid 1 side is given by the frontal area on fluid 1 side minus the area blocked by the fins at the entrance of the core on that side:

$$A_{0,1} = b_1 \cdot L_2 \cdot N_p - [(b_1 - \delta) + p_f] \cdot \delta \cdot n_f \quad (53)$$

Moreover, the hydraulic diameter can be expressed using surface parameters as follows:

$$D_{h,1} = \frac{4 \cdot A_{0,1} \cdot L_1}{A_1} \quad (54)$$

In this chapter some basic heat transfer equations for a heat exchanger were given. In Appendix A, sample calculations using above equations for one experiment are given in details and for other experiments, calculated results are given in Appendix B.

## **CHAPTER 4**

### **EXPERIMENTAL PROCEDURES AND RESULTS**

This chapter is devoted to a thorough presentation of all the aspects of the procedure followed in designing and manufacturing of the microchannel heat exchanger and constructing the experimental setup, including preliminary stages and various difficulties encountered. The experimental data are given concisely at the end of the chapter, detailed test results are reported in Appendix B.

#### **4.1 Design of the Microchannel Heat Exchanger**

The first step of the work leading to a set of experimental results on the thermal performance of a microchannel heat exchanger was to investigate the manufacturing methods suitable for the geometry. Preliminary research revealed that the common methods available for manufacturing a microchannel heat exchanger were laser machining, micromachining, electron discharge machining, chemical etching, welding and brazing. Laser machining offers high accuracy, but the channel depth that can be machined is limited to a few microns. EDM is a conventional machining method that can be applied easily to microgeometries by employing fine wire, and aspect ratios up to 15 can be machined with good accuracy. Microsawing is a purely mechanical process that is typically employed in silicon micromachining. Chemical etching is commonly employed together with lithographic techniques and is also typically applied in the silicon industry.

In order to select the most appropriate manufacturing method, various design parameters such as channel geometry and material, and applicability of the

method within Turkey was considered. For military applications that require rugged designs, the heat exchanger material would preferably be a metal with high thermal conductivity, such as aluminum or copper. Because chemical etching and microsawing are not commonly employed with metals, and because they are not commonly available in Turkey, these methods were dismissed. Laser machining was also dismissed due to the channel depth restriction imposed by this method, as the channels would preferably have a depth on the order of a few millimeters to provide a large surface area for heat transfer and a high aspect ratio to achieve better heat transfer coefficients. Although in EDM machining, channel widths as small as 300 microns with channel depth as large as 5 mm to be machined with good accuracy, EDM is not able to machine undercut details which means that hot fluid side, in this study water side, cannot be machined.

For use in a military radar application, the final product must be resistant to failure in harsh environments involving shock and vibration. Joining the parts using adhesives or using silicon to seal the mating sections, therefore, are not appropriate methods, considering the intended application of the heat exchanger. Although soldering provided satisfactory sealing of the mating interfaces, the joined structure would not be appropriate for use in a military application subject to vibration. The most reliable joining method is brazing, in which the mating parts are brought together and exposed to very high temperatures in the presence of a compatible filler material so that the filler penetrates into the mating interface and bonds with both mating parts when cooled. The filler to be used and the temperature to which the parts are to be exposed depend on the material of the mating parts. For copper, typical brazing temperatures exceed 1000 °C, while aluminum is typically brazed at temperatures about 600 °C.

Generally, the brazed joints are considered ideal from the heat transfer point of view. This is in fact true for a well brazed heat exchanger. However, good brazing requires a lot of development time and painstaking efforts by experienced people, first by making small samples, cutting them and analyzing before a full

scale heat exchanger is brazed. If sufficient care is not exercised, either a metallic bond in 100% of the joints may not be achieved, the fins may warp or partially plug up due to the flow of the braze alloy (filler metal), or burn through (complete melting of base metal by the braze alloy). This may result in reduced performance of as much as 15-20%, and consequently, the incremental higher performance of improved interrupted fin geometry may not be realized. Any brazing induced surface roughness may increase the pressure drop for highly compact heat exchanger surfaces.

After the selection of manufacture method as brazing, heat exchanger type and fin type was decided. In ASELSAN's stock, two plain fins whose heights are 4 mm and 10 mm were available. Importing fins from abroad would take more than six months. Due to time shortage, available fins were decided to be used. The coolant fluid in our project in general is water or mixtures of ethylene glycol and water. A mixture's composition complicates the test and adds some parameters to be analyzed. To simplify the number of parameters for the experiments water was chosen as coolant fluid. Also, availability and simple usage compared to the mixture was taken into consideration when selecting water. To cool the hot water, a fan is used to exchange the heat by air flow. The flow directions of water and air have to be normal each other so that the design becomes more simple and can be manufactured in a short period. Crossflow is the most suitable flow type for ASELSAN's project's requirement. In design, if air flows normal to water, the designers are better able to manage assembling all products.

In the next step, a preliminary heat exchanger was designed using available fins, according to flow type. A sandwich type construction was selected. Fins were placed between two parting plates. For water side 4 mm height plain fin was used, for air side 10 mm height plain fin was used. The heat exchanger was designed such that water flows in six layers. Hot water enters at one side and exits at the other side after being cooled. Fan's mounting detail was opened on the heat

exchanger so that the fan can be assembled normal to the water's flow direction. Fig. 4.1 represents the construction design of the heat exchanger to be produced.

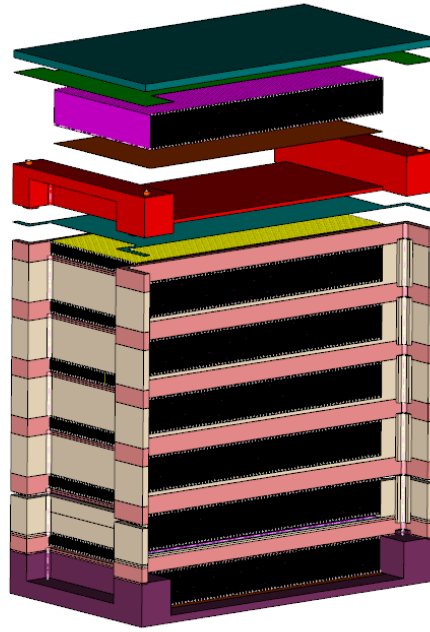


**Figure 4.1:** A view of the sandwich construction design of the microchannel heat exchanger

Moreover, a finger protection part for the fan was designed. The material for the heat exchanger was selected as aluminum 6061 series. These series alumina are able to be brazed, manufactured and obtained easily through subcontractors. The preliminary design of the heat exchanger is presented in Fig. 4.2.

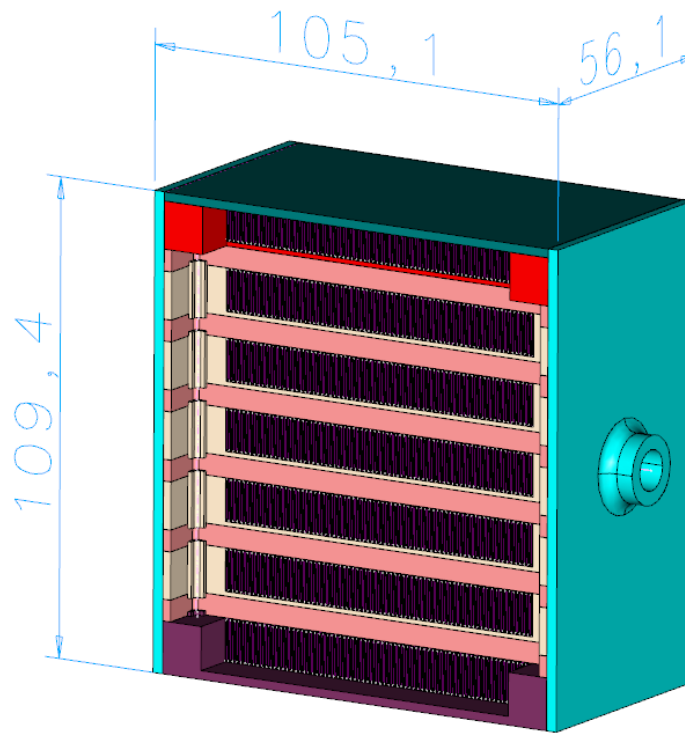


**Figure 4.2:** The preliminary design of the microchannel heat exchanger.

## 4.2 Manufacturing of the Microchannel Heat Exchanger

After finishing the design of the heat exchanger, brazing method was selected. Two alternatives were available: dip brazing and vacuum brazing. Dip brazing capability is available at ASELSAN subcontractor, EMD Inc. and ASELSAN has vacuum brazing capability. Vacuum brazing in ASELSAN was constructed two years ago. The staff working in vacuum brazing did not have enough experience to braze the heat exchanger. In addition, the staff claimed that in vacuum brazing vertical joints were not possible to be brazed well. As the heat exchanger sides had to be brazed vertically, only alternative left was dip brazing. Before problems faced in manufacturing of the heat exchanger some basic information will be given about brazing and brazing methods.

#### 4.2.1 Manufacturing Process: Brazing

When two pieces of clean, oxide free metal are brought within 4 angstroms ( $4 \times 10^{-10}$  m or  $1.6 \times 10^{-8}$  in.) of each other, the inter-atomic attraction will bind them together in a permanent metallurgical joint. This is the basis of brazing and soldering. It is accomplished by "wetting" the metals to be joined (referred to as base metals or parent metals) with a molten metal. If the temperature of the wetting metal is above  $450^{\circ}\text{C}$  ( $840^{\circ}\text{F}$ ), the process is called brazing and the molten metal is referred to as filler metal or braze alloy. If the wetting metal is at temperatures below  $450^{\circ}\text{C}$  ( $840^{\circ}\text{F}$ ), the process is called soldering and the molten metal is referred to as solder. In contrast, in welding both the base metals to be joined are locally molten at the time of joining. Conventional welding can cause distortion of the base parts, and dissimilar metals may not join if metallurgically incompatible [39].

A filler metal (braze alloy) is used in brazing two or more parts. The molten filler metal is drawn by capillary attraction into the space between closely adjacent surfaces of the parts to be joined. This filler metal has a liquidus temperature above  $450^{\circ}\text{C}$  ( $840^{\circ}\text{F}$ ), but below the solidus temperature of the base metals, and must also wet the base metals without melting them. For making complicated joints by brazing, generally the whole parts are heated to the desired temperature of the filler metal. Precleaning of the joints is essential for good brazing. Greases and oils must be removed from the workpiece surfaces because these can form non-wetting carbon deposits when the components are heated to braze. Further, most metal surfaces are covered by oxide films which are non-wetted by conventional braze alloys and must be removed if joints are to be formed. This can be achieved by fluxing or by special alloying elements in the base metal or filler metal to chemically/mechanically remove the oxide films during the brazing process. A vacuum or controlled atmosphere is used when the flux-bath is not used to prevent the reoxidation of the oxide-free surface.

Cleanliness of base metal, filler metal, flux and purity of atmosphere should be as high as practical to obtain high quality joints [39, 21].

Since the base materials do not melt at the brazing temperature, practically any two materials can be joined by brazing. This includes similar and dissimilar metals, cast materials and wrought metals, metals and nonmetals, porous metal components, metals of significantly different thicknesses, and fiber and dispersion-strengthened composites. The only requirement is to find/develop a suitable brazing filler metal that is compatible with the base metals, wets them and has a melting point below those of the base metals.

Brazing has many advantages over welding and other joining techniques. More importantly highly complicated long and/or multiple joints between two or more parts can be made without burning or distorting the joints. Large assemblies with multiple joints can be fabricated in stress-free conditions. However, stresses may develop in brazed joints of dissimilar materials upon cooling due to different thermal expansion coefficients. Metals as thin as 0.05 mm (0.002 in.) and as thick as 152 mm (6 in.) can be brazed. Because of the inter-atomic bond in brazing, the properly designed and fabricated joints, free of oxide films, can have overall strength equal to that of the base metal. Brazed joints generally exhibit excellent resistance to thermal and mechanical shock and vibration. In brazing, one can protect special metal coating, cladding, or important metallurgical characteristics of base materials. High quality, reproducible, extremely leak tight, close tolerance joints can be produced in mass production. The brazing process can be automated readily. Brazing is usually suited for relatively small assemblies with thin parts. Since materials are generally fully annealed after brazing, the brazements are designed for strength considering fully annealed conditions after brazing [39, 41].

The major disadvantages of brazing are as follows: The brazing process of parts and assemblies is often considered an art today. It requires considerable expenditure, development time, research, and capital investment before ideal

brazed joints can be manufactured, particularly for complicated parts. If any one variable of the brazing process (i.e., flux, filler metals, temperature, brazing cycle time, atmosphere, etc.), base materials (alloying components, surface structure and preparation, joint clearances, etc.), or equipment and fixturing is changed, in general one needs to redefine the brazing process for ideal joints. Clean surfaces free of grease, oil, oxide or dirt are essential for uniform quality brazed joints. Chemical and/or mechanical cleaning with or without subsequent fluxing can be used to prepare the surfaces before brazing. In most applications, these fluxes must be removed after brazing. If not properly removed, they can corrode the joined parts reducing their desired life significantly. In many brazing processes, the major elements in the filler metal are the same as the base metal except for some additional melting point temperature depressant elements. In the case of aluminum, the brazing is usually done at a temperature which is within 22 to 70°C (40 to 125° F) of the solidus temperature of the base metal. Hence, close temperature control during brazing is essential. Due to diffusion of alloying elements, brazing produces an alloyed zone, near the joint, whose mechanical and thermal properties may be different from the base metal. In some systems, brittle intermetallic compounds are formed at braze-workpiece interfaces, and their growth can have very detrimental effects on mechanical properties [39,41].

#### **4.2.1.1 Brazing Processes**

A compact heat exchanger, particularly the plate-fin, tube-fin or regenerative type, has thousands of joints many of which may not be easily accessible. The thin fins make brazing difficult due to sagging or distortion. Hence, specialized brazing processes are required which can uniformly heat all interior parts without overheating the external surfaces of the brazements, and the brazements must be protected from oxidation at elevated brazing temperatures throughout the brazing cycle. The most commonly used brazing methods for

compact heat exchangers are dip brazing, vacuum brazing, and controlled atmosphere (inert or reduced gas) furnace brazing [39, 42, 43].

#### **4.2.1.2 Dip Brazing**

Dip brazing in molten salt bath is also referred to as salt-bath or salt-pot brazing or molten chemical-bath dip brazing. The molten salt bath is used as a heating medium and it may provide fluxing action depending upon the selected salts for the bath. If the molten salt acts as a flux, the process is also referred to as flux-bath brazing. The molten flux is maintained at the brazing temperature (slightly above the liquidus temperature of the filler metal but below the solidus temperature of the base metal). Advantages are: the flux (if needed) is applied without a separate operation, all interior parts are heated uniformly without overheating the outside surfaces of the brazement, and the brazement is continuously protected by the flux during the brazing operation. The brazements are immersed in the "pot" for about one minute to 20 minutes depending upon their material, geometry and mass [39, 43].

Dip brazing has been used extensively in industry for daily production of aluminum alloy parts, although it can be used for many metals (such as magnesium, silver, brass, nickel, copper, titanium, and steel). The machined, ground or fabricated parts are deburred and filed; the joint surfaces are cleaned for oil, grease, paint, scale or oxides; parts to be brazed are fixtured or jigged after preplacing the filler material (if not clad); preheating is done to within about 55°C (100° F) of the brazing temperature to remove all moisture, to minimize thermal distortion, and to reduce the temperature drop of the molten salt bath to within 6°C or 10° F when the preheated brazements are dipped; the brazements are dipped into the bath for the exact scheduled time necessary for the flux to remove all oxide layers from the brazement surfaces and for the filler metal to melt and flow into the joints; the brazed parts are carefully lifted from the bath to

minimize the disturbance to the still molten filler material in the joints and held there until the filler metal solidifies; the flux (molten salt) is removed from the brazed parts first by properly draining it (the drain paths are designed into the brazements before brazing), and then immersing in a hot water bath which also provides cooling; any remaining traces of the flux (salt) may be removed by acid pickling or a second water washing. Postbrazing treatment may include conversion coating of the base metal to add corrosion resistance to the exposed base metals [39].

The selection of the salt depends upon how easily it can remove the oxides on the base metal surface and its temperature in the molten state for proper brazing. When the brazements are dipped, the salt bath protects the base metal from reoxidation. Generally, chloride salts are used which are chemically aggressive to dissolve or disrupt the oxide film on the surface. If neutral chloride salts are used (as with silver-based filler metals), borax or cryolite is added to produce the salt as fluxing. For aluminum brazing, sometimes a small amount of sodium fluoride is added to remove any oxides in the salt bath; lithium chloride is added to lower the melting point of the salt (flux). Any water entering into the molten salt bath is highly undesirable since it violently reacts with the molten salt. It enters either through the moisture in the dry salt or moisture absorbed by the free surface of the bath because the salt is very hygroscopic. Furnaces used for dip brazing are usually made of steel lined with high-alumina acid-proof fire bricks. They are either externally heated by gas, oil, or electrical resistance, or internally heated by immersed or submerged electrodes. Internally heated furnaces are suited for continuous high-volume production brazing. The salt in the molten state is an electrical conductor; the current passing through the salt from one electrode to the other produces the resistance heating. The close spacing of electrodes also induces an electromagnetic stirring action within the salt that helps maintain the uniform temperature of the salt bath within  $\pm 3^{\circ}\text{C}$  or  $\pm 5^{\circ}\text{F}$ . The electrodes used are generally made up of carbon, wrought nickel or Inconel 600 depending upon the

cost, desired life, physical size requirement and possible reaction with the molten salt [39, 40].

Dip brazing has some unique advantages as: The time required for heating is about one-fourth of that required for furnace brazing. The possibility of gravitational distortion of brazements during heating is less because they weigh less when immersed in the bath. The entire metal part comes up to the brazing temperature more uniformly. A protruding joint can be selectively brazed by just dipping it in the salt bath. Several assemblies can be brazed at the same time since the only limitation is the heating capacity and size of the salt bath. The salt on the surface, when a workpiece is removed from the pot, protects the workpiece from scaling or decarburization. For a few special applications, carburizing or hardening can follow brazing without a separate reheating [40].

The limitations of dip brazing are as follows: It is used for continuous daily production brazing rather than for intermittent operation, and hence, must be heated day and night regardless of the volume throughput. Unless the joints protrude, the whole assembly must be dipped into the bath thus utilizing considerable energy in heating. The parts and assembly must be designed properly to avoid trapping of air during brazing and the incomplete draining of salt after brazing. The brazements must be completely dry before being dipped in the salt bath. Chloride fluxes usually leave hygroscopic corrosive residue on the surface of the workpiece. Hence, extensive postbrazing treatment is necessary to remove the salt and corrosive residues, and obtain adequate corrosion resistance for the brazements. The water used to rinse the salt is polluted, and may require water treatment before being drained to the sewer. Salt pots produce continuously irritating toxic gases, and should be forced vented properly, and may pose air pollution problems. The maintenance of the salt-bath furnace is difficult and expensive [39, 43, 41].

#### 4.2.1.3 Vacuum Brazing

Vacuum brazing is a common brazing process for medium to high production brazing of compact heat exchangers. In this method, brazing is done in a vacuum with absolute pressures of  $1.3 \times 10^{-4}$  Pa thus preventing serious oxidation of the brazements; heating is done by radiation; special filler metals are used; and usually no flux is used, thus eliminating the need for any postbrazing treatment. It is an environmentally very clean process, and is used where entrapped fluxes cannot be tolerated or reactive metals are brazed. It is used extensively in aerospace, automotive, and nuclear fields. Vacuum brazing is not suitable for base metals and filler metals having high vapor pressure or low boiling point constituents. From the cleaning, fixturing and tolerances of the joint clearances, the vacuum brazing process is less forgiving compared to other controlled atmospheric brazing processes. The maintenance of proper vacuum in the furnace is critical. Also, better surface cleanliness and part fit-up are essential. The moisture dew point must be maintained at  $-60^{\circ}\text{C}$  ( $-75^{\circ}\text{F}$ ) to maintain a relatively water vapor (and oxygen) free atmosphere at high vacuums [39, 42].

Operations associated with vacuum brazing are cleaning, assembling and fixturing, loading into the brazing furnace, vacuum brazing using a simultaneous pump-down and the fastest practical continuous radiant heating, back filling, unloading vacuum furnace chamber, cooling, and defixturing. In a three-zone vacuum furnace, preheating, brazing, and cooling zones are separate. Vacuum brazing sheets and/or filler metals must be clean, should not be handled with bare hands (molten filler metal won't wet the base metal at fingerprints), and should be stored in a dry place at a temperature that prevents water condensation from atmosphere [40, 42].

Three types of vacuum braze furnaces are used: single-pumped retort furnace (a sealed retort of thick material), double-pumped retort furnace (an inner retort contained within a vacuum chamber), and cold-wall vacuum furnaces (a single

vacuum chamber with thermal insulation and heating elements inside the chamber). These furnaces can be side-loading with rectangular work zone, or top or bottom loading with circular work zone. Both batch type and semi-continuous furnaces are used. The semi-continuous furnace could have multizones: preheating, brazing and cooling. While in the batch-type furnace, the parts to be brazed are stationary, they are moving in a semi-continuous furnace. Also, a pressure excursion occurs in the brazing chamber of a multizone furnace. The large vacuum brazing furnaces have main brazing chambers up to 28 m<sup>3</sup> (1000 ft<sup>3</sup>), and can accept a single heat exchanger of 1.2 x 1.2 x 6m (4 x 4 x 20 ft). Vacuum pressures of 10<sup>-3</sup> torr (0.13 Pa) and lower are maintained in the furnace, particularly for metals (such as aluminum) that form very stable oxides. For base materials (such as Cr, Si) that form oxides of intermediate stability, vacuum pressures of 10<sup>-3</sup> to 10<sup>-2</sup> torr (0.13 to 1.3 Pa) are required. The aforementioned ranges of vacuum pressures are rough guidelines. The constituents of gases that make up the vapor pressure in the furnace are more important from the brazing point of view (oxidizing versus nonoxidizing) than the absolute value of the vacuum pressure. In vacuum brazing, the gas from the furnace is analyzed before and during brazing to determine its precise composition and to monitor the furnace atmosphere [39].

The furnace is heated electrically, and parts are heated by radiation only. Heating elements are made from nichrome or metallic alloys of molybdenum, tungsten, or tantalum depending upon the required temperature range and the furnace size. Other selection criteria are high electrical resistivity, excellent scale stability, high strength at elevated temperatures, and low vapor pressure [42].

### **4.3 The Preliminary Heat Exchangers**

Before dip brazing of the preliminary heat exchanger, some test specimens were performed. Plain fin material was aluminum 3003 O. In literature the series

of aluminum 3003 is able to be brazed. Fins between two flat plates were brazed. After success of this test specimen, the preliminary brazed heat exchanger was produced. Fig. 4.3 and Fig 4.4 shows steps of production of preliminary heat exchanger in dip brazing. In leakage test at some points leakage occurred. Investigation of the heat exchanger showed that the plates were very thin and end of the plates were not able to be brazed in about 600 ° C. The ends of the plates bended so that a good contact between two adjacent plates did not occur.

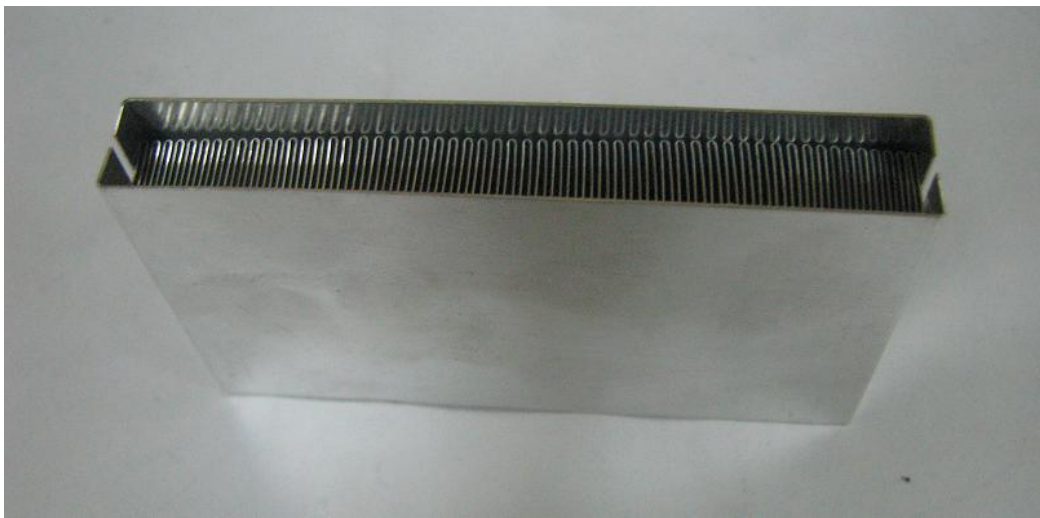


**Figure 4.3:** A view of the sandwich construction of the air side plain fins for the preliminary heat exchanger before dip brazing



**Figure 4.4:** A view of the assembly step of the preliminary heat exchanger before dip brazing

To overcome this problem, the box profile with rectangular sections was considered. However the thickness of the box profile had to be about 1-1.5 mm due to restriction on the production method and ability. If the thickness of the box profile were higher, the wall resistance and weight of the heat exchanger would also be higher. One of the main aims of this study was producing the heat exchanger as light as possible. The first test box profile was manufactured. However the material composition was not suitable for dip brazing. Then the box profile was produced again. It took about two months to produce the correct box profile. In Turkey most of the subcontractors are boss firms, which means if the boss is abroad or ill, no work progresses. Because of this, the box profile had some healthy problem; the production time took more than expected.

Although the last produced box profile also had some problems in flatness and homogeneous thickness, the secondary heat exchanger was brazed because of the time shortage of this study. The secondary heat exchanger with box profile in dip brazing is shown in Fig. 4.5.



**Figure 4.5:** Secondary heat exchanger in dip brazing

In leakage tests, leaking points decreased however the heat exchanger was not leakproof. Moreover, in the preliminary heat exchanger, salt was detected in the microchannels of the heat exchanger. Then, the preliminary heat exchanger was slice into four parts to investigate the microchannel at water sides. Fig. 4.6 and Fig.4.7 present photographic views of sliced parts of the preliminary heat exchanger. After a week or longer period it was observed that the heat exchanger vomited salt particles. As seen Fig. 4.6 and Fig. 4.7, the salt filled the channels at the water side.

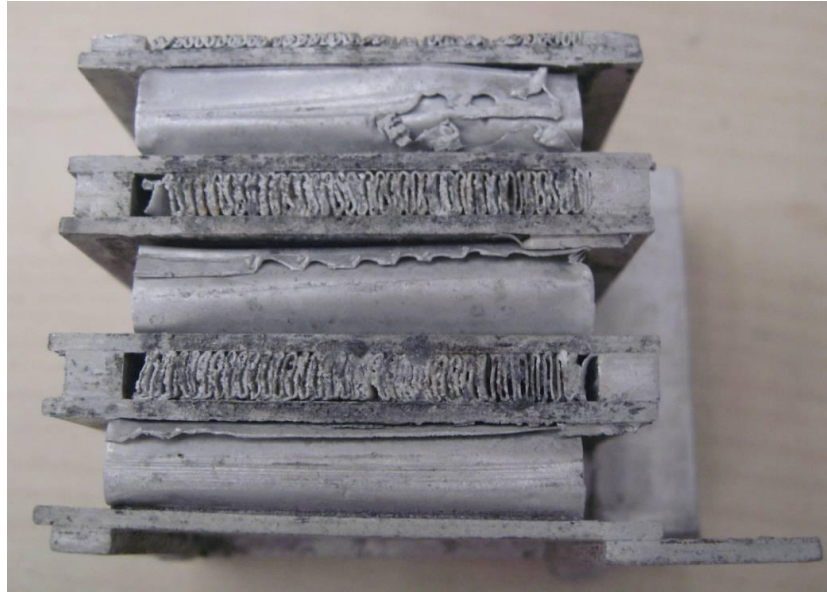


**Figure 4.6:** A view of the first quarter specimen of the preliminary microchannel heat exchanger produced in dip brazing, after being sliced into four specimens



**Figure 4.7:** A view of the second quarter specimen of the preliminary microchannel heat exchanger produced in dip brazing, after being sliced into four specimens

#### 4.4 The Test Heat Exchanger

After these experiences in dip brazing, it was decided not to produce the heat exchanger in dip brazing. By the same time, some good news was heard from vacuum brazing; vertical joints up to 20 cm in height were able to be brazed in the vacuum furnace. The design of the heat changer was modified to suit vacuum brazing. The modified design of the heat exchanger is presented in Fig. 4.8.

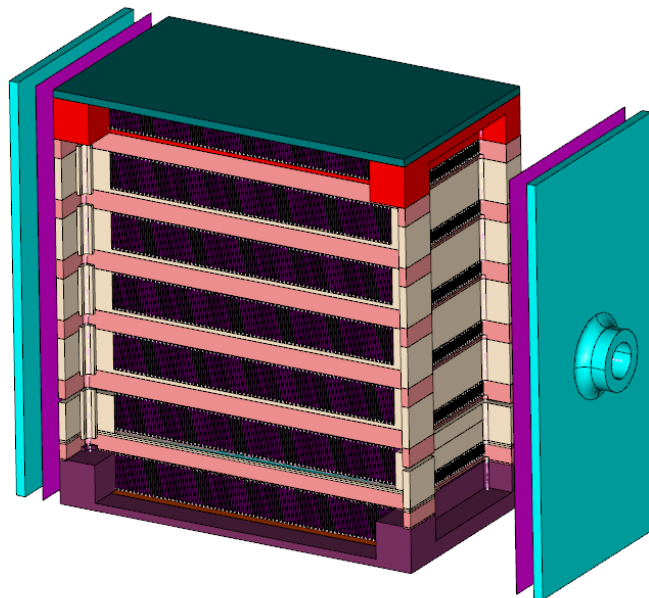


**Figure 4.8:** A view of the microchannel heat exchanger assembled vertically

The box profile usage was no longer used. Then the plates were redesigned to form leakage proof joints and also to form the water channels. Detailed drawings of the heat exchanger are given Appendix C. Before brazing the heat exchanger in the vacuum furnace, some test specimens were brazed as shown in Fig. 4.9. All parts of the heat exchanger were remanufactured and are presented in Fig. 4.10. Then, the test specimen of the microchannel heat exchanger was brazed in vacuum brazing furnace at ASELSAN. Fig. 4.11 shows jig and fixture of microchannel heat exchanger. At the leakage test of the test specimen, it was

observed that at some small points there was leakage. A conductive glue was applied these points. The leakage test was remade. Finally the test specimen, shown in Fig. 4.12, was leak proof and was ready for the experiments.



**Figure 4.9:** The test specimen produced in vacuum brazing



**Figure 4.10:** All parts require to assemble the microchannel heat exchanger in vacuum brazing

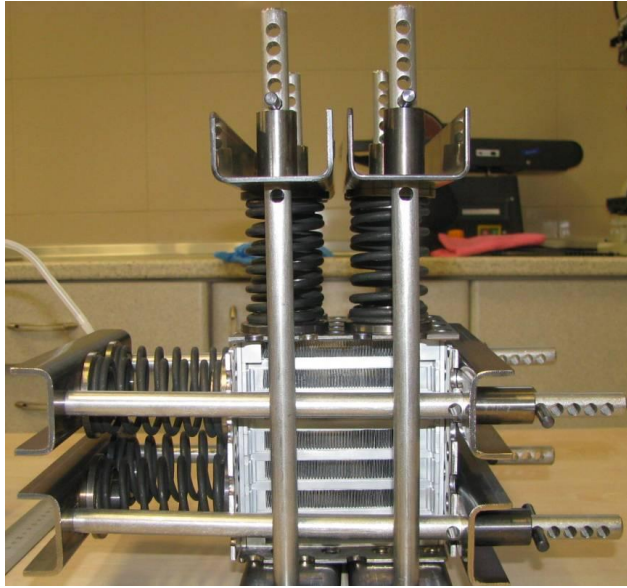


**Figure 4.11:** The jig and fixture of the microchannel heat exchanger in vacuum brazing



**Figure 4.12:** The test microchannel heat exchanger

## 4.5 Test Setup

A new experimental setup was constructed to perform the experiments of the microchannel heat exchanger. The experimental setup was designed to simulate a typical liquid cooling system. In addition to the flow of coolant circulating in a closed loop, the system required a sophisticated measurement facility to record data such as pressures, temperatures, and flow rates. The test setup mainly consists of a heating tank with heaters, a pump, a flow meter, a fan, transducers, a data logger and the heat exchanger, view of the test setup is provided in Fig. 4.13. All instruments of the experimental setup and their properties are given in Table 4.1

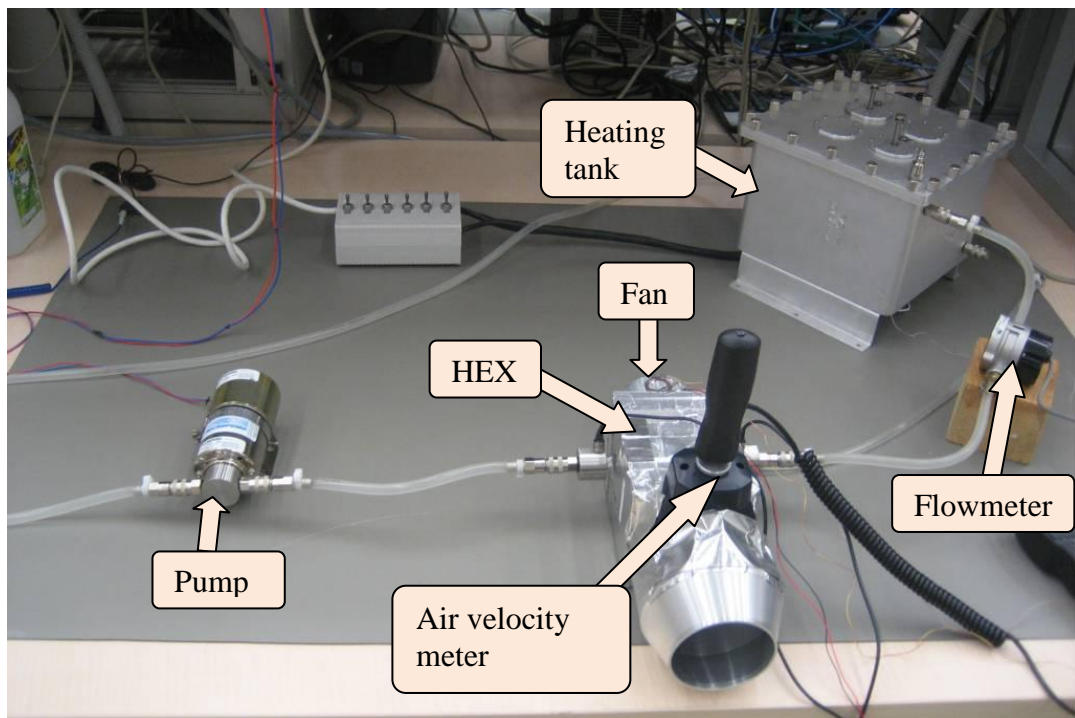


**Figure 4.13:** A view of experimental setup

**Table 4.1:** Measurement instruments of experimental setup

<b>COMPONENT</b>	<b>DESCRIPTION</b>	<b>PROPERTIES</b>
	<p>DIGITAL DATA LOGGER <b>AGILENT HP 34970A</b></p>	<p>60 channel multiplexer and data logger capable of measuring and recording voltage, current, temperature, frequency etc. at a sampling interval of 2 seconds</p>
	<p>ROTARY DIGITAL FLOWMETER <b>GEMS RFO 2500</b></p>	<p>RotorFlow type flowmeter with digital frequency output capable of measuring flow rates up to 5 lpm</p>
	<p>TEMPERATURE / PRESSURE TRANSDUCER <b>KULITE HKL/T-1- 235-3.5 BARA</b></p>	<p>Miniature and rugged temperature and pressure transducer up to 3.5 bar pressure range</p>
	<p>AXIAL FAN <b>AMATEK ROTRON 011384</b></p>	<p>26 VDC military spec. fan max. 18400 RPM, free flow rate 119 CFM (cubic feet per minute)</p>
	<p>PUMP <b>MICROPUMP GB P25</b></p>	<p>Maximum Speed 10,000 rpm with pump head 0.34 kg</p>
	<p>EXPANSION UNIT <b>BELLOWS TECH 0150A-034</b></p>	<p>Edge welded bellow with operating stroke 31.5 mm</p>
	<p>HEATING TANK</p>	<p>8 lt heating capacity up to 1200 W</p>

	<p style="text-align: center;">AIR VELOCITY METER <b><i>AIRFLOW LCA501</i></b></p>	<p style="text-align: center;">Temperature and velocity meter of air, with velocity range 0.25 to 3 m/s</p>
	<p style="text-align: center;">QUICK COUPLING <b><i>LEGRIS</i></b></p>	<p style="text-align: center;">Male or female metal quick acting couplers with threaded end and sealed</p>
	<p style="text-align: center;">J-TYPE THERMOCOUPLE <b><i>OMEGA J-32 SLE</i></b></p>	<p style="text-align: center;">J-type thermocouple appropriate for measurements at 0-750 °C at special limits of error corresponding to 1.1 °C</p>

To heat thus condition water, a heating tank, which is shown in Fig.4.14, was designed and manufactured. The volume of heating tank is about 8 liters. In the heating tank there are 6 heaters where each heater can supply about 200W energy to water. Heating tank has a switch box to turn on or off each heater. For this setup each heater was made of Inconel alloy, which is a nickel-chromium alloy with good oxidation resistance at high temperatures and resistance to chloride-ion stress-corrosion cracking, corrosion by high-purity water, and caustic corrosion. Inconel alloy is used for furnace components, in chemical and food processing, in nuclear engineering, and for sparking electrodes. The profile of the heater was selected as M profile to reduce the length of the heater. The total length of the heater is 30 cm. Four expansion units were assembled to the heating tank to compensate for volumetric expansion of hot water. Gaskets were used in all joints to prevent leakage. Four connectors were assembled to the heating tank. The connectors used for the entrance and exit of water were placed so that the distance between these connectors was maximized in order to mix the water for homogeneity. For the exit of hot water the bottom connector was used. The upper

connector was used for addition of extra cold water. The connector at the top of the cover was used to discharge extra air in closed loop.

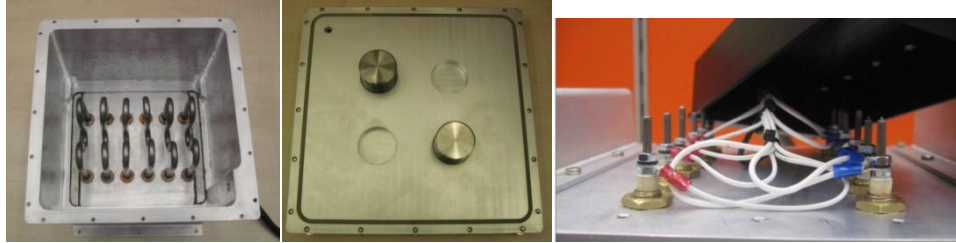


**Figure 4.14:** Heating tank

The pump was used to circulate the water and adjust the flow rate of the hot water. The pump was placed prior to the microchannel heat exchanger and next to the heating tank. The connection between these equipments was established by hoses and connectors. The mounting interface of the pump was G1/8. The connectors were selected to be suitable this detail. Because clean water was used in all experiments, no filter was needed. The maximum and minimum voltage supplied to the pump was 30 VDC and 10 VDC respectively. Changing the voltage of pump, the flow rate of the water was adjusted. For all experiments, voltage of pump was set to 10 VDC, 15 VDC, 20 VDC and 28 VDC.

To ensure flow of air, a military fan was assembled to the front of the microchannel heat exchanger. The maximum revolution per minute of the fan is 18000. Previous experience in military projects has shown that when the fan is used to suck air from the hot spot instead of blowing, the thermal performance is better. Therefore, the fan was placed so that heated air was sucked. A finger protector was used to prevent any accidents. Fig 4.15 shows the assembly of the fan and finger protector to microchannel heat exchanger.



**Figure 4.15:** The finger protector part of the fan

The transducers were placed at the entrance and exit of the microchannel heat exchanger. They measured inlet and outlet pressures and temperatures of water. The maximum capacity of the transducer was 3.5 bars. The transducers were rugged and miniature. The output of the transducers for pressure was in voltage. This value was converted to the pressure unit, bar by linear interpolation. Defining RTD, temperature sensing value, the output of the transducers for temperature was in Celsius. The mounting detail of the transducers was M6x0.75.

A rotary flowmeter was used to adjust the flow of water. The maximum operating pressure of the flowmeter was 14 bars and it work until to 100 °C. The output of the flowmeter was Hertz. The value in Hertz was converted into GPM (gallon per minute) through a graph supplied by the firm of the flow meter. The flow rate of the water was measured after the microchannel heat exchanger.

To measure the volumetric flow rate of the air, an air velocity meter was placed at air inlet side of the microchannel heat exchanger. The air velocity meter is capable of the measuring temperature and velocity of the inlet air. Fig. 4.16 is an assembly view of air velocity meter and microchannel heat exchanger.



**Figure 4.16:** A view of air velocity meter assembled to the microchannel heat exchanger

For the purposes of this study, the measurement facility is vital. An Agilent HP 34901 data logger and 20-channel multiplexer were used to collect all data. The digital data logger enabled the recording of all temperature, pressure, and flow rate data on a single file. In addition to the two temperature and pressure transducers integrated onto the microchannel heat exchanger, four J-type thermocouples, placed outside of the heating tank, on the top surface of the microchannel heat exchanger, entrance and exit of the air, were included to complete the temperature measurements required. In all connections leak proof connectors was used. Details of the experimental setup are given in Appendix D.

#### **4.6 Experiments**

The changeable and manageable variables of the test setup were selected as flow rates of water and air. The flow rates of water were adjusted by changing pump input voltage. The flow rates of water were selected as 0.009 kg/s, 0.013 kg/s, 0.019 kg/s, 0.024 kg/s. For air, current value of the fan was changed to adjust

the flow rate of air. The maximum current applicable to the fan was 1.2 A. Then the current of the fan was set to 1.2 A, 1A, 0.9 A, 0.8 A, 0.7 A, 0.6 A, 0.5 A, 0.4 A. All experimental input parameters are listed in Table 4.2. The heat load could be changed from 200 W to 1200 W. In most of the experiments it was selected as average heat load which is 800 W. However, in last experiments it was set to 1200 W so that the response of the setup could be observed.

During tests, instantaneous measurements of temperature, pressure and flow rate taken at 10 second intervals were transferred from the data logger to a PC via the *Agilent Benchlink* software. Fig. 4.17 shows data logger and power supply.

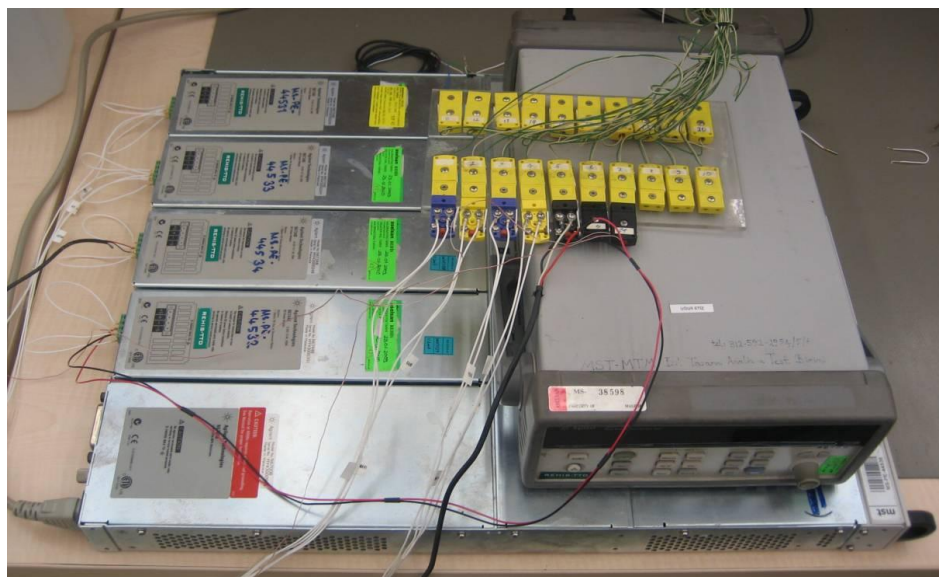


**Figure 4.17:** Data logger and the power supply used in experiments

**Table 4.2:** Input variables of the experiments

<i>Experiment Number</i>	<i>Input Heat to water in heating tank [W]</i>	<i>Pump Input Voltage [V]/ Current [A]</i>	<i>Fan Input Voltage [V]/ Current [A]</i>
1	800	10 / 0.088	26 / 1.090
2	800	15 / 0.130	26 / 1.090
3	800	20 / 0.180	26 / 1.073
4	800	28 / 0.286	26 / 1.064
5	800	10 / 0.081	22.858 / 0.9
6	800	15 / 0.124	22.858 / 0.9
7	800	20 / 0.174	23.040 / 0.9
8	800	28 / 0.284	22.898 / 0.9
9	800	10 / 0.077	20.994 / 0.8
10	800	15 / 0.110	21.102 / 0.8
11	800	20 / 0.161	20.998 / 0.8
12	800	28 / 0.262	21.066 / 0.8
13	800	10 / 0.077	19.214 / 0.7
14	800	15 / 0.114	19.205 / 0.7
15	800	20 / 0.163	19.196 / 0.7
16	800	28 / 0.263	19.050 / 0.7
17	800	10 / 0.076	17.170 / 0.6
18	800	15 / 0.112	17.232 / 0.6
19	800	20 / 0.163	17.285 / 0.6
20	800	28 / 0.248	17.270 / 0.6
21	800	10 / 0.077	15.191 / 0.5
22	800	15 / 0.117	15.201 / 0.5
23	800	20 / 0.165	15.201 / 0.5
24	800	28 / 0.273	15.156 / 0.5
25	800	10 / 0.081	13.025 / 0.4
26	800	15 / 0.120	13.075 / 0.4
27	800	20 / 0.173	13.070 / 0.4
28	800	28 / 0.278	13.086 / 0.4
29	1200	10 / 0.078	26 / 1.054
30	1200	15 / 0.126	26 / 1.060
31	1200	20 / 0.168	26 / 1.054
32	1200	28 / 0.285	26 / 1.057

The measurements were thus monitored continuously so that it could be judged easily whether or not the system reached thermal steady state conditions at

each flow rate and heat load tested. Moreover for all experiments the inlet and outlet temperature of water versus time graph were drawn and they also helped to establish the steady state condition. Fig. 4.18 shows temperature versus time interval for experiment 5. The graph is plotted in Excel. Because the maximum number of data in row is limited in Excel, the time scale is only monitoring the number of time intervals not real time.

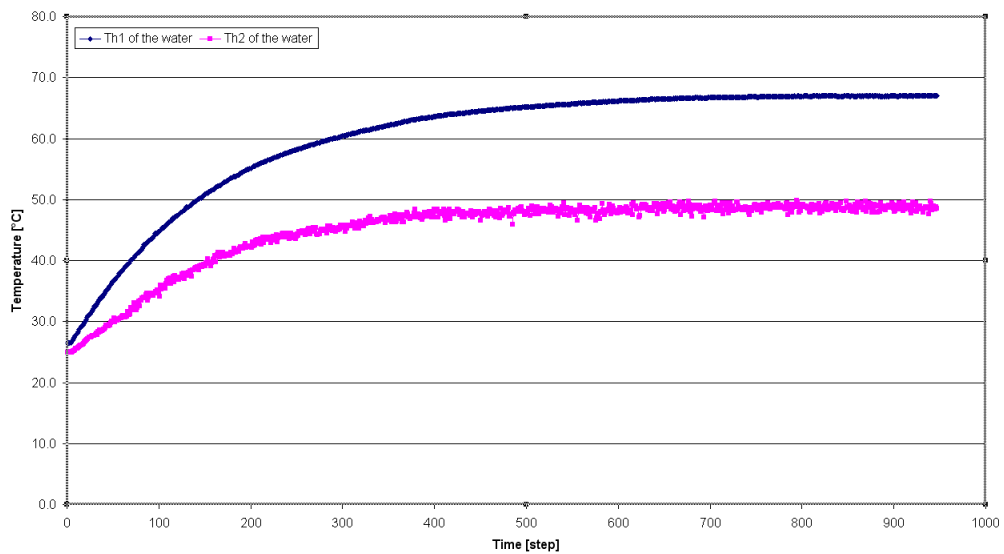


**Figure 4.18:** Inlet and outlet temperatures of the water & time step for experiment 5

Once steady state conditions were confirmed, the flow rate or heat load variable was changed to the next test value for the microchannel heat exchanger.

#### 4.7 Experimental Results

In experiments, according to input parameters given in Table 4.2, measured parameters of water are tabulated in Tables 4.3 and 4.4. Table 4.5 provides measured parameters of air in all experiments.

**Table 4.3:** Measured parameters of water for all experiments

<i>Experiment Number</i>	<i>Flow rate of water [kg/s]</i>	<i>Inlet Temperature of water [°C]</i>	<i>Outlet Temperature of water [°C]</i>	<i>Temperature Difference of water [°C]</i>
1	0.009	63.8	44.9	18.9
2	0.013	61.3	48.2	13.1
3	0.019	59.1	49.9	9.2
4	0.024	57.8	51.3	6.5
5	0.009	67.0	48.6	18.4
6	0.013	65.0	53.2	11.8
7	0.019	64.4	56.5	7.9
8	0.024	64.6	59.5	5.1
9	0.009	70.7	52.9	17.8
10	0.013	67.6	55.9	11.7
11	0.019	66.4	58.1	8.3
12	0.024	64.5	58.4	6.1
13	0.009	71.8	54.4	17.4
14	0.013	70.6	58.0	12.6
15	0.019	69.0	61.0	8.0
16	0.024	67.5	61.8	5.7
17	0.009	75.4	60.7	14.7
18	0.013	73.3	62.1	11.2
19	0.019	73.2	66.2	7.0
20	0.024	72.2	67.5	4.7
21	0.009	80.7	64.4	16.3
22	0.013	79.0	68.1	10.9
23	0.019	78.5	72.8	5.7
24	0.024	77.8	73.9	3.9
25	0.009	88.0	72.2	15.8
26	0.013	86.9	77.1	9.8
27	0.019	86.7	80.5	6.2
28	0.024	86.8	83.3	3.5
29	0.009	86.6	60.8	25.8
30	0.013	79.5	63.8	15.7
31	0.019	79.2	66.8	12.4
32	0.024	78.5	70.9	7.6

**Table 4.4:** Pressure drop of water for all experiments

<i>Experiment Number</i>	<i>Inlet Pressure of water [bar]</i>	<i>Outlet Pressure of water [bar]</i>	<i>Pressure drop of water [bar]</i>
1	1.334	1.302	0.032
2	1.316	1.276	0.040
3	1.344	1.297	0.047
4	1.468	1.409	0.059
5	1.339	1.306	0.033
6	1.323	1.286	0.037
7	1.370	1.327	0.043
8	1.505	1.453	0.052
9	0.866	0.833	0.033
10	1.433	1.393	0.040
11	1.428	1.382	0.046
12	1.490	1.437	0.053
13	1.546	1.511	0.035
14	1.169	1.113	0.056
15	1.145	1.102	0.043
16	1.217	1.168	0.049
17	1.298	1.266	0.032
18	1.211	1.172	0.039
19	1.220	1.178	0.042
20	1.300	1.256	0.044
21	1.444	1.412	0.032
22	1.335	1.298	0.037
23	1.328	1.291	0.037
24	1.411	1.366	0.045
25	1.675	1.645	0.030
26	1.543	1.506	0.037
27	1.530	1.490	0.040
28	1.611	1.572	0.039
29	1.825	1.792	0.033
30	1.386	1.349	0.037
31	1.483	1.441	0.042
32	1.538	1.495	0.043

**Table 4.5:** Measured parameters of air for all experiments

<i>Experiment Number</i>	<i>Flow rate of air [m<sup>3</sup>/s]</i>	<i>Velocity of air [m/s]</i>	<i>Inlet Temperature of air [°C]</i>	<i>Outlet Temperature of air [°C]</i>	<i>Temperature Difference of air [°C]</i>
1	0.02118	3.25	23.4	45.0	21.6
2	0.02118	3.25	23.5	47.7	24.2
3	0.02118	3.25	23.6	48.6	25.0
4	0.02118	3.25	23.7	49.6	25.9
5	0.01950	3.10	23.4	49.8	26.4
6	0.01950	3.10	24.3	53.0	28.7
7	0.01950	3.10	25.4	54.2	28.8
8	0.01950	3.10	26.0	56.0	30.0
9	0.01868	2.80	24.4	56.0	31.6
10	0.01868	2.80	23.4	56.8	33.4
11	0.01868	2.80	23.1	57.4	34.3
12	0.01868	2.80	23.3	57.4	34.1
13	0.01595	2.45	23.8	57.3	33.5
14	0.01595	2.45	23.4	59.6	36.2
15	0.01595	2.45	23.4	60.1	36.7
16	0.01595	2.45	23.4	60.6	37.2
17	0.01372	2.10	24.0	60.9	36.9
18	0.01372	2.10	23.6	63.1	39.5
19	0.01372	2.10	24.7	64.8	40.1
20	0.01372	2.10	23.9	65.4	41.5
21	0.01141	1.75	23.9	66.6	42.7
22	0.01141	1.75	24.1	69.0	44.9
23	0.01141	1.75	23.9	70.3	46.4
24	0.01141	1.75	24.0	71.0	47.0
25	0.00886	1.35	24.3	74.7	50.4
26	0.00886	1.35	24.2	77.1	52.9
27	0.00886	1.35	24.3	78.3	54.0
28	0.00886	1.35	24.4	79.6	55.2
29	0.02118	3.25	25.0	62.3	37.3
30	0.02118	3.25	23.5	62.9	39.4
31	0.02118	3.25	24.6	66.0	41.4
32	0.02118	3.25	25.4	67.7	42.3

## CHAPTER 5

### DISCUSSION AND COMPARISON OF RESULTS

This chapter is devoted to the comparison of the results obtained from the experiments among each other, and to the discussion of possible reasons for the particular trends observed.

#### 5.1 Outlet Temperatures of water

Outlet temperatures of water obtained for all experiments where mass flow rate of air was changing from 0.01296 kg/s to 0.00537 kg/s is given in Fig. 5.1.

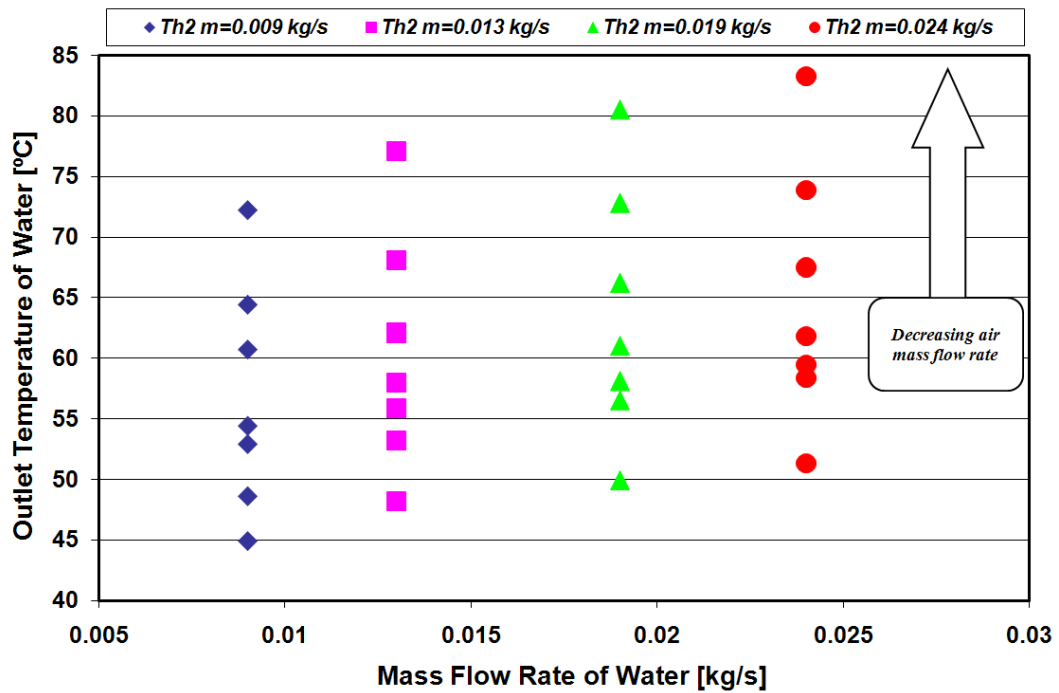


Figure 5.1: Outlet temperatures of water

As seen from Fig. 5.1, while mass flow rate of water increases, the outlet temperatures of water increases slightly. The time elapsed from the entrance of water to the microchannel heat exchanger to its, decreases as mass flow rate of water increases. This results in less heat transfer duration and thus less heat transfer. Decrease in heat transfer from water to air causes increase in the outlet temperature of water.

In Fig. 5.1, in upward direction, mass flow rate of air decreases by reducing the revolution of the fan. The mass flow rate of air was reduced from 0.01296 kg/s to 0.00537 kg/s. This time, heat transfer from water to air becomes less because of decrease in mass flow rate of air. Two and a half times decrease of mass flow rate of air causes approximately one and a half times increase of the outlet temperature of water. Actually, in heat transfer equation, heat transfer is directly proportional to mass flow rate of air. However, all heat transferred from water does not go to air also it goes to surroundings. In experiments, surroundings are at almost room temperature or the inlet temperature of air. The microchannel heat exchanger could not be isolated from the surroundings in the experiments.

## **5.2 Pressure Drop of Water**

Pressure drop of water obtained for all experiments where the mass flow rate of air was changed from 0.01296 kg/s to 0.00537 kg/s is given in Fig. 5.2. Table 4.4, presented earlier, provides the pressure drop of water in all experiments.

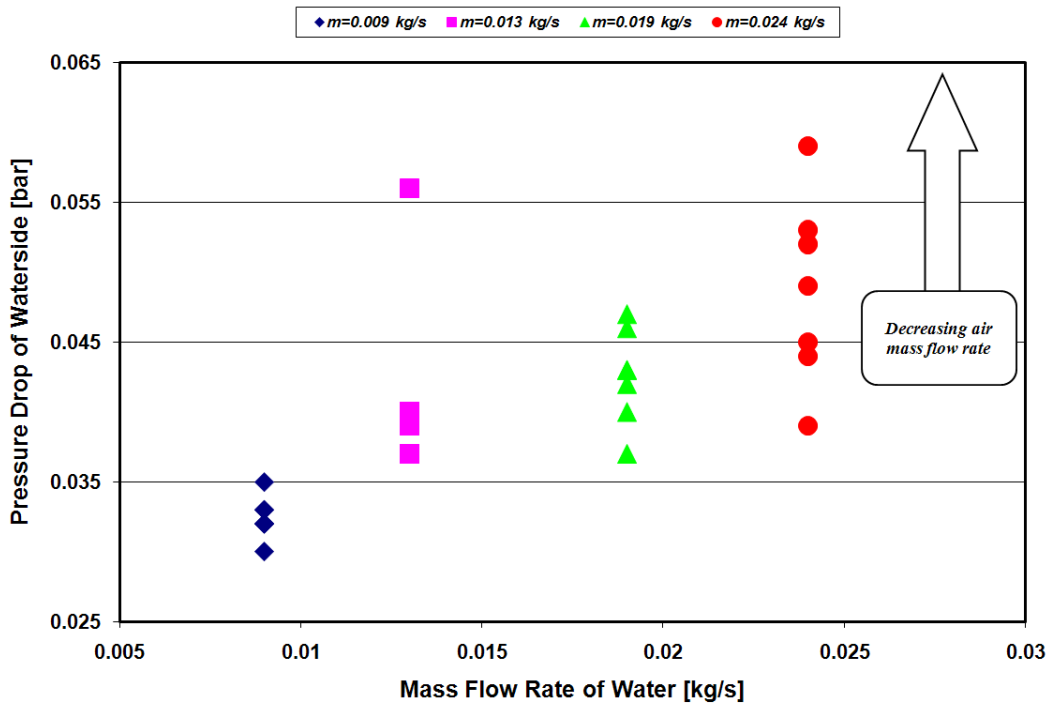


**Figure 5.2:** Pressure drop of water

Fig. 5.2 shows that pressure drop increases slightly as mass flow rate of water increases from 0.009 kg/s to 0.024 kg/s. In upward direction mass flow rate of air is being reduced. In this direction, pressure differences of inlet of water and exit of water increase. In addition, the pressure drop for higher mass flow rate of water and lower mass flow rate of air are almost two times that for lower mass flow rate of water and higher mass flow rate of air. In our project, the system pressure is almost 4-5 bars. Pressure drops about 30-50 mbar do not make any considerable change for the system. As a result, these small pressure drops can be tolerated in the system.

#### 5.4 Number of Transfer Units

Experimental overall thermal coefficient and number of transfer units obtained for all experiments where mass flow rate of air was changing from 0.01296 kg/s to 0.00537 kg/s are given in Table 5.1, 5.2, 5.3 and 5.4.

**Table 5.1:** Experimental overall thermal coefficient  $(U \cdot A)_{exp}$ , number of transfer units  $NTU_{exp}$  where  $\dot{m}_h = 0.009 \text{ kg/s}$  and air mass flow rate is changing

<i>Experiment Number</i>	$(U \cdot A)_{exp}$ [ $\frac{W}{K}$ ]	$NTU_{exp}$
1	16.91	1.29
5	15.68	1.26
9	14.70	1.31
13	13.41	1.36
17	10.22	1.21
21	9.88	1.41
25	8.09	1.49
29	15.81	1.22

**Table 5.2:** Experimental overall thermal coefficient  $(U \cdot A)_{exp}$ , number of transfer units  $NTU_{exp}$  where  $\dot{m}_h = 0.013 \text{ kg/s}$  and air mass flow rate is changing

<i>Experiment Number</i>	$(U \cdot A)_{exp}$ [ $\frac{W}{K}$ ]	$NTU_{exp}$
2	17.21	1.32
6	15.08	1.21
10	13.86	1.23
14	13.24	1.34
18	11.43	1.35
22	9.61	1.37
26	7.34	1.36
30	15.11	1.16

**Table 5.3:** Experimental overall thermal coefficient  $(U \cdot A)_{exp}$ , number of transfer units  $NTU_{exp}$  where  $\dot{m}_h = 0.019 \text{ kg/s}$  and air mass flow rate is changing

<i>Experiment Number</i>	$(U \cdot A)_{exp}$ [ $\frac{W}{K}$ ]	$NTU_{exp}$
3	17.77	1.36
7	14.54	1.17
11	13.83	1.23
15	12.27	1.25
19	10.26	1.22
23	7.78	1.11
27	6.85	1.26
31	16.34	1.25

**Table 5.4:** Experimental overall thermal coefficient  $(U \cdot A)_{exp}$ , number of transfer units  $NTU_{exp}$  where  $\dot{m}_h = 0.024 \text{ kg/s}$  and air mass flow rate is changing

<i>Experiment Number</i>	$(U \cdot A)_{exp}$ [ $\frac{W}{K}$ ]	$NTU_{exp}$
4	16.44	1.26
8	12.51	1.01
12	13.49	1.20
16	11.63	1.18
20	9.33	1.11
24	7.19	1.02
28	5.60	1.03
32	13.76	1.06

While mass flow rate of water was 0.009 kg/s, overall thermal coefficient  $(U \cdot A)$  decreases as mass flow rate of air decreases from 0.01296 kg/s to 0.00537 kg/s. On other hand, number of transfer units ( $NTU = U \cdot A / C_{min}$ ) does not show the expected trend that is proportional to the overall thermal coefficient, while mass flow rate of air is reduced. This may result from the fact that the decrease in the overall thermal coefficient is less than the decrease in minimum heat capacity

rate,  $C_{\min}$ , which is the heat capacity rate of air. Similar changes in overall thermal coefficient are observed for other mass flow rates of water, which are 0.013 kg/s, 0.019 kg/s and 0.024 kg/s.

### 5.5 Effectiveness

Effectiveness of the microchannel heat exchanger for all experiments where mass flow rate of air was changing from 0.01296 kg/s to 0.00537 kg/s is given in Fig. 5.3. In Appendix B, Table B.21, Table B.22, Table B.23, Table B.24 show effectiveness of microchannel heat exchanger for each experiments.

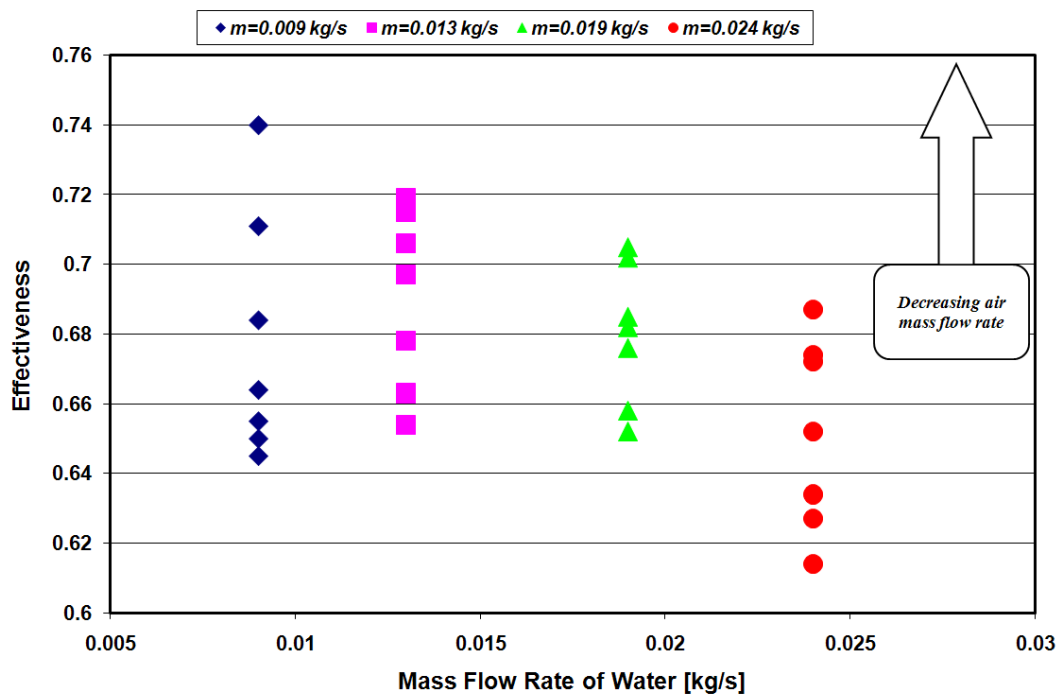


**Figure 5.3:** Effectiveness of the microchannel heat exchanger

While mass flow rate of water is 0.009 kg/s, effectiveness slightly increases as the mass flow rate of air decreases. The increase in effectiveness is about 10%. The same trend is observed when mass flow rate of water is 0.013 kg/s. However, the increase in effectiveness for this flow rate is about 6%. While

mass flow rate of water is 0.019 kg/s, effectiveness of microchannel heat exchanger for maximum flow rate of air is 0.71. On other hand, for minimum flow rate of air, effectiveness of microchannel heat exchanger becomes 0.70. In change of mass flow rate of air from 0.01296 kg/s to 0.00537 kg/s, effectiveness shows small variations. For highest mass flow rate of water, effectiveness of microchannel heat exchanger decreases from 0.69 to 0.63.

### 5.6 Colburn Factor of Air

Experimental Colburn factor of air for all experiments where mass flow rate of water was changing from 0.009 kg/s to 0.024 kg/s is given in Fig. 5.4. In Appendix B, Table B.25, Table B.26, Table B.27, Table B.28 show experimental convection heat transfer coefficient and Colburn factor of air for each experiments. Experimental Colburn factor,  $j_{exp,air}$  means that it is evaluated from experimental convection coefficient of air,  $h_{exp,air}$ .

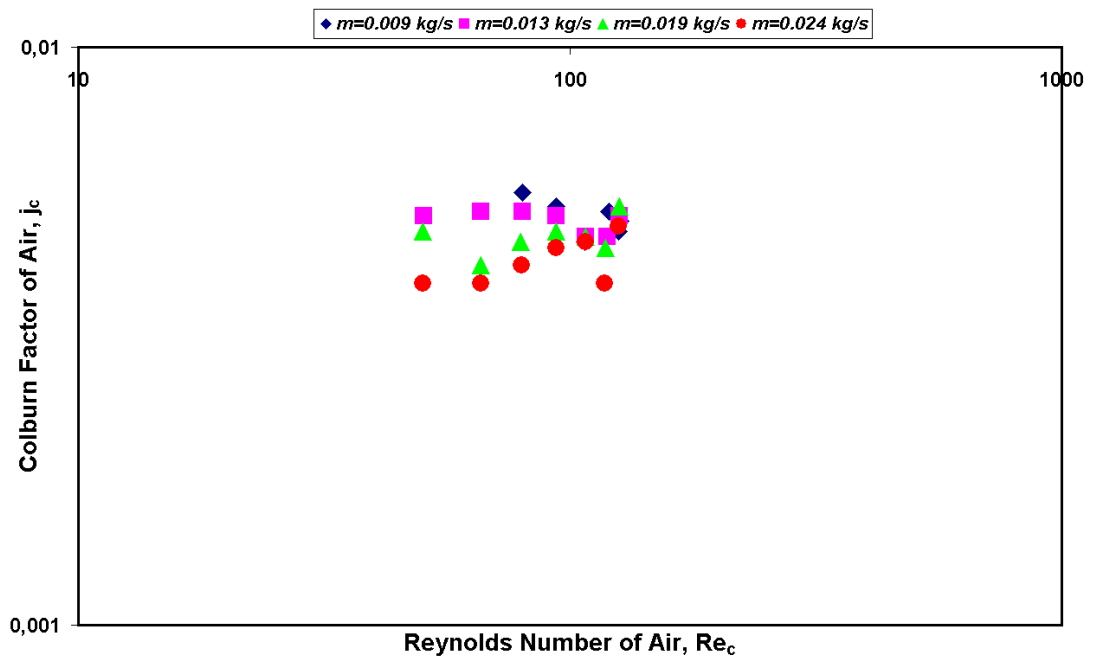


**Figure 5.4:** Experimental Colburn factor of air

Fig 5.4 shows that experimental Colburn factor does not decrease linearly as Reynolds number of air increases (in the logarithmic plot) as expected. In microchannel heat exchanger, convection resistance of air dominates because water side has a convection coefficient of  $7000 \frac{W}{m^2 \cdot K}$ , which is much higher than the air side. Theoretical convection coefficient of air side calculated from Nusselt correlations is not correct. Overall thermal coefficient is not uniform all over the microchannel heat exchanger. Therefore, any theoretical overall thermal coefficient calculated from Nusselt number correlations that assume uniform flow would be significantly different. In microchannels, air flow is not uniform as fan section area is circular on the other hand; all air channels have rectangular cross section area. This means that some portion of air flow area, especially in the corners of the heat exchanger, is not utilized. In theoretical convection heat transfer coefficient calculations, the fins at top and bottom rows are twice as long as at middle rows. Therefore they have higher fin efficiency, which means overall surface efficiency is also higher in reality. Overall surface efficiency is not uniform and not easy to determine accurately. All these calculations difficulties may cause to calculate convection resistance of air incorrectly. Because of these reasons mentioned before, experimental overall thermal coefficient calculated from heat transfer equation is more suitable to evaluate the convection coefficient of air and also convection resistance by iterations. Moreover, Colburn factor of air has to be evaluated from experimental heat transfer coefficient and not from theoretical Nusselt correlations.

## **5.6 Comparison The Microchannel Heat Exchanger with a Commercial Heat Exchanger**

In ASELSAN projects, a commercial heat exchanger is used and the microchannel heat exchanger is produced as an alternative to this commercial heat exchanger. The dimensions of the commercial heat exchanger are 195 x 167 x 77 mm while the microchannel heat exchanger's dimensions are 110 x 110 x 56 mm.

The weights of the commercial heat exchanger and the microchannel heat exchanger are 1041 and 640 grams respectively. The commercial heat exchanger was tested at the same configuration of the experimental setup as the microchannel heat exchanger. Temperature differences of water for both heat exchangers at the same heat loads were obtained for four mass flow rates of water and three mass flow rates of air. Mass flow rates of water, which are 0.009 kg/s, 0.013 kg/s, 0.019 kg/s and 0.024 kg/s, were set to the same for the comparison of both heat exchangers. Not to increase the number of experiments, three mass flow rates of air were selected, as maximum, intermediate and minimum.

Temperature differences of water for the microchannel heat exchanger and the commercial heat exchanger where mass flow rate of air was changing from 0.01296 kg/s to 0.00537 kg/s is given in Fig. 5.5.

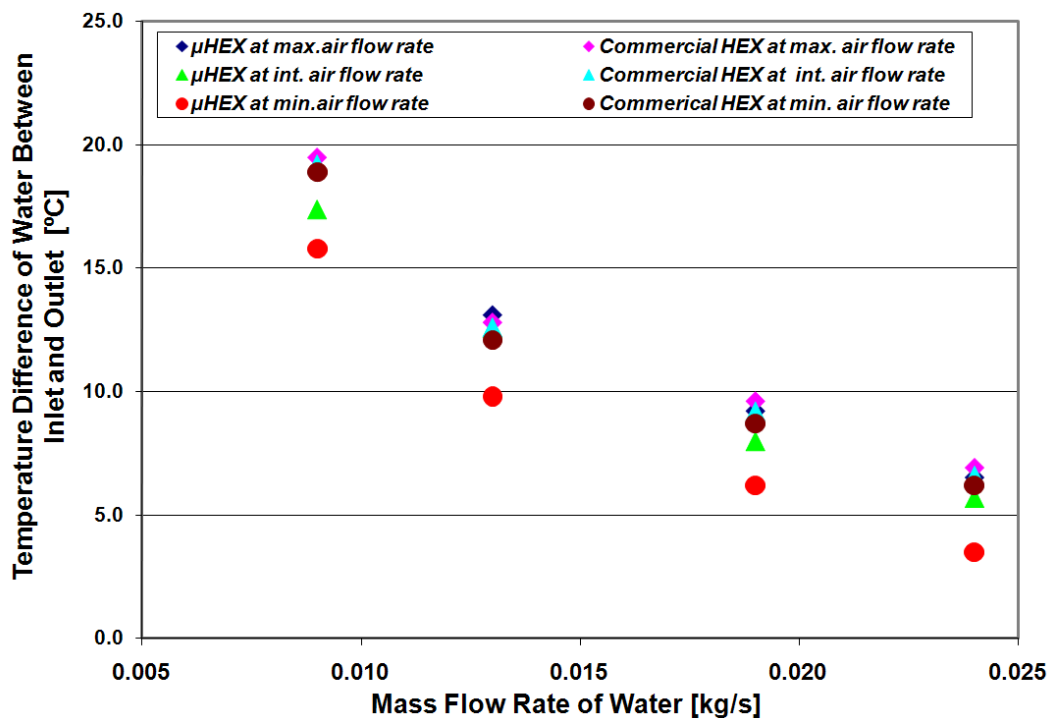


**Figure 5.5:** Temperature differences of water for the microchannel heat exchanger and the commercial heat exchanger where mass flow rate of air decreasing

Fig. 5.5 shows that at the maximum air flow rate, temperature differences of water for the microchannel heat exchanger and the commercial heat exchanger are almost the same. As mass flow rate of air decreases, temperature differences of water for both heat exchangers show some variations, whose magnitudes are about 2-3 °C. These small differences in temperature, compared to temperature differences in all systems can be ignored in military applications. The microchannel heat exchanger performs as well as the commercial heat exchanger in a smaller volume and it is lighter in mass. The volumetric profit is about 73% if the microchannel heat exchanger is used instead of the commercial heat exchanger. Moreover the microchannel heat exchanger is about 40% of the commercial heat exchanger in mass.

### **5.7 Critic of Experimental Setup**

Care was taken to construct the experimental setup so as to resemble an actual liquid cooling application as closely as possible. This was achieved by incorporating heating water by six heaters and forcing to flow in the microchannel heat exchanger by a pump to simulate the heat load and flow rates in applications. Therefore, it may be said that heat load and flow rates in experimental setup simulated a real life electronics cooling application very well.

Measuring of the flow rate of air is difficult and it needs comprehensive measurement tools. Exact velocity or flow rate of air throughout the microchannels cannot be measured. Air velocity meter could be assembled a distance 10 cm away from the microchannel heat exchanger. Velocity measured and used to calculate the mass flow rate of air may not be correct. Even though the flowmeter is used to measure the flow rate of water, flow rate of water may not be measured accurately. Because, output of the flowmeter is frequency and this value has to be converted flow rate in gallon per minute by using a graph. Graphical interpretations of flowmeter data may lead to errors in flow rate of water. Despite the high accuracy of the thermo couples used to measure inlet and outlet

temperatures of air, they had to be placed a distance approximately 10 cm away from air inlet of microchannel heat exchanger and at outlet of air and they had to be placed on the front surface of the finger protector of fan. This caused errors in measuring exact inlet and outlet temperatures of air. Although the temperature and pressure transducers used for measuring temperature and pressure at inlet and outlet of water were of high accuracy, they had to be placed a distance of approximately 1-2 cm away from the heat exchanger inlet and outlet sections due to physical restrictions. This led to some measurement error. In addition to these measurement error sources, accuracy of measurement devices, rounding off numbers of calculations may lead to some errors.

## **CHAPTER 6**

### **CONCLUSION**

Heat dissipation becomes a major problem in military systems. Heat exchangers are significant parts of these systems. Microchannels provide high heat transfer coefficients because of their small hydraulic diameters. Since high heat fluxes have to be removed from military systems, the structure of the heat exchanger was selected as microchannel. Then, available plain fins, whose heights were 4 mm and 10 mm, were used to form the microchannel structure of the heat exchanger.

In order to select the most appropriate manufacturing method, various design parameters such as channel geometry and material, and applicability of the method within Turkey was considered. Dip brazing and vacuum brazing were selected as manufacturing techniques to produce the heat exchanger. The detailed design of the heat exchanger was performed. Some test specimens and two heat exchangers were produced with dip brazing. Failure in leakage test and clogged microchannels by salts used in dip brazing led to a change in the manufacturing method from dip brazing to vacuum brazing. The design of the heat exchanger was modified according to the requirements of vacuum brazing. The final heat exchanger was produced with vacuum brazing.

An experimental setup was constructed to heat and pump the coolant fluid through the heat exchanger. Water and air were used as the working fluids and flowed through microchannels. To heat water, a heating tank and heaters were designed and produced. This heating tank, which is a constant heat source, provided constant wall heat flux to water. For forced convection cooling of air, a military fan was used. 32 experiments were performed at various flow rates of

water and air. Some of these experiments were repeated with the commercial heat exchanger. From the data obtained from experiments, the rate of heat transfer, effectiveness and various other parameters have been computed and the results have been compared with those from an available commercial heat exchanger. The results indicate that the heat exchanger performs as well as the commercial heat exchanger. The volumetric profit is about 73% while the weight profit is about 40%. In addition, air-side Colburn modulus has been obtained with respect to Reynolds number.

### 6.1 Future Work

Although the present study has produced satisfactory results as a pioneering study in the field of microchannel heat exchanger in Turkey, much additional work is required to reach state-of-the art quality. Fig. 6.1 shows a thermal image of the microchannel heat exchanger.

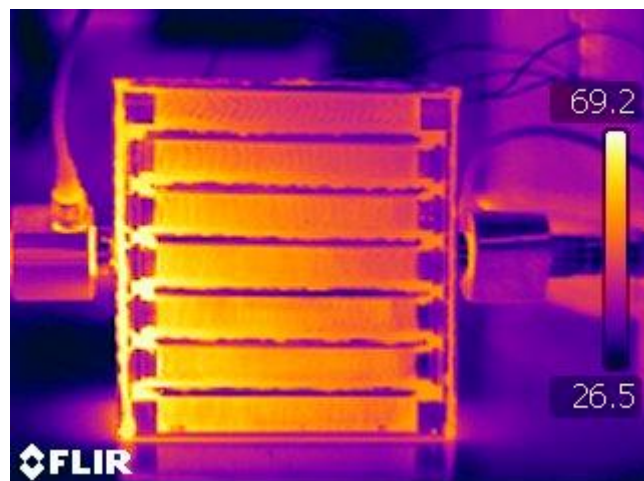


**Figure 6.1:** A thermal view of the microchannel heat exchanger

From Fig. 6.1, it is observed that the surface temperature of microchannel heat exchanger changes rather much from left upper corner of microchannel heat exchanger to right bottom corner of microchannel heat exchanger. In other words almost half of microchannel heat exchanger is not used to heat transfer as

effectively as the other half of the microchannel heat exchanger. Due to manufacturing restrictions in vacuum brazing, the microchannel heat exchanger was produced with six rows for water flow. However, as it is seen from Fig.6.1, in three rows of water, heat transfer is very small. After water enters the microchannel heat exchanger, it descends due to gravity and insufficient flow rate. Therefore, water almost does not pass through the upper three rows. In the future, the microchannel heat exchanger has to be redesigned with less rows and so that the microchannel is a two pass heat exchanger. In redesigned microchannel heat exchanger, upper rows may be used for entering water and after one pass of water, lower rows may be used for exit the water. As water passes twice, air may be cooled much more effectively. This will result in a decrease of the outlet temperature of water and an increase in the effectiveness of microchannel heat exchanger.

To increase surface area on both sides, offset strip fins may be used. Therefore turbulent flow may be achieved to increase heat transfer rate from water to air. Geometrical dimensions can be determined according to fan outside dimensions. In this way usage of surface area will be increased and non-used surface area will decrease.

Possible improvements regarding the experimental setup may be using a more reliable flowmeter to measure the mass flow rate of water. Machining sensor tabs directly into the microchannel heat exchanger, smaller temperature and pressure sensors of greater accuracy may also be used to allow for better temperature and pressure measurements especially at the airside. For exact heat transfer measurement, an insulating material to the outer surface area of microchannel heat exchanger may be used to obstruct heat transfer to surroundings.

## REFERENCES

- [1] R. K. Shah and D. P. Sekulic, Fundamentals of Heat Exchanger Design, John Wiley & Sons, 2003
- [2] S. Kakaç and H. Liu, Heat Exchangers Selection, Rating and Thermal Design, 2<sup>nd</sup> Edition, CRC Press LLC, 2002
- [3] S. Kakaç, A.E. Bergles, F. Mayinger, Heat Exchangers Thermal-Hydraulic Fundamentals and Design, Hemisphere Publishing Corporation, 1981
- [4] Geoffrey F. Hewitt, HEDH : Heat Exchanger Design Handbook, New York: Begell House, 2002
- [5] R.P. Feynman, “There’s Plenty of Room at the Bottom”, Miniaturization, H.D. Gilbert, ed., 282-296, Reinhold Publishing, New York, 1961.
- [6] D.B. Tuckerman, R.F.W. Pease, “High-Performance Heat Sinking for VLSI”, IEEE Electron Device Letters, Vol. EDL-2, No.5, 1981.
- [7] Alpsan Emrah, Experimental Investigation and Numerical Analysis of Microchannel Heat sinks for Phased Array Radar Cooling Applications, Msc Thesis, Mechanical Engineering Department, METU, Ankara, 2008
- [8] S.S Mehendale, A.M. Jacobi, R.K. Shah, "Fluid Flow and Heat Transfer at Micro- and Meso-scales with Application to Heat Exchanger Design," Applied Mechanics Reviews, Vol.53, pp.175-193, 2000.
- [9] S.G. Kandlikar, W.J. Grande, “Evolution of Microchannel Flow Passages – Thermohydraulic Performance and Fabrication Technology”, Heat Transfer Engineering, Vol.24, pp.3-17, 2003.

[10] N.T. Obot, “Toward a Better Understanding of Friction and Heat/Mass Transfer in Microchannels – A Literature Review”, *Microscale Thermophysical Engineering*, Vol.6, pp.155-173, 2003.

[11] M. Bahrami, M.M. Jovanovich, “Pressure Drop of Fully Developed Laminar Flow in Microchannels of Arbitrary Cross-Section”, *Journal of Fluids Engineering*, Vol.128, pp.1036-1044, 2006.

[12] M. Bahrami, M.M. Jovanovich, J.R. Culham, “Pressure Drop of Fully Developed, Laminar Flow in Rough Microtubes”, *Journal of Fluids Engineering*, Vol.128, pp.632-637, 2006.

[13] T. Bayraktar, S.B. Pidugu, “Characterization of Liquid Flows in Microfluidic Systems”, *International Journal of Heat and Mass Transfer*, Vol.49, pp.815-824, 2006.

[14] S. G. Kandlikar, S. Garimella, D. Li, S. Colin and M. R. King, *Heat Transfer and Fluid Flow In Minichannels and Microchannels*, Elsevier, 2006

[15] M. Gad-el-Hak, “The Fluid Mechanics of Microdevices – The Freeman Scholar Lecture”, *Journal of Fluids Engineering*, Vol.121, pp.5-33, 1999.

[16] D. Bharathan, K. Gawlik, B. Kramer, S. Rogers, T.J. Hendricks, “Advanced Power Electronics - Thermal Management”, National Renewable Energy Laboratory (NREL) Publications, 2003

[http://www.nrel.gov/vehiclesandfuels/powerelectronics/pdfs/advanced\\_power\\_electronics\\_thermal\\_mgmt.pdf](http://www.nrel.gov/vehiclesandfuels/powerelectronics/pdfs/advanced_power_electronics_thermal_mgmt.pdf), last accessed on April 10<sup>th</sup>, 2010

[17] R.S. Prasher, J. Chang, I. Sauciuc, S. Narasimhan, D. Chau, D. G. Chrysler, A. Myers, S. Prstic, C. Hu, C., “Nano and Micro Technology-Based Next-

Generation Package-Level Cooling Solutions”, INTEL Technology Journal Vol.9, pp.285-296, 2005.

[18] Melcor™ Product Catalogue, [www.melcor.com](http://www.melcor.com), 2007, last accessed on April 10<sup>th</sup>, 2010

[19] M.A. Al-Nimr, M. Maqableh, A.F. Khadrawi, S.A. Ammourah, Fully developed thermal behaviors for parallel flow microchannel heat exchanger, International Communications in Heat and Mass Transfer, Vol. 36, pp. 385-390, 2009

[20] B. Mathew, H. Hegab, Application of effectiveness-NTU relationship to parallel flow microchannel heat exchangers subjected to external heat transfer, International Journal of Thermal Sciences Vol. 30, pp.1-10, 2009

[21] D. Dovic, B. Palm, S. Svaic, Generalized correlations for predicting heat transfer and pressure drop in plate heat exchanger channels of arbitrary geometry, International Journal of Heat and Mass Transfer, Vol. 52, pp. 4553-4563, 2009

[22] Dović, The analysis of single-phase flow in chevron channels of plate heat exchangers, Int. MSc Thesis, Energy Department, Royal Institute of Technology, Stockholm, 2000

[23] Nobuyoshi Tsuzuki, Motoaki Utamura, Tri Lam Ngo, Nusselt number correlations for a microchannel heat exchanger hot water supplier with S-shaped fins, Applied Thermal Engineering, Vol. 29, pp. 3299-3308, 2009

[24] Mushtaq I. Hasan, A.A. Rageb, M. Yaghoubi, Homayon Homayoni, Influence of channel geometry on the performance of a counter flow microchannel heat exchanger, International Journal of Thermal Sciences, Vol. 48, pp. 1607-1618, 2009

- [25] N. Garcia-Hernando, A. Acosta-Iborra, U. Ruiz-Rivas, M. Izquierdo, Experimental investigation of fluid flow and heat transfer in a single-phase liquid flow micro-heat exchanger, *International Journal of Heat and Mass Transfer*, Vol. 52, pp. 5433-5446, 2009
- [26] Ulrich Schygulla, Jürgen J. Brandner, Eugen Anurjew, Edgar Hansjosten, Klaus Schubert, Micro heat changers and surface-micro-coolers for high heat flux, *Proceedings of the Sixth International ASME Conference on Nanochannels, Microchannels and Minichannels ICNMM2008*, Darmstadt, Germany, 2008
- [27] Shung-Wen Kang, Shin-Chau Tseng, Analysis of effectiveness and pressure drop in micro cross-flow heat exchanger, *Applied Thermal Engineering*, Vol. 27, pp. 877-885, 2007
- [28] Gowreesan Vamadevan, Fank F. Kraft, Processing effects in aluminum micro-channel tube for brazed R744 heat exchangers, *Journal of Materials Processing Technology*, Vol. 191, pp. 30-33, 2007
- [29] Jian Wen, Yanzhong Li, Aimin Zhou, Ke Zhang, An experimental and numerical investigation of flow patterns in the entrance of plate-fin heat exchanger, *International Journal of Heat and Mass Transfer*, Vol. 49, pp. 1667-1678, 2006
- [30] Kwasi Foli, Tatsuya Okabe, Markus Olhofer, Yaochu Jin, Bernhard Sendhoff, Optimization of micro heat exchanger-CFD, analytical approach and multi-objective evolutionary algorithms, *International Journal of Heat and Mass Transfer*, Vol. 49, pp. 1090-1099, 2006
- [31] Philippe Nika, Yannick Bailly, François Guermeur, Thermoacoustics and related oscillatory heat and fluid flows in micro heat exchangers, Vol. 48, pp. 3773-3792, 2005

- [32] K. Kanlayasiri, B.K. Paul, A nickel aluminide microchannel array heat exchanger for high-temperature applications, *Journal of Manufacturing Processes*, Vol. 6, No.1, 2004
- [33] Pei-Xue Jiang, Ming-Hong Fan, Guang-Shu Si, Ze-Pei Ren, Thermal-hydraulic performance of small scale micro-channel and porous-media heat-exchangers, *International Journal of Heat and Mass Transfer*, Vol. 44, pp. 1039-1051, 2001
- [34] Philips Wyne Allen, *Experimental and Numerical Investigation of Fluid Flow and Heat Transfer in Microchannels*, Msc Thesis, Mechanical Engineering Department, Louisiana State University, 2007
- [35] S. Kakaç, R. K. Shah, A. E. Bergles, *Low Reynolds Number Flow Heat Exchangers*, Hemisphere Publishing Corporation, 1983
- [36] R. K. Shah and A. L. London, *Laminar Flow Forced Convection In Ducts*, Academic Press, 1978
- [37] B. Sunden and M. Faghri, *Computer Simulations in Compact Heat Exchangers*, Vol. 1, Computational Mechanical Publications, 1998
- [38] F. P. Incropera and D. P. DeWitt, *Fundamentals of Heat and Mass Transfer*, 4<sup>th</sup> Edition, John Wiley & Sons, 1996
- [39] R. K. Shah, A. D. Kras and D. Metzger, *Compact Heat Exchangers*, Hemisphere Publishing Corporation, 1990
- [40] P. Roberts, *Industrial Brazing Practice*, CRC Press LLC, 2004

- [41] N. Lashko and S. Lashko, *Brazing and Soldering of Metals*, Mir Publishers, 1979
- [42] R. Fabian, *Vacuum Technology, Practical Heat Treating and Brazing*, ASM International, 1993
- [43] M. M. Schwartz, *Brazing*, ASM International, 1987
- [44] Material Property Data, [www.matweb.com](http://www.matweb.com), last accessed on April 15<sup>th</sup>, 2010
- [45] B. Sunden and R.H. Shah, *Compact heat exchangers*, R.T. Edwards Inc., 2007
- [46] W. M. Kays and A. London, *Compact Heat Exchangers – A summary of basic heat transfer and flow friction design data*, McGraw-Hill Book Company Inc., 1958
- [47] Ehsan Sadeghi, Majid Bahrami, Ned Djilali, Estimation of Nusselt number in microchannels of arbitrary cross section with constant axial heat flux, *Heat Transfer Engineering*, Vol. 31, pp. 666-674, 2010
- [48] Yu-Tang Chen, Shung-Wen Kang, Wen-Chian Tuh and Tsung-Hsin Hsiao, Experimental investigation of fluid flow and heat transfer in microchannels, *Tamkang Journal of Science and Engineering*, Vol.7, No.1, pp. 11-16, 2004
- [49] W. M. Kays and A.L. London, *Compact heat exchangers*, 2<sup>nd</sup> Edition, McGraw-Hill Series in Mechanical Engineering, 1964
- [50] Ralph L. Webb, Nae-Hyun Kim, *Principles of Enhanced Heat Transfer*, Taylor & Francis Group, 2005

[51] Ramesh K. Shah, Compact Heat Exchangers and Enhancement Technology for the Process Industries, Begell House, 1999

[52] W. Roetzel, P.J. Heggs and D. Butterworth, Design and Operation of Heat Exchangers, Springer-Verlag, 1991

[53] C. J. Thwaites, Capillary Joining – Brazing and Soft-Soldering, Research Studies Press, 1982

[54] J. J. Ginoux, Heat Exchangers, North Atlantic Treaty Organization Advisory Group For Aerospace Research And Development, 1972

[55] Lytron™ Application Note and Product Catalogue, [www.lytron.com](http://www.lytron.com), 2007, last accessed on, April 10<sup>th</sup>, 2010

## APPENDIX A

### SAMPLE CALCULATIONS

In this chapter performance of the heat exchanger for experiment 1 will be performed. Theoretical and experimental calculations of the heat exchanger will be done. First design geometry of the heat exchanger will be investigated to determine geometrical properties on each fluid side. This includes the minimum free flow area  $A_0$ , heat transfer surface area  $A$  (both primary and secondary area), flow length  $L$ , hydraulic diameters  $D_h$ , fin geometry for fin efficiency determination and any specialized dimensions used for heat transfer. Next, the mean temperatures of both fluids will be calculated and then thermophysical properties of water and air on each side will be found. For inlet conditions, the air is assumed an ideal gas then mass flow rate of air will be calculated. The fluid properties needed for the analysis are  $\rho, c_p, k, \mu$  and  $Pr$ . Then Reynolds numbers and any other pertinent dimensionless group (Nu, St, j) will be calculated. Nusselt number, corrected for variable fluid property effects in the heat exchanger, will be calculated. Next, heat transfer coefficients  $h$  for both sides will be computed. Subsequently fin efficiency  $\eta_f$  and the extended surface efficiency  $\eta_0$  will be determined. Individual convective resistances, wall thermal resistances and fouling resistances will be calculated. Then theoretical overall thermal resistance  $R_t$  will be computed. With experimental results, mean temperature of the heat exchanger  $\Delta T_{lm}$ , heat transferred from water and heat transferred to air ( $Q_h, Q_c$ ) will be calculated. As heat is transferred not only from water to air but also the surroundings absorb heat, the average heat transfer will be computed. The maximum heat duty,  $Q_{max}$ , will be calculated. The experimental overall thermal conductance  $(U \cdot A)_{exp}$  will be determined. After calculating heat capacity rates on each fluid side, number of transfer units  $NTU$  will be found. Then, effectiveness of the heat exchanger will be determined. Heat transfer coefficient for air will be calculated from experimental overall thermal conductance and thermal resistance assuming that theoretical calculated heat transfer coefficient for water is not

significantly different in the experiments. Pressure drop in water side will be evaluated from measured inlet and outlet pressures of water.

### A.1 Geometrical Parameters

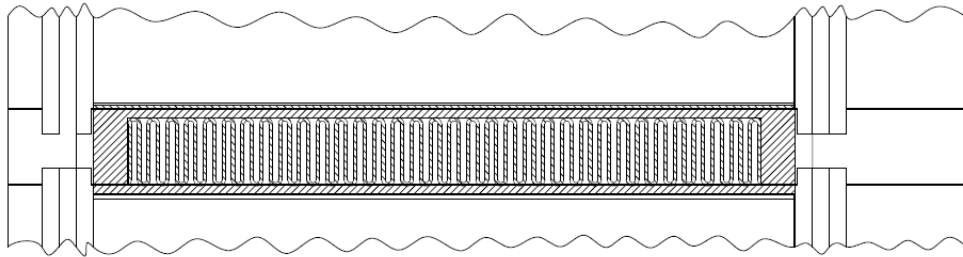


**Figure A.1:** Section view of the heat exchanger

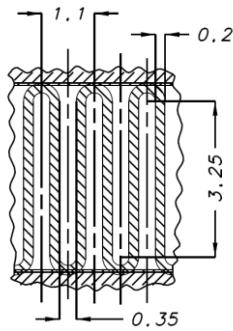


**Figure A.2:** Detailed section view of water side of the heat exchanger

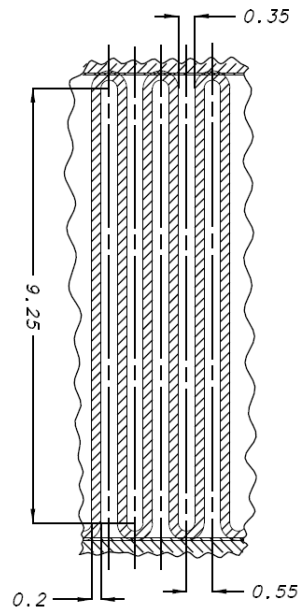


**Figure A.3:** Detailed section view of air side of the heat exchanger

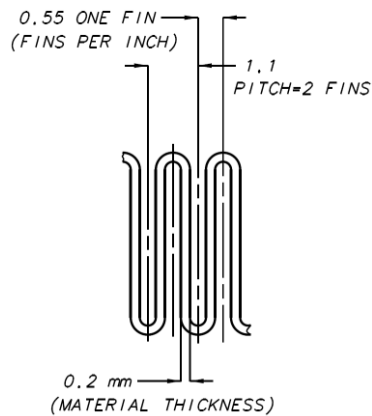


**Figure A.4:** Detailed view of plain fin of both sides of the heat exchanger

All detailed drawings of the heat exchanger is given in Appendix C. From drawings in Appendix C and Fig. A.2, A.3 and A.4, geometrical parameters for the heat exchanger may be determined.

Fin thickness for both air and water side

$$\delta_c = \delta_h = 0.2 \text{ mm}$$

Fin height for airside

$$b_c = b_2 = 10 \text{ mm}$$

Fin height for waterside	$b_h = b_1 = 4 \text{ mm}$
One fin width for both sides	$p_f = 0.55 \text{ mm}$
Fin flow length for airside	$L_{f,c} = 40 \text{ mm}$
Fin flow length for waterside	$L_{f,h} = 80 \text{ mm}$
Number of fins per unit length for air side	$N_{f,c} = 46 \text{ fin/inch}$
Number of fins per unit length for water side	$N_{f,h} = 46 \text{ fin/inch}$
Total number of water passage	$N_{p,h} = 6$
Total number of air passage	$N_{p,c} = N_{p,h} + 1$ $N_{p,c} = 7$
Wall thickness between air and water passage	$\delta_w = 1 \text{ mm}$
Length of heat exchanger in flow direction of water	$L_1 = 85 \text{ mm}$
Length of heat exchanger in flow direction of air for water side	$L_{2,h} = 37 \text{ mm}$
Length of heat exchanger in flow direction of water for air side	$L_{2,c} = 41 \text{ mm}$
Height of heat exchanger	$L_3 = 110 \text{ mm}$

From Fig. A.2 and A.3 it can be assumed that flow passages of both side rectangular channel. After assuming rectangular channel of flow passages first aspect ratio of both sides will be calculated.

For water sides From Fig. A.2, the dimensions of rectangular will be:

$$a_h = 0.35 \text{ mm}$$

$$b_h = 3.55 + 0.2 = 3.75 \text{ mm}$$

Then, aspect ratio for water channel:

$$\alpha_{c,h} = \frac{a_h}{b_h} = \frac{(0.35 \text{ mm})}{(3.75 \text{ mm})} = 0.0933$$

For air side From Fig. A.3, the dimensions of rectangular will be:

$$a_c = 0.35 \text{ mm}$$

$$b_c = 9.55 + 0.2 = 9.75 \text{ mm}$$

Then, aspect ratio for air channel:

$$\alpha_{c,c} = \frac{a_c}{b_c} = \frac{(0.35 \text{ mm})}{(9.75 \text{ mm})} = 0.0359$$

## A.2 Surface Geometrical Properties

To find hydraulic diameter of both sides, primary and secondary surface areas will be calculated.

### Water Side

Total plate area

$$= 2 \cdot L_1 \cdot L_2 \cdot N_p = 2 \cdot (85 \text{ mm}) \cdot (37 \text{ mm}) \cdot (6) = 37740 \text{ mm}^2$$

Fin base area covering plates

$$= 2 \cdot \delta \cdot L_f \cdot n_f = 2 \cdot \delta \cdot L_f \cdot N_f \cdot L_2 \cdot N_p$$

$$= 2 \cdot (0.2 \text{ mm}) \cdot (80 \text{ mm}) \cdot \left(46 \frac{\text{fin}}{25.4 \text{ mm}}\right) \cdot (37 \text{ mm}) \cdot (6) = 12865.512 \text{ mm}^2$$

Area of header bars on the side for water

$$= 2 \cdot b_1 \cdot L_1 \cdot N_p = 2 \cdot (4 \text{ mm}) \cdot (85 \text{ mm}) \cdot (6) = 4080 \text{ mm}^2$$

Area of header bars and plates of air at water core inlet and outlet faces

$$\begin{aligned}
&= 2 \cdot (b_2 + 2 \cdot \delta_w) \cdot (N_p + 1) \cdot L_2 \\
&= 2 \cdot (10 \text{ mm} + 2 \cdot (1 \text{ mm})) \cdot (6 + 1) \cdot (37 \text{ mm}) = 6216 \text{ mm}^2
\end{aligned}$$

The total primary surface area on the water side is then

$$\begin{aligned}
A_{p,1} &= 2 \cdot L_1 \cdot L_2 \cdot N_p - 2 \cdot \delta \cdot L_f \cdot N_f \cdot L_2 \cdot N_p + 2 \cdot b_1 \cdot L_1 \cdot N_p \\
&\quad + 2 \cdot (b_2 + 2 \cdot \delta_w) \cdot (N_p + 1) \cdot L_2 \\
&= (37740 \text{ mm}^2) - (12865.512 \text{ mm}^2) + (4080 \text{ mm}^2) + (6216 \text{ mm}^2) = 35170.488 \text{ mm}^2
\end{aligned}$$

The three components of the secondary (fin) area are:

Fin height area

$$\begin{aligned}
&= 2 \cdot (b_1 - \delta) \cdot L_f \cdot n_f \\
&= 2 \cdot (4 - 0.2) \cdot (80 \text{ mm}) \cdot \left(46 \frac{\text{fin}}{25.4 \text{ mm}}\right) \cdot (37 \text{ mm}) \cdot (6) = 244444.724 \text{ mm}^2
\end{aligned}$$

Fin edge height area

$$\begin{aligned}
&= 2 \cdot (b_1 - \delta) \cdot \delta \cdot n_f \\
&= 2 \cdot (4 - 0.2) \cdot (0.2) \cdot \left(46 \frac{\text{fin}}{25.4 \text{ mm}}\right) \cdot (37 \text{ mm}) \cdot (6) = 611.112 \text{ mm}^2
\end{aligned}$$

Fin edge width area

$$\begin{aligned}
&= 2 \cdot p_f \cdot \delta \cdot n_f \\
&= 2 \cdot (0.55 \text{ mm}) \cdot (0.2) \cdot \left(46 \frac{\text{fin}}{25.4 \text{ mm}}\right) \cdot (37 \text{ mm}) \cdot (6) = 88.450 \text{ mm}^2
\end{aligned}$$

The total secondary area on water side is:

$$\begin{aligned}
A_{f,1} &= 2 \cdot (b_1 - \delta) \cdot L_f \cdot n_f + 2 \cdot (b_1 - \delta) \cdot \delta \cdot n_f + 2 \cdot p_f \cdot \delta \cdot n_f \\
&= (244444.724 \text{ mm}^2) + (611.112 \text{ mm}^2) + (88.450 \text{ mm}^2) = 245144.287 \text{ mm}^2
\end{aligned}$$

The total surface area on water side is:

$$A_1 = A_{p,1} + A_{f,1}$$

$$=(35170.488 \text{ mm}^2)+(245144.287) \text{ mm}^2=280314.775 \text{ mm}^2$$

The free flow area on water side is given by the frontal area on water side minus the area blocked by the fins at the entrance of the core on that side:

$$A_{0,1} = b_1 \cdot L_2 \cdot N_p - [(b_1 - \delta) + p_f] \cdot \delta \cdot n_f$$

$$= (4 \text{ mm}) \cdot (37 \text{ mm}) \cdot (6) - [(4 \text{ mm} - 0.2 \text{ mm}) + (0.55 \text{ mm})]$$

$$\cdot (0.2 \text{ mm}) \cdot \left(46 \frac{\text{fin}}{25.4 \text{ mm}}\right) \cdot (37 \text{ mm}) \cdot (6)=538.219 \text{ mm}^2$$

Hydraulic diameter of water side

$$D_{h,1} = \frac{4A_{0,1} \cdot L_1}{A_1} = \frac{4 \cdot (538.219 \text{ mm}^2) \cdot (85 \text{ mm})}{280314.775 \text{ mm}^2} = 0.653 \text{ mm}$$

### Air Side

Total plate area

$$= 2 \cdot L_2 \cdot L_1 \cdot (N_p + 1)$$

$$= 2 \cdot (41 \text{ mm}) \cdot (85 \text{ mm}) \cdot (7) = 48790 \text{ mm}^2$$

Fin base area covering plates

$$= 2 \cdot \delta \cdot L_f \cdot n_f = 2 \cdot \delta \cdot L_f \cdot N_f \cdot L_1 \cdot (N_p + 1)$$

$$= 2 \cdot (0.2 \text{ mm}) \cdot (40 \text{ mm}) \cdot \left(46 \frac{\text{fin}}{25.4 \text{ mm}}\right) \cdot (85 \text{ mm}) \cdot (7) = 17240.945 \text{ mm}^2$$

Area of header bars on the side for air

$$= 2 \cdot b_1 \cdot L_1 \cdot N_p$$

$$= 2 \cdot (10 \text{ mm}) \cdot (41 \text{ mm}) \cdot (7) = 5740 \text{ mm}^2$$

Area of header bars and plates of water at air core inlet and outlet faces

$$\begin{aligned} &= 2 \cdot (b_1 + 2 \cdot \delta_w) \cdot N_p \cdot L_1 \\ &= 2 \cdot (4 \text{ mm} + 2 \cdot (1 \text{ mm})) \cdot (6) \cdot (85 \text{ mm}) = 6120 \text{ mm}^2 \end{aligned}$$

The total primary surface area on the air side is then

$$\begin{aligned} A_{p,2} &= 2 \cdot L_2 \cdot L_1 \cdot (N_p + 1) - 2 \cdot \delta \cdot L_f \cdot N_f \cdot L_1 \cdot (N_p + 1) \\ &\quad + 2 \cdot b_2 \cdot L_2 \cdot (N_p + 1) + 2 \cdot (b_1 + 2 \cdot \delta_w) \cdot N_p \cdot L_1 \\ &= (48790 \text{ mm}^2) - (17240.945 \text{ mm}^2) + (5740 \text{ mm}^2) + (6120 \text{ mm}^2) = 43409.055 \text{ mm}^2 \end{aligned}$$

The three components of the secondary (fin) area are:

Fin height area

$$\begin{aligned} &= 2 \cdot (b_2 - \delta) \cdot L_f \cdot n_f \\ &= 2 \cdot (10 - 0.2) \cdot (40 \text{ mm}) \cdot \left(46 \frac{\text{fin}}{25.4 \text{ mm}}\right) \cdot (85 \text{ mm}) \cdot (7) = 844806.299 \text{ mm}^2 \end{aligned}$$

Fin edge height area

$$\begin{aligned} &= 2 \cdot (b_2 - \delta) \cdot \delta \cdot n_f \\ &= 2 \cdot (10 - 0.2) \cdot (0.2) \cdot \left(46 \frac{\text{fin}}{25.4 \text{ mm}}\right) \cdot (85 \text{ mm}) \cdot (7) = 4224.031 \text{ mm}^2 \end{aligned}$$

Fin edge width area

$$\begin{aligned} &= 2 \cdot p_f \cdot \delta \cdot n_f \\ &= 2 \cdot (0.55) \cdot (0.2) \cdot \left(46 \frac{\text{fin}}{25.4 \text{ mm}}\right) \cdot (85 \text{ mm}) \cdot (7) = 237.063 \text{ mm}^2 \end{aligned}$$

The total secondary area on air side is:

$$A_{f,2} = 2 \cdot (b_2 - \delta) \cdot L_f \cdot n_f + 2 \cdot (b_2 - \delta) \cdot \delta \cdot n_f + 2 \cdot p_f \cdot \delta \cdot n_f$$

$$=(844806.299 \text{ mm}^2)+(4224.031 \text{ mm}^2)+(237.063 \text{ mm}^2) = 849267.961 \text{ mm}^2$$

The total surface area on water side is:

$$A_2 = A_{p,2} + A_{f,2}$$

$$=(43409.055 \text{ mm}^2)+(849267.961 \text{ mm}^2)=892677.512 \text{ mm}^2$$

The free flow area on water side is given by the frontal area on water side minus the area blocked by the fins at the entrance of the core on that side:

$$A_{0,2} = b_2 \cdot L_1 \cdot (N_p + 1) - [(b_2 - \delta) + p_f] \cdot \delta \cdot n_f$$

$$= (10 \text{ mm}) \cdot (85 \text{ mm}) \cdot (7) - [(10 \text{ mm} - 0.2 \text{ mm}) + 0.55] \cdot (0.2 \text{ mm})$$

$$\cdot \left(46 \frac{\text{fin}}{25.4 \text{ mm}}\right) \cdot (85 \text{ mm}) \cdot (7)=3719.453 \text{ mm}^2$$

Hydraulic diameter of air side

$$D_{h,2} = \frac{4A_{0,2}L_2}{A_2} = \frac{4 \cdot (3719.453 \text{ mm}^2) \cdot (41 \text{ mm})}{892677.512 \text{ mm}^2} = 0.683 \text{ mm}$$

### **A.3 Mean Temperatures and Fluid Properties**

#### For Water

Water properties are available in Ref [38] and for some temperatures water thermophysical properties are given as below in Appendix E.

**Table A.1:** Water thermophysical properties

Temperature ° C	Density $\rho$ [kg/m <sup>3</sup> ]	Conductivity k [W/m·C]	Specific Heat $c_p$ [J/kg·C]	Viscosity $\mu$ [kg/m·s]	Prandtl Number Pr
51.85	987.2	0.645	4182	0.000528	3.42
56.85	984.3	0.650	4184	0.000489	3.15

For experiment 1 the mean temperature of water  $T_{ave,h}=54.35$  °C. All air thermophysical properties are calculated at this mean temperature by means of linear interpolation and given in Table A.2.

**Table A.2:** Water properties at  $T = 54.35$  °C for experiment 1

Temperature ° C	Density $\rho$ [kg/m <sup>3</sup> ]	Conductivity k [W/m·C]	Specific Heat $c_p$ [J/kg·C]	Viscosity $\mu$ [kg/m·s]	Prandtl Number Pr
54.35	985.7	0.6489	4178.9	0.0005137	3.285

For all experiments water thermophysical properties at the mean temperature of each experiment are calculated and given in Appendix E.

For air

Air thermophysical properties are available in Ref [38] and for some temperatures water thermophysical properties are given as below in Appendix E.

**Table A.3:** Air thermophysical properties

Temperature ° C	Density $\rho$ [kg/m <sup>3</sup> ]	Conductivity k [W/m·C]	Specific Heat $c_p$ [J/kg·C]	Viscosity $\mu$ [kg/m·s]	Prandtl Number Pr
20	1.2045	0.0257	1005	0.0000182	0.713
40	1.1267	0.0271	1009	0.0000191	0.711

For experiment 1 the mean temperature of air  $T_{ave,c}=34.2$  ° C. All air thermophysical properties are calculated at this mean temperature by means of linear interpolation and given in Table A.4.

**Table A.4:** Air properties at  $T = 34.2$  °C for experiment 1

Temperature ° C	Density $\rho$ [kg/m <sup>3</sup> ]	Conductivity k [W/m·C]	Specific Heat $c_p$ [J/kg·C]	Viscosity $\mu$ [kg/m·s]	Prandtl Number Pr
34.2	1.1492	0.0267	1007.84	0.0000188	0.71158

For all experiments air thermophysical properties at the mean temperature of each experiment are calculated and given in Appendix E

#### A.4 Compactness of the Heat Exchanger

Total area of the heat exchanger is sum of areas at both sides.

Total area of the heat exchanger

$$\begin{aligned}
 A_T &= A_1 + A_2 \\
 &= 280314.775 \text{ mm}^2 + 892677.512 \text{ mm}^2 = 1.173 \text{ m}^2
 \end{aligned}$$

Outside dimensions of the heat exchanger are 105.1 mm, 56.1 mm and 109.4 mm.

Total volume of the heat exchanger

$$\begin{aligned} V_T &= l_x \cdot l_y \cdot l_z \\ &= 105.1 \cdot 56.1 \cdot 109.4 = 0.645 \text{ m}^3 \end{aligned}$$

Then, surface density of the heat exchanger

$$\beta = \frac{\text{Total area}}{\text{Total volume}} = \frac{1.173 \text{ m}^2}{0.645 \text{ m}^3} = 1818.494 \text{ m}^2/\text{m}^3$$

In Ref [3], a heat exchanger is considered as a compact heat exchanger if surface density of the heat exchanger is roughly greater than  $700 \text{ m}^2/\text{m}^3$

As  $\beta = 1818.494 \text{ m}^2/\text{m}^3 > 700 \text{ m}^2/\text{m}^3$  then the designed heat exchanger is a compact heat exchanger.

#### **A.4 Mass Flow Rates**

Mass flow rate of water for experiment 1 is measures as

$$\dot{m}_h = 0.009 \text{ kg/s}$$

Pressure of inlet air equals to atmospheric pressure. According to Governmental Meteorology Institute, the maximum measured atmospheric pressure in Ankara is 936.5 mbar and the minimum measured atmospheric pressure in Ankara 882.6 mbar. Average atmospheric pressure in Ankara can be assumed as mean value of these pressure values.

$$P_{atm,ave,Ankara} = 912.7 \text{ mbar}$$

Assuming air as ideal gas then density of air will be calculated from ideal gas equation:

$$\rho_{air} = \frac{P}{R \cdot T}$$

where  $R$  is ideal gas constant and equals to  $0.287 \frac{kPa \cdot m^3}{kg \cdot K}$ . The inlet temperature of air for experiment 1 is measured as  $23.4^\circ C$ . Then

$$\rho_{air} = \frac{912.7 \text{ mbar}}{\left(0.287 \frac{kPa \cdot m^3}{kg \cdot K}\right) \cdot (23.4^\circ C)} = 1.072 \frac{kg}{m^3}$$

Velocity of inlet air for experiment 1 is measured as  $u = 3.25 \text{ m/s}$ . Then mass flow rate of air will be calculated as

$$\dot{m}_c = \rho_c \cdot A_{0,2} \cdot u$$

$$\dot{m}_c = \left(1.072 \frac{kg}{m^3}\right) \cdot (3719.453 \text{ mm}^2) \cdot (3.25 \text{ m/s}) = 0.01296 \text{ kg/s}$$

Then

$$G_h = \frac{\dot{m}_h}{A_{0,1}} = \frac{0.009 \frac{kg}{s}}{538.219 \text{ mm}^2} = 16.722 \frac{kg}{m^2 \cdot s}$$

$$G_c = \frac{\dot{m}_c}{A_{0,2}} = \frac{0.01296 \frac{kg}{s}}{3719.453 \text{ mm}^2} = 3.485 \frac{kg}{m^2 \cdot s}$$

## A.5 Reynolds Number

Reynolds numbers will be calculated as below

$$Re_h = \frac{G_h \cdot D_{h,1}}{\mu_h} = \frac{\left(16.722 \frac{kg}{m^2 \cdot s}\right) \cdot (0.653 \text{ mm})}{\left(0.0005137 \frac{kg}{m \cdot s}\right)} = 21.468$$

$$Re_c = \frac{G_c \cdot D_{h,2}}{\mu_c} = \frac{\left(3.485 \frac{kg}{m^2 \cdot s}\right) \cdot (0.683 \text{ mm})}{\left(0.0000188 \frac{kg}{m \cdot s}\right)} = 126.416$$

For both flows, Reynolds numbers are less than 2300 then laminar flow assumption of each flow is correct.

## A.6 Nusselt Number

### Water side

For fully developed laminar flow in rectangular flow and taking into account temperature variations:

$$Nu_h = 8.235 \cdot (1 - 1.883 \cdot \alpha_c + 3.767 \cdot \alpha_c^2 - 5.814 \cdot \alpha_c^3 + 5.361 \cdot \alpha_c^4 - 2 \cdot \alpha_c^5) \cdot \left(\frac{\mu_b}{\mu_w}\right)^{-0.14}$$

Measured wall temperature of the heat exchanger is  $T_w = 37.1 \text{ }^\circ\text{C}$  and at this temperature, viscosity of water is  $\mu_w = 0.0006922 \text{ kg/m} \cdot \text{s}$ .

$$Nu_h = 8.235 \cdot (1 - 1.883 \cdot (0.0933) + 3.767 \cdot (0.0933^2) - 5.814 \cdot (0.0933^3) + 5.361 \cdot (0.0933^4) - 2 \cdot (0.0933^5)) \cdot \left(\frac{0.0005137}{0.0006922}\right)^{-0.14}$$

$$Nu_h = 7.321$$

For air side

For fully developed laminar flow in rectangular flow:

$$Nu_c = 8.235 \cdot (1 - 1.883 \cdot \alpha_c + 3.767 \cdot \alpha_c^2 - 5.814 \cdot \alpha_c^3 + 5.361 \cdot \alpha_c^4 - 2 \cdot \alpha_c^5)$$

$$Nu_c = 8.235 \cdot (1 - 1.883 \cdot (0.0359) + 3.767 \cdot (0.0359^2) - 5.814 \cdot (0.0359^3) + 5.361 \cdot (0.0359^4) - 2 \cdot (0.0359^5))$$

$$Nu_c = 7.716$$

### **A.7 Convection Heat Transfer Coefficient, h**

The convection heat transfer coefficient h can be calculated:

$$h = \frac{Nu \cdot k}{D_h}$$

For water side

$$h_h = \frac{7.321 \cdot (0.6489 \frac{W}{m \cdot K})}{0.653 \cdot 10^{-3} mm} = 7277.844 \frac{W}{m^2 \cdot K}$$

For air side

$$h_c = \frac{7.716 \cdot (0.0267 \frac{W}{m \cdot K})}{0.683 \cdot 10^{-3} mm} = 301.431 \frac{W}{m^2 \cdot K}$$

### **A.7 Stanton Number**

$$St = \frac{h}{G \cdot c_p}$$

For water side

$$St_h = \frac{7277.844 \frac{W}{m^2 \cdot K}}{16.722 \frac{kg}{s \cdot m^2} \cdot 4178.918 \frac{J}{kg \cdot K}} = 0.1041$$

For air side

$$St_c = \frac{301.431 \frac{W}{m^2 \cdot K}}{3.485 \frac{kg}{s \cdot m^2} \cdot 1007.84 \frac{J}{kg \cdot K}} = 0.0858$$

### **A.8 Colburn Factor**

$$j = St \cdot Pr^{2/3}$$

For water side

$$j_h = (0.1041) \cdot (3.285)^{2/3} = 0.2302$$

For air side

$$j_c = (0.0858) \cdot (0.71158)^{2/3} = 0.0684$$

### **A.9 Fin Efficiency**

Materials of fin at both sides are Aluminum 3003-O and its thermo physical properties are given in Appendix E. Let calculate the fin efficiency for water and air sides.

$$m = \left[ \frac{2 \cdot h}{k_f \cdot \delta} \left( 1 + \frac{\delta}{L_f} \right) \right]^{\frac{1}{2}}$$

For water side

$$m_h = \left[ \frac{2 \cdot 7277.844 \frac{W}{m^2 \cdot K}}{193 \frac{W}{m \cdot K} \cdot 0.2 \text{ mm}} \left( 1 + \frac{0.2 \text{ mm}}{80} \right) \right]^{1/2} = 614.844 \text{ m}^{-1}$$

For air side

$$m_c = \left[ \frac{2 \cdot 301.431 \frac{W}{m^2 \cdot K}}{193 \frac{W}{m \cdot K} \cdot 0.2 \text{ mm}} \left( 1 + \frac{0.2 \text{ mm}}{40} \right) \right]^{1/2} = 125.285 \text{ m}^{-1}$$

For overall extended surface efficiency adiabatic fin lengths are

$$l_{1,h} = \frac{b_h}{2} - \delta_h = \frac{4 \text{ mm}}{2} - 0.2 \text{ mm} = 1.8 \text{ mm} = 0.0018 \text{ m}$$

$$l_{1,c} = \frac{b_c}{2} - \delta_c = \frac{10 \text{ mm}}{2} - 0.2 \text{ mm} = 4.8 \text{ mm} = 0.0048 \text{ m}$$

Fin efficiency

$$\eta_f = \frac{\tanh(m \cdot l_1)}{m \cdot l_1}$$

For water side

$$\eta_{f_h} = \frac{\tanh(614.844 \text{ m}^{-1} \cdot 0.0018 \text{ m})}{614.844 \text{ m}^{-1} \cdot 0.0018 \text{ m}} = 0.725$$

For air side

$$\eta_{fc} = \frac{\tanh (125.285 \text{ m}^{-1} \cdot 0.0048 \text{ m})}{125.285 \text{ m}^{-1} \cdot 0.0048 \text{ m}} = 0.895$$

### **A.10 The Overall Surface Efficiency**

$$\eta_o = \left[ 1 - (1 - \eta_f) \frac{A_f}{A} \right]$$

For water side

$$\eta_{oh} = \left[ 1 - (1 - 0.725) \cdot \frac{245144.2866 \text{ mm}^2}{280314.778 \text{ mm}^2} \right] = 0.76$$

For air side

$$\eta_{oc} = \left[ 1 - (1 - 0.894) \cdot \frac{849267.9606 \text{ mm}^2}{892677.5118 \text{ mm}^2} \right] = 0.9$$

It should be pointed out that the fin conduction length  $l$  for the end passages on the airside will be  $b$  and not  $\frac{b}{2} - \delta$ . This will result in lower fin efficiency for the end passages. However, its influence will be smaller on the weighted average fin efficiency considering all air passages. Hence it has been neglected.

### **A.11 The Convection Resistance of Water Side**

$$R_h = \frac{1}{\left( \eta_{o,h} \cdot h \cdot A \right)_h}$$

$$R_h = \frac{1}{\left[0.76 \cdot 7277.844 \frac{W}{m^2 \cdot K} \cdot 280314.778 \text{ mm}^2\right]_{f,d,h}} = 6.45 \cdot 10^{-4} \frac{K}{W}$$

### A.12 The Fouling Resistance of Water Side

In all experiments well water was used. Fouling resistance of the well water can be read from Table 3.1 in Ref [2] is given as  $R_{fh} = 0.000352 \frac{m^2 \cdot K}{W}$ . Then fouling resistances of the both water side is:

$$R_{f,h} = \frac{R_{fh}}{\eta_{0,h} A_h}$$

$$R_{f,h} = \frac{0.000352 \frac{m^2 \cdot K}{W}}{0.76 \cdot (280314.778 \text{ mm}^2)} = 1.652 \cdot 10^{-3} \frac{K}{W}$$

### A.13 The Wall Resistance

Material of the heat exchanger is Aluminum 6061-T6 and its thermophysical properties are given in Appendix E. For the  $R_w$  determination, first the wall conduction area  $A_w$  must be calculated.

$$A_w = L_1 \cdot L_2 \cdot (2N_p + 2) = 85 \text{ mm} \cdot 41 \text{ mm} \cdot (2 \cdot 6 + 2) = 0.0488 \text{ m}^2$$

$$R_w = \frac{\delta_w}{k_w A_w} = \frac{1 \text{ mm}}{\left(167 \frac{W}{K \cdot m}\right) \cdot (0.0488 \text{ m}^2)} = 1.2273 \cdot 10^{-4} \frac{K}{W}$$

### A.14 The Convection Resistance of Air Side

$$R_c = \frac{1}{\left(\eta_{0,c} \cdot h \cdot A\right)_c}$$

$$R_c = \frac{1}{\left[0.9 \cdot 301.431 \frac{W}{m^2 \cdot K} \cdot (892677.512 \text{ mm}^2)\right]_{fd,c}} = 4.130 \cdot 10^{-3} \frac{K}{W}$$

### A.15 The Fouling Resistance of Air Side

In the experiments air can be assumed as compressed, so fouling resistance of the compressed air can be read from Table 3.2 Ref [2] is given as

$R_{fh} = 0.000176 \frac{m^2 \cdot K}{W}$ . Then fouling resistances of the both air side is:

$$R_{f,c} = \frac{R_{fc}}{\eta_{0,c} \cdot A_c}$$

$$R_{f,c} = \frac{0.000176 \frac{m^2 \cdot K}{W}}{0.9 \cdot (892677.512 \text{ mm}^2)} = 2.191 \cdot 10^{-4} \frac{K}{W}$$

### A.16 The Total Thermal Resistance

$$R_t = R_h + R_{h,f} + R_w + R_{c,f} + R_c$$

$$R_t = 6.45 \cdot 10^{-4} \frac{K}{W} + 1.652 \cdot 10^{-3} \frac{K}{W} + 1.2273 \cdot 10^{-4} \frac{K}{W} + 2.191 \cdot 10^{-4} \frac{K}{W} + 4.130 \cdot 10^{-3} \frac{K}{W} = 0.00677 \frac{K}{W}$$

### A.17 Experimental Heat Transfer from Water

$$Q_h = (\dot{m} \cdot c_p)_h \cdot (T_{h1} - T_{h2})$$

$$Q_h = \left(0.009 \frac{kg}{s} \cdot 4183 \frac{J}{kg \cdot C}\right)_h (63.8 \text{ } ^\circ C - 44.9 \text{ } ^\circ C) = 710.833 \text{ W}$$

### A.18 Experimental Heat Transfer to Air

$$Q_c = (\dot{m} \cdot c_p)_c \cdot (T_{c2} - T_{c1})$$

$$Q_c = \left( 0.01246 \frac{\text{kg}}{\text{s}} \cdot 1007.845 \frac{\text{J}}{\text{kg} \cdot \text{C}} \right) (45 \text{ }^\circ\text{C} - 23.4 \text{ }^\circ\text{C}) = 282.199 \text{ W}$$

As heat transfer from water not only to transfer to the air also it was transferred to ambient, average heat transfer may be more suitable to define the transferred heat. Then,

$$Q_{ave} = \frac{Q_h + Q_c}{2} = \frac{710.833 + 282.199}{2} = 496.517 \text{ W}$$

### A.19 Maximum Heat Transfer

$$Q_{\max} = (\dot{m} \cdot c_p)_c \cdot (T_{h1} - T_{c1}) \text{ if } C_c < C_h$$

$$Q_{\max} = \left( 0.01246 \frac{\text{kg}}{\text{s}} \cdot 1007.845 \frac{\text{J}}{\text{kg} \cdot \text{C}} \right) \cdot (63.8 \text{ }^\circ\text{C} - 23.4 \text{ }^\circ\text{C}) = 527.817 \text{ W}$$

### A.20 Experimental Overall Thermal Coefficient

$$P = \frac{T_{c2} - T_{c1}}{T_{h1} - T_{c1}} = \frac{\Delta T_c}{\Delta T_{\max}} = \frac{45.0 \text{ }^\circ\text{C} - 23.4 \text{ }^\circ\text{C}}{63.8 \text{ }^\circ\text{C} - 23.4 \text{ }^\circ\text{C}} = 0.534$$

$$R = \frac{C_c}{C_h} = \frac{T_{h1} - T_{h2}}{T_{c2} - T_{c1}} = \frac{\Delta T_h}{\Delta T_c} = \frac{24.531}{37.610} = \frac{63.8 \text{ }^\circ\text{C} - 44.9 \text{ }^\circ\text{C}}{45.0 \text{ }^\circ\text{C} - 23.4 \text{ }^\circ\text{C}} = 0.652$$

From Fig.3.1 F can be read as  $F = 0.89$

$$\begin{aligned}\Delta T_{lm,cf} &= \frac{(T_{h2} - T_{c1}) - (T_{h1} - T_{c2})}{\ln \left[ \frac{T_{h2} - T_{c1}}{T_{h1} - T_{c2}} \right]} \\ &= \frac{(44.94^\circ\text{C} - 23.4^\circ\text{C}) - (63.8^\circ\text{C} - 45.0^\circ\text{C})}{\ln \left[ \frac{44.9^\circ\text{C} - 23.4^\circ\text{C}}{63.8^\circ\text{C} - 45.0^\circ\text{C}} \right]} \\ &= 29.963^\circ\text{C}\end{aligned}$$

$$U \cdot A = \frac{Q_{ave}}{F \cdot \Delta T_{lm,cf}} = \frac{496.517 \text{ W}}{0.89 \cdot 29.963^\circ\text{C}} = 18.619 \frac{\text{W}}{\text{K}}$$

### A.21 Heat Capacity Rates

$$C_h = (\dot{m} \cdot c_p)_h = \left( 0.009 \frac{\text{kg}}{\text{s}} \cdot 4183 \frac{\text{J}}{\text{kg} \cdot \text{C}} \right) = 37.647 \frac{\text{W}}{\text{K}}$$

$$C_c = (\dot{m} \cdot c_p)_c = \left( 0.01246 \frac{\text{kg}}{\text{s}} \cdot 1007.845 \frac{\text{J}}{\text{kg} \cdot \text{C}} \right) = 13.065 \frac{\text{W}}{\text{K}}$$

$$C_{\min} = \min(C_c, C_h) = 13.065 \frac{\text{W}}{\text{K}}$$

$$C_{\max} = \max(C_c, C_h) = 37.647 \frac{\text{W}}{\text{K}}$$

$$C^* = \frac{C_{\min}}{C_{\max}} = \frac{13.065}{37.647} = 0.347$$

### A.22 Number of Transfer Unit

$$\text{NTU} = \frac{U \cdot A}{C_{\min}}$$

$$\text{NTU} = \frac{18.619 \frac{\text{W}}{\text{K}}}{13.065 \frac{\text{W}}{\text{K}}} = 1.425$$

### A.23 Effectiveness

$$\begin{aligned}\varepsilon &= 1 - e^{-(1+C^*) \cdot NTU} \cdot [I_0(2 \cdot NTU \cdot \sqrt{C^*}) + \\ &\quad \sqrt{C^*} \cdot I_1(2 \cdot NTU \cdot \sqrt{C^*}) - \frac{1-C^*}{C^*} \cdot \sum_{n=2}^{\infty} C^{*\frac{n}{2}} \cdot I_n(2 \cdot NTU \cdot \sqrt{C^*})] \\ \varepsilon &= 1 - e^{-(1+0.347) \cdot 1.425} \cdot [I_0(2 \cdot 1.425 \cdot \sqrt{0.347}) \\ &\quad + \sqrt{0.347} \cdot I_1(2 \cdot 1.425 \cdot \sqrt{0.347}) \\ &\quad - \frac{1-0.347}{0.347} \cdot \sum_{n=2}^{\infty} 0.347^{\frac{n}{2}} \cdot I_n(2 \cdot 1.425 \cdot \sqrt{0.347})] = 0.679\end{aligned}$$

### A.24 Experimental Effectiveness

$$\varepsilon = \frac{Q_{ave}}{Q_{max}} = \frac{496.517 \text{ W}}{527.817 \text{ W}} = 0.941$$

### A.25 Experimental Heat Transfer Coefficient of Air

$$\begin{aligned}h_{c,exp} &= \frac{\left( \frac{1}{(U \cdot A)_{exp}} - \frac{1}{(\eta_{0,h} \cdot h \cdot A)_h} - \frac{R_{fh}}{\eta_{0,h} \cdot A_h} - \frac{\delta_w}{k_w \cdot A_w} - \frac{R_{fc}}{\eta_{0,c} \cdot A_c} \right)^{-1}}{(\eta_{0,c} \cdot A)_c} \\ &= \left( \frac{1}{18.619 \frac{W}{K}} - 6.45 \cdot 10^{-4} \frac{K}{W} - 1.652 \cdot 10^{-3} \frac{K}{W} - 1.2273 \cdot 10^{-4} \frac{K}{W} \right. \\ &\quad \left. - 2.191 \cdot 10^{-4} \frac{K}{W} \right)^{-1} / (0.9 \cdot (892677.512 \text{ mm}^2)) \\ h_{c,exp} &= 24.379 \frac{W}{m^2 \cdot K}\end{aligned}$$

### A.26 Pressure Drop of Water

The inlet and outlet pressure of water are measured as 1.334 *bar* and 1.302 *bar*

$$\Delta p_h = p_{h1} - p_{h2}$$

$$\Delta p_h = 1.334 \text{ bar} - 1.302 \text{ bar} = 0.032 \text{ bar} = 3.2 \text{ kpa}$$

## APPENDIX B

### THEORETICAL AND EXPERIMENTAL CALCULATION RESULTS

**Table B.1:** Mass flow rates and Reynolds numbers of water and air side for each experiment

<i>Experiment Number</i>	<i>Flow rate of the water [kg/s]</i>	$G_h$ <i>[<math>\frac{kg}{m^2 \cdot s}</math>]</i>	$Re_h$	<i>Flow rate of the air [kg/s]</i>	$G_c$ <i>[<math>\frac{kg}{m^2 \cdot s}</math>]</i>	$Re_c$
1	0.009	16.722	21.250	0.01296	8.180	296.711
2	0.013	24.154	30.918	0.01296	8.142	294.330
3	0.019	35.302	45.028	0.01295	8.128	293.480
4	0.024	44.592	56.911	0.01295	8.114	292.632
5	0.009	16.722	22.402	0.01236	7.470	269.357
6	0.013	24.154	33.015	0.01233	7.417	266.162
7	0.019	35.302	49.285	0.01228	7.389	264.468
8	0.024	44.592	63.866	0.01226	7.362	262.755
9	0.009	16.722	23.850	0.01113	7.069	252.783
10	0.013	24.154	34.428	0.01117	7.071	252.918
11	0.019	35.302	50.728	0.01118	7.067	252.648
12	0.024	44.592	63.255	0.01117	7.065	252.513
13	0.009	16.722	24.367	0.00976	6.029	215.379
14	0.013	24.154	35.902	0.00977	6.012	214.346
15	0.019	35.302	53.100	0.00977	6.007	214.003
16	0.024	44.592	66.675	0.00977	6.003	213.774
17	0.009	16.722	26.184	0.00836	5.156	183.395
18	0.013	24.154	37.659	0.00837	5.142	182.515
19	0.019	35.302	56.443	0.00834	5.121	181.152
20	0.024	44.592	71.436	0.00836	5.122	181.249
21	0.009	16.722	27.749	0.00697	4.252	150.249
22	0.013	24.154	40.618	0.00696	4.235	149.206
23	0.019	35.302	61.080	0.00697	4.229	148.806
24	0.024	44.592	77.379	0.00697	4.224	148.487
25	0.009	16.722	30.621	0.00537	3.186	111.496
26	0.013	24.154	45.323	0.00537	3.174	110.779
27	0.019	35.302	67.385	0.00537	3.169	110.422
28	0.024	44.592	86.844	0.00537	3.162	110.006
29	0.009	16.722	28.178	0.01289	7.931	281.302
30	0.013	24.154	39.608	0.01296	7.943	282.055
31	0.019	35.302	58.925	0.02936	7.893	278.902
32	0.024	44.592	76.165	0.02924	7.862	276.966

**Table B.2:** Dimensionless numbers and convection heat transfer coefficient,  $h$  of water side where  $\dot{m}_h = 0.009 \text{ kg/s}$  and air mass flow rate is changing

<i>Experiment Number</i>	$Re_h$	$Nu_h$	$St_h$	$j_h$	$\frac{h_h}{W}$ [ $\frac{W}{m^2 \cdot K}$ ]
1	21.25	7.32	0.1041	0.2302	7277.84
5	22.40	7.22	0.1032	0.2194	7210.65
9	23.85	7.24	0.1040	0.2107	7270.09
13	24.37	7.11	0.1023	0.2045	7155.41
17	26.18	7.10	0.1029	0.1950	7198.26
21	27.75	7.06	0.1028	0.1857	7200.44
25	30.62	7.05	0.1034	0.1744	7247.94
29	28.18	7.12	0.1038	0.1855	7266.95

**Table B.3:** Dimensionless numbers and convection heat transfer coefficient,  $h$  of water side where  $\dot{m}_h = 0.013 \text{ kg/s}$  and air mass flow rate is changing

<i>Experiment Number</i>	$Re_h$	$Nu_h$	$St_h$	$j_h$	$\frac{h_h}{W}$ [ $\frac{W}{m^2 \cdot K}$ ]
2	30.92	7.26	0.0715	0.1573	7217.49
6	33.02	7.14	0.0707	0.1481	7139.55
10	34.43	7.26	0.0722	0.1464	7292.78
14	35.90	7.25	0.0723	0.1427	7305.45
18	37.66	7.06	0.0708	0.1347	7156.45
22	40.62	7.06	0.0712	0.1275	7202.89
26	45.32	7.05	0.0718	0.1192	7269.95
30	39.61	7.11	0.0717	0.1305	7245.32

**Table B.4:** Dimensionless numbers and convection heat transfer coefficient,  $h$  of water side where  $\dot{m}_h = 0.019 \text{ kg/s}$  and air mass flow rate is changing

<i>Experiment Number</i>	$Re_h$	$Nu_h$	$St_h$	$j_h$	$\frac{h_h}{W}$ [ $\frac{W}{m^2 \cdot K}$ ]
3	45.03	7.19	0.0485	0.1069	7149.83
7	49.29	7.11	0.0483	0.0995	7126.04
11	50.73	7.23	0.0492	0.0992	7260.34
15	53.10	7.24	0.0494	0.0969	7301.36
19	56.44	7.07	0.0486	0.0905	7184.56
23	61.08	7.08	0.0489	0.0859	7233.29
27	67.39	7.06	0.0492	0.0807	7284.29
31	58.93	7.10	0.0490	0.0881	7240.72

**Table B.5:** Dimensionless numbers and convection heat transfer coefficient,  $h$  of water side where  $\dot{m}_h = 0.024 \text{ kg/s}$  and air mass flow rate is changing

<i>Experiment Number</i>	$Re_h$	$Nu_h$	$St_h$	$j_h$	$\frac{h_h}{W}$ [ $\frac{W}{m^2 \cdot K}$ ]
4	56.91	7.12	0.0380	0.0657	7074.63
8	63.87	7.10	0.0383	0.0773	7134.21
12	63.26	7.10	0.0382	0.0777	7123.19
16	66.68	7.09	0.0384	0.0754	7152.43
20	71.44	7.07	0.0385	0.0716	7189.31
24	77.38	7.08	0.0387	0.0679	7234.90
28	86.84	7.07	0.0390	0.0632	7300.14
32	76.17	7.11	0.0389	0.0689	7260.17

**Table B.6:** Overall surface efficiency, convection and fouling resistance of water side where  $\dot{m}_h = 0.009 \text{ kg/s}$  and air mass flow rate is changing

<i>Experiment Number</i>	$\eta_{0_h}$	$R_{T,h}$ [ $\frac{K}{W}$ ]	$R_{T,h,f}$ [ $\frac{K}{W}$ ]
1	0.760	0.000645	0.001652
5	0.761	0.000650	0.001649
9	0.760	0.000646	0.001652
13	0.763	0.000654	0.001647
17	0.762	0.000651	0.001649
21	0.762	0.000650	0.001649
25	0.761	0.000647	0.001651
29	0.760	0.000646	0.001652

**Table B.7:** Overall surface efficiency, convection and fouling resistance of water side where  $\dot{m}_h = 0.013 \text{ kg/s}$  and air mass flow rate is changing

<i>Experiment Number</i>	$\eta_{0_h}$	$R_{T,h}$ [ $\frac{K}{W}$ ]	$R_{T,h,f}$ [ $\frac{K}{W}$ ]
1	0.761	0.000649	0.001650
5	0.763	0.000655	0.001646
9	0.760	0.000644	0.001653
13	0.759	0.000643	0.001654
17	0.763	0.000654	0.001647
21	0.762	0.000650	0.001649
25	0.760	0.000646	0.001652
29	0.761	0.000647	0.001651

**Table B.8:** Overall surface efficiency, convection and fouling resistance of water side where  $\dot{m}_h = 0.019 \text{ kg/s}$  and air mass flow rate is changing

<i>Experiment Number</i>	$\eta_{0_h}$	$R_{T,h}$ [ $\frac{K}{W}$ ]	$R_{T,h,f}$ [ $\frac{K}{W}$ ]
1	0.763	0.000654	0.001646
5	0.763	0.000656	0.001645
9	0.760	0.000646	0.001652
13	0.759	0.000643	0.001654
17	0.762	0.000652	0.001648
21	0.761	0.000648	0.001650
25	0.760	0.000645	0.001653
29	0.761	0.000648	0.001651

**Table B.9:** Overall surface efficiency, convection and fouling resistance of water side where  $\dot{m}_h = 0.024 \text{ kg/s}$  and air mass flow rate is changing

<i>Experiment Number</i>	$\eta_{0_h}$	$R_{T,h}$ [ $\frac{K}{W}$ ]	$R_{T,h,f}$ [ $\frac{K}{W}$ ]
1	0.764	0.000660	0.001643
5	0.763	0.000655	0.001645
9	0.763	0.000656	0.001645
13	0.763	0.000654	0.001646
17	0.762	0.000651	0.001648
21	0.761	0.000648	0.001650
25	0.759	0.000643	0.001654
29	0.760	0.000646	0.001652

**Table B.10:** Dimensionless numbers and convection heat transfer coefficient,  $h$  of air side where  $\dot{m}_h = 0.009 \text{ kg/s}$  and air mass flow rate is changing

<i>Experiment Number</i>	$Re_c$	$St_c$	$j_c$	$\frac{h_c}{W}$ [ $\frac{W}{m^2 \cdot K}$ ]
1	126.42	0.0858	0.0684	301.43
5	119.87	0.0905	0.0721	303.41
9	107.01	0.1014	0.0808	306.17
13	93.74	0.1158	0.0922	306.49
17	79.94	0.1358	0.1082	307.99
21	66.20	0.1641	0.1307	310.21
25	50.51	0.2153	0.1713	313.53
29	122.95	0.0883	0.0703	308.94

**Table B.11:** Dimensionless numbers and convection heat transfer coefficient,  $h$  of air side where  $\dot{m}_h = 0.013 \text{ kg/s}$  and air mass flow rate is changing

<i>Experiment Number</i>	$Re_c$	$St_c$	$j_c$	$\frac{h_c}{W}$ [ $\frac{W}{m^2 \cdot K}$ ]
2	125.95	0.0861	0.0686	302.54
6	118.94	0.0912	0.0727	304.99
10	107.40	0.1010	0.0805	306.09
14	93.67	0.1159	0.0923	307.20
18	79.87	0.1359	0.1083	308.70
22	65.96	0.1648	0.1312	311.23
26	50.38	0.2159	0.1718	314.47
30	123.71	0.0878	0.0699	308.55

**Table B.12:** Dimensionless numbers and convection heat transfer coefficient,  $h$  of air side where  $\dot{m}_h = 0.019 \text{ kg/s}$  and air mass flow rate is changing

<i>Experiment Number</i>	$Re_c$	$St_c$	$j_c$	$\frac{h_c}{W}$ [ $\frac{W}{m^2 \cdot K}$ ]
3	125.76	0.0863	0.0687	302.93
7	118.19	0.0918	0.0731	305.86
11	107.46	0.1010	0.0804	306.25
15	93.60	0.1160	0.0924	307.44
19	79.32	0.1369	0.1090	309.81
23	65.92	0.1649	0.1312	311.63
27	50.30	0.2163	0.1721	314.95
31	122.66	0.0886	0.0705	310.21

**Table B.13:** Dimensionless numbers and convection heat transfer coefficient,  $h$  of air side where  $\dot{m}_h = 0.024 \text{ kg/s}$  and air mass flow rate is changing

<i>Experiment Number</i>	$Re_c$	$St_c$	$j_c$	$\frac{h_c}{W}$ [ $\frac{W}{m^2 \cdot K}$ ]
4	125.57	0.0864	0.0689	303.33
8	117.62	0.0923	0.0735	306.81
12	107.36	0.1011	0.0805	306.33
16	93.56	0.1160	0.0924	307.60
20	79.55	0.1365	0.1087	309.73
24	65.84	0.1651	0.1314	311.94
28	50.20	0.2167	0.1724	315.50
32	121.96	0.0891	0.0709	311.23

**Table B.14:** Overall surface efficiency, convection and fouling resistance of air side where  $\dot{m}_h = 0.009 \text{ kg/s}$  and air mass flow rate is changing

<i>Experiment Number</i>	$\eta_{0_c}$	$R_c$ [ $\frac{K}{W}$ ]	$R_{f.c}$ [ $\frac{K}{W}$ ]
1	0.900	0.004130	0.000219
5	0.899	0.004106	0.000219
9	0.898	0.004073	0.000219
13	0.898	0.004069	0.000219
17	0.898	0.004051	0.000220
21	0.897	0.004025	0.000220
25	0.896	0.003986	0.000220
29	0.898	0.004040	0.000220

**Table B.15:** Overall surface efficiency, convection and fouling resistance of air side where  $\dot{m}_h = 0.013 \text{ kg/s}$  and air mass flow rate is changing

<i>Experiment Number</i>	$\eta_{0_c}$	$R_c$ [ $\frac{K}{W}$ ]	$R_{f.c}$ [ $\frac{K}{W}$ ]
2	0.899	0.004117	0.000219
6	0.899	0.004087	0.000219
10	0.898	0.004073	0.000219
14	0.898	0.004060	0.000220
18	0.898	0.004042	0.000220
22	0.897	0.004013	0.000220
26	0.896	0.003976	0.000220
30	0.898	0.004044	0.000220

**Table B.16:** Overall surface efficiency, convection and fouling resistance of air side where  $\dot{m}_h = 0.019 \text{ kg/s}$  and air mass flow rate is changing

<i>Experiment Number</i>	$\eta_{0_c}$	$R_c$ [ $\frac{K}{W}$ ]	$R_{f,c}$ [ $\frac{K}{W}$ ]
3	0.899	0.004112	0.000219
7	0.899	0.004076	0.000219
11	0.898	0.004072	0.000219
15	0.898	0.004057	0.000220
19	0.897	0.004029	0.000220
23	0.897	0.004008	0.000220
27	0.896	0.003970	0.000220
31	0.897	0.004025	0.000220

**Table B.17:** Overall surface efficiency, convection and fouling resistance of air side where  $\dot{m}_h = 0.024 \text{ kg/s}$  and air mass flow rate is changing

<i>Experiment Number</i>	$\eta_{0_c}$	$R_c$ [ $\frac{K}{W}$ ]	$R_{f,c}$ [ $\frac{K}{W}$ ]
4	0.899	0.004107	0.000219
8	0.898	0.004065	0.000219
12	0.898	0.004071	0.000219
16	0.898	0.004056	0.000220
20	0.897	0.004030	0.000220
24	0.897	0.004005	0.000220
28	0.896	0.003964	0.000220
32	0.897	0.004013	0.000220

**Table B.18:** Heat capacity rates

<i>Experiment Number</i>	$C_h$ [ $\frac{W}{K}$ ]	$C_c$ [ $\frac{W}{K}$ ]	$C_{min}$ [ $\frac{W}{K}$ ]	$C_{max}$ [ $\frac{W}{K}$ ]	$C^*$
1	37.61	13.07	13.07	37.61	0.347
2	54.33	13.06	13.06	54.33	0.240
3	79.40	13.06	13.06	79.40	0.164
4	100.30	13.06	13.06	100.30	0.130
5	37.61	12.47	12.47	37.61	0.331
6	54.33	12.44	12.44	54.33	0.229
7	79.41	12.39	12.39	79.41	0.156
8	100.33	12.37	12.37	100.33	0.123
9	37.62	11.23	11.23	37.62	0.299
10	54.34	11.27	11.27	54.34	0.207
11	79.43	11.28	11.28	79.43	0.142
12	100.32	11.27	11.27	100.32	0.112
13	37.63	9.85	9.85	37.63	0.262
14	54.37	9.86	9.86	54.37	0.181
15	79.47	9.86	9.86	79.47	0.124
16	100.38	9.86	9.86	100.38	0.098
17	37.66	8.44	8.44	37.66	0.224
18	54.39	8.45	8.45	54.39	0.155
19	79.52	8.42	8.42	79.52	0.106
20	100.45	8.44	8.44	100.45	0.084
21	37.69	7.03	7.03	37.69	0.187
22	54.45	7.03	7.03	54.45	0.129
23	79.61	7.03	7.03	79.61	0.088
24	100.57	7.03	7.03	100.57	0.070
25	37.74	5.42	5.42	37.74	0.144
26	54.53	5.42	5.42	54.53	0.099
27	79.72	5.42	5.42	79.72	0.068
28	100.73	5.42	5.42	100.73	0.054
29	37.70	13.01	13.01	37.70	0.345
30	54.42	13.08	13.08	54.42	0.240
31	79.57	13.03	13.03	79.57	0.164
32	100.54	12.99	12.99	100.54	0.129

**Table B.19:** Heat transfer rates

<b>Experiment Number</b>	<b><math>Q_h</math> [W]</b>	<b><math>Q_c</math> [W]</b>	<b><math>Q_{ave}</math> [W]</b>	<b><math>Q_{max}</math> [W]</b>
1	710.83	282.20	496.52	527.82
2	711.68	316.15	513.92	493.82
3	730.49	326.52	528.51	463.66
4	651.92	338.20	495.06	445.27
5	692.04	329.16	510.60	543.60
6	641.06	356.89	498.97	506.11
7	627.32	356.89	492.10	483.29
8	511.69	371.03	441.36	477.39
9	669.68	354.90	512.29	519.99
10	635.82	376.38	506.10	498.08
11	659.28	386.91	523.10	488.43
12	611.96	384.40	498.18	464.43
13	654.78	329.87	492.33	472.65
14	685.03	356.94	520.98	465.40
15	635.76	361.87	498.81	449.62
16	572.15	366.80	469.47	434.83
17	553.59	311.23	432.41	433.53
18	609.21	333.61	471.41	419.76
19	556.64	337.43	447.03	408.11
20	472.10	350.15	411.13	407.52
21	614.28	300.23	457.25	399.37
22	593.47	315.49	454.48	385.75
23	453.79	326.24	390.02	383.90
24	392.21	330.35	361.28	378.15
25	596.31	273.00	434.66	345.05
26	534.42	286.64	410.53	339.74
27	494.29	292.50	393.40	338.00
28	352.55	298.90	325.73	337.89
29	972.53	485.26	728.90	801.39
30	854.46	515.17	684.82	732.22
31	986.62	539.32	762.97	711.28
32	764.12	549.57	656.84	689.89

**Table B.20:** Experimental overall thermal coefficients

<i>Experiment Number</i>	<i>P</i>	<i>R</i>	<i>F</i>	$\Delta T_{lm,cf}$ [°C]
1	0.535	0.347	0,98	29.96
2	0.640	0.240	0,97	30.79
3	0.704	0.164	0,97	30.67
4	0.760	0.130	0,98	30.74
5	0.606	0.331	0,97	33.56
6	0.705	0.229	0,96	34.46
7	0.738	0.156	0,97	34.90
8	0.777	0.123	0,98	35.99
9	0.683	0.299	0,95	36.68
10	0.756	0.207	0,96	38.05
11	0.792	0.142	0,97	39.00
12	0.828	0.112	0,97	38.07
13	0.698	0.262	0,95	38.65
14	0.767	0.181	0,97	40.57
15	0.805	0.124	0,98	41.47
16	0.844	0.098	0,98	41.18
17	0.718	0.224	0,97	43.64
18	0.795	0.155	0,94	43.86
19	0.827	0.106	0,97	44.91
20	0.859	0.084	0,96	45.91
21	0.752	0.187	0,96	48.19
22	0.818	0.129	0,96	49.25
23	0.850	0.088	0,97	51.70
24	0.874	0.070	0,97	51.83
25	0.791	0.144	0,97	55.43
26	0.844	0.099	0,97	57.66
27	0.865	0.068	0,97	59.25
28	0.885	0.054	0,96	60.63
29	0.606	0.345	0,97	47.54
30	0.704	0.240	0,95	47.72
31	0.758	0.164	0,97	48.13
32	0.797	0.129	0,97	49.20

**Table B.21:** Total thermal resistance  $R_t$ , experimental overall thermal coefficient

$(U \cdot A)_{exp}$ , number of transfer units  $NTU_{exp}$  where

$\dot{m}_h = 0.009 \text{ kg/s}$  and air mass flow rate is changing

<i>Experiment Number</i>	$R_t$ [ $\frac{K}{W}$ ]	$(U \cdot A)_{exp}$ [ $\frac{W}{K}$ ]	$NTU_{exp}$	$\epsilon_{exp}$
1	0.006770	16.91	1.29	0.65
5	0.006747	15.68	1.26	0.65
9	0.006712	14.70	1.31	0.66
13	0.006711	13.41	1.36	0.68
17	0.006692	10.22	1.21	0.66
21	0.006666	9.88	1.41	0.71
25	0.006627	8.09	1.49	0.74
29	0.006680	15.81	1.22	0.63

**Table B.22:** Total thermal resistance  $R_t$ , experimental overall thermal coefficient

$(U \cdot A)_{exp}$ , number of transfer units  $NTU_{exp}$  where

$\dot{m}_h = 0.013 \text{ kg/s}$  and air mass flow rate is changing

<i>Experiment Number</i>	$R_t$ [ $\frac{K}{W}$ ]	$(U \cdot A)_{exp}$ [ $\frac{W}{K}$ ]	$NTU_{exp}$	$\epsilon_{exp}$
2	0.006757	17.21	1.32	0.68
6	0.006730	15.08	1.21	0.65
10	0.006713	13.86	1.23	0.66
14	0.006699	13.24	1.34	0.70
18	0.006685	11.43	1.35	0.71
22	0.006655	9.61	1.37	0.72
26	0.006616	7.34	1.36	0.72
30	0.006685	15.11	1.16	0.64

**Table B.23:** Total thermal resistance  $R_t$ , experimental overall thermal coefficient

$(U \cdot A)_{exp}$ , number of transfer units  $NTU_{exp}$  where

$\dot{m}_h = 0.019 \text{ kg/s}$  and air mass flow rate is changing

<i>Experiment Number</i>	$R_t$ [ $\frac{K}{W}$ ]	$(U \cdot A)_{exp}$ [ $\frac{W}{K}$ ]	$NTU_{exp}$	$\epsilon_{exp}$
3	0.006754	17.77	1.36	0.71
7	0.006719	14.54	1.17	0.66
11	0.006712	13.83	1.23	0.68
15	0.006697	12.27	1.25	0.69
19	0.006671	10.26	1.22	0.68
23	0.006649	7.78	1.11	0.65
27	0.006610	6.85	1.26	0.70
31	0.006666	16.34	1.25	0.68

**Table B.24:** Total thermal resistance  $R_t$ , experimental overall thermal coefficient

$(U \cdot A)_{exp}$ , number of transfer units  $NTU_{exp}$  where

$\dot{m}_h = 0.024 \text{ kg/s}$  and air mass flow rate is changing

<i>Experiment Number</i>	$R_t$ [ $\frac{K}{W}$ ]	$(U \cdot A)_{exp}$ [ $\frac{W}{K}$ ]	$NTU_{exp}$	$\epsilon_{exp}$
4	0.006751	16.44	1.26	0.69
8	0.006708	12.51	1.01	0.61
12	0.006714	13.49	1.20	0.67
16	0.006698	11.63	1.18	0.67
20	0.006672	9.33	1.11	0.65
24	0.006646	7.19	1.02	0.63
28	0.006604	5.60	1.03	0.63
32	0.006653	13.76	1.06	0.63

**Table B.25:** Experimental convection heat transfer coefficient  $h_{exp}$ ,

Stanton number  $St_{exp}$  and colburn factor  $j_{exp}$  of air side

where  $\dot{m}_h = 0.009 \text{ kg/s}$  and air mass flow rate is changing

<i>Experiment Number</i>	$h_{exp}$ [ $\frac{W}{m^2 \cdot K}$ ]	$St_{exp}$	$j_{exp}$
1	22.04	0.0063	0.0050
5	20.38	0.0061	0.0048
9	19.07	0.0063	0.0050
13	17.34	0.0065	0.0052
17	13.10	0.0058	0.0046
21	12.67	0.0067	0.0053
25	10.33	0.0071	0.0056
29	20.59	0.0059	0.0047

**Table B.26:** Experimental convection heat transfer coefficient  $h_{exp}$ ,

Stanton number  $St_{exp}$  and colburn factor  $j_{exp}$  of air side

where  $\dot{m}_h = 0.013 \text{ kg/s}$  and air mass flow rate is changing

<i>Experiment Number</i>	$h_{exp}$ [ $\frac{W}{m^2 \cdot K}$ ]	$St_{exp}$	$j_{exp}$
2	22.45	0.0064	0.0051
6	19.58	0.0059	0.0047
10	17.93	0.0059	0.0047
14	17.11	0.0065	0.0051
18	14.71	0.0065	0.0052
22	12.32	0.0065	0.0052
26	9.36	0.0064	0.0051
30	19.63	0.0056	0.0044

**Table B.27:** Experimental convection heat transfer coefficient  $h_{exp}$ ,

Stanton number  $St_{exp}$  and colburn factor  $j_{exp}$  of air side

where  $\dot{m}_h = 0.019 \text{ kg/s}$  and air mass flow rate is changing

<i>Experiment Number</i>	$h_{exp}$ [ $\frac{W}{m^2 \cdot K}$ ]	$St_{exp}$	$j_{exp}$
3	23.22	0.0066	0.0053
7	18.85	0.0057	0.0045
11	17.89	0.0059	0.0047
15	15.82	0.0060	0.0048
19	13.17	0.0058	0.0046
23	9.92	0.0052	0.0042
27	8.72	0.0060	0.0048
31	21.32	0.0061	0.0048

**Table B.28:** Experimental convection heat transfer coefficient  $h_{exp}$ ,

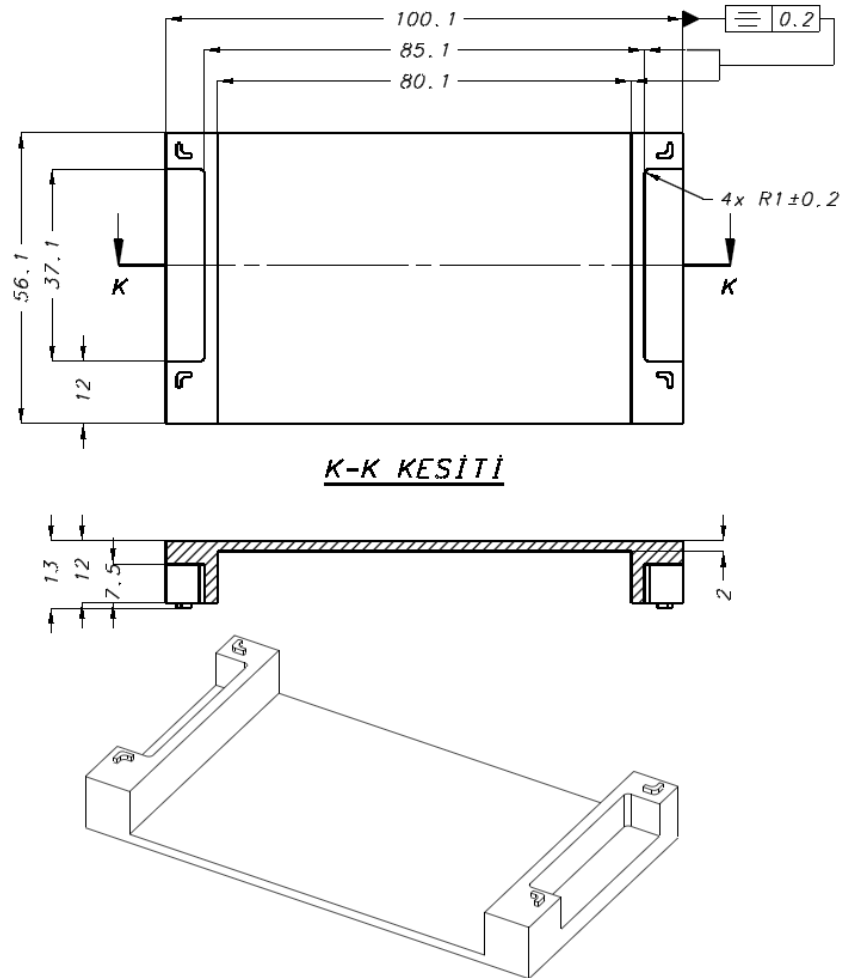
Stanton number  $St_{exp}$  and colburn factor  $j_{exp}$  of air side

where  $\dot{m}_h = 0.024 \text{ kg/s}$  and air mass flow rate is changing

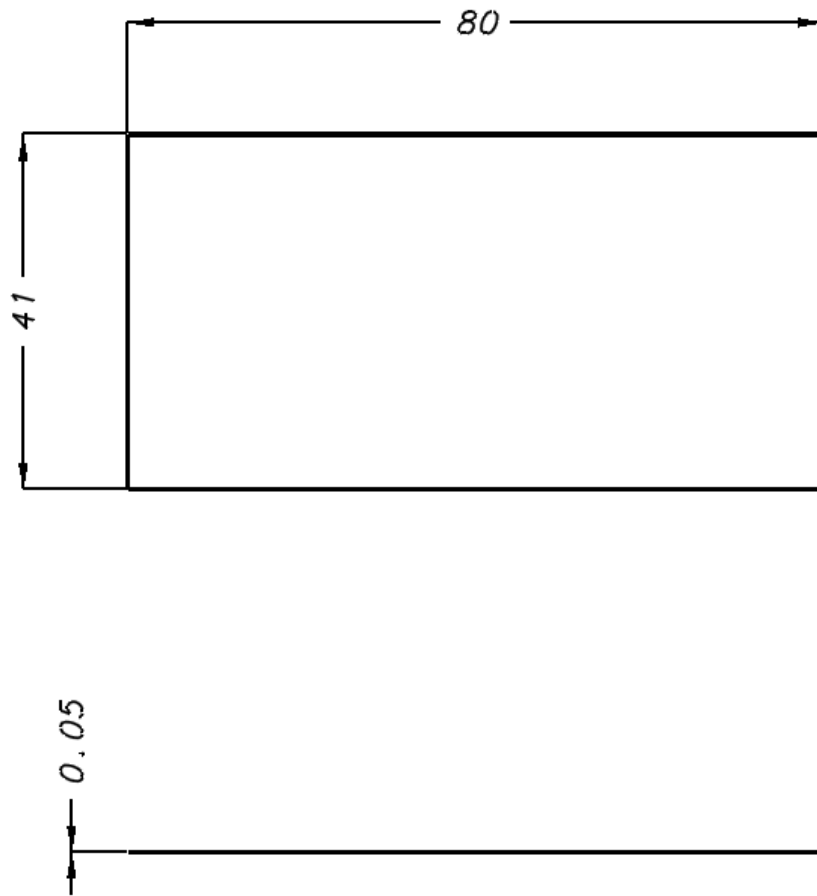
<i>Experiment Number</i>	$h_{exp}$ [ $\frac{W}{m^2 \cdot K}$ ]	$St_{exp}$	$j_{exp}$
4	21.41	0.0061	0.0049
8	16.14	0.0049	0.0039
12	17.45	0.0058	0.0046
16	14.97	0.0056	0.0045
20	11.94	0.0053	0.0042
24	9.15	0.0048	0.0039
28	7.10	0.0049	0.0039
32	17.84	0.0051	0.0041

## APPENDIX C

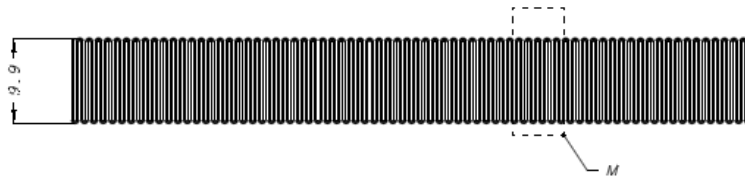
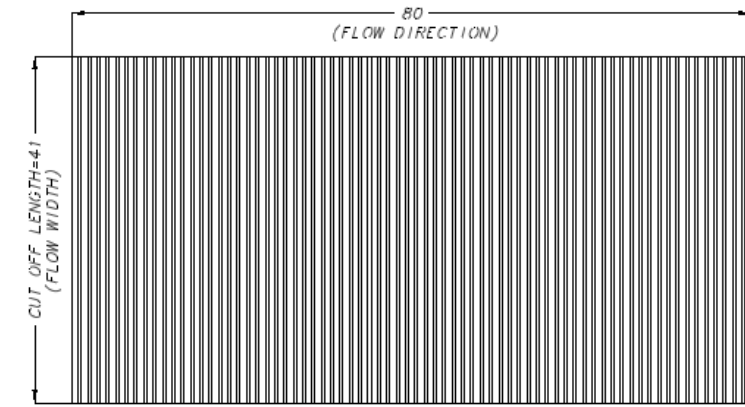
### DRAWINGS OF THE MICROCHANNEL HEAT EXCHANGER



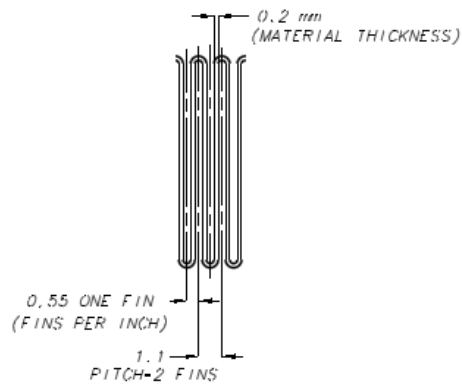
<b>1</b>		<b>BASE PLATE</b>			
<i>Part number</i>		<i>Part description</i>			
<i>Scale</i>	<i>Unit</i>	<i>General Roughness</i>	<i>Tolerances unless otherwise stated</i>	<i>Material</i>	<i>Burrfree</i>
<b>1:1</b>	<b>mm</b>	<b>3.2µm</b> ✓	<b>± 0.1 mm / ± 30'</b>	<b>AL 6061-T6</b>	



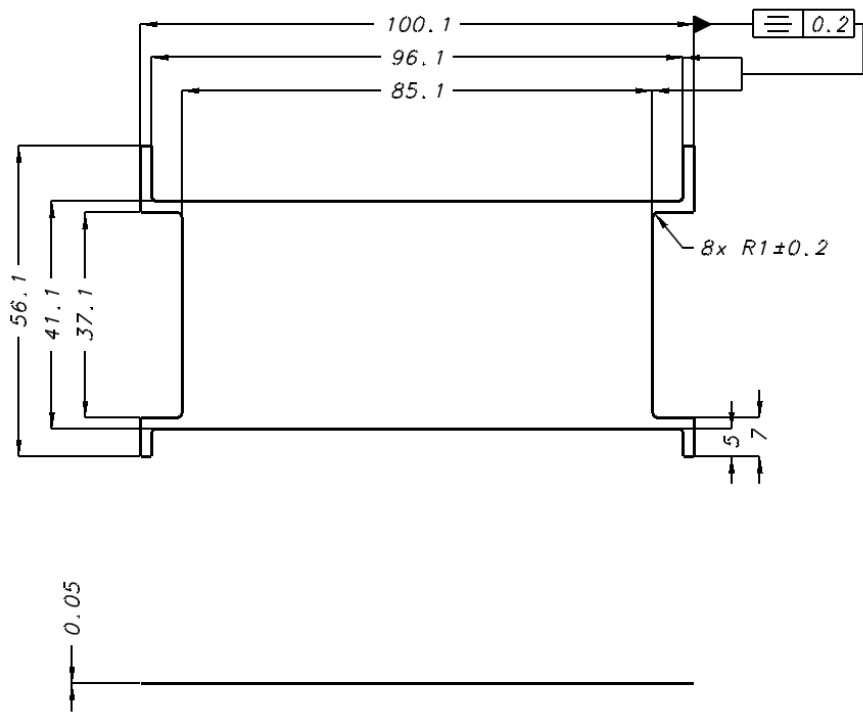
<b>2</b>		<b>FOIL BASE PLATE SIDE</b>			
<i>Part number</i>		<i>Part description</i>			
<i>Scale</i>	<i>Unit</i>	<i>General Roughness</i>	<i>Tolerances unless otherwise stated</i>	<i>Material</i>	<i>Burrfree</i>
<b>1:1</b>	<b>mm</b>	<b>3.2 μm</b> ✓	<b>± 0.1 mm / ± 30'</b>	<b>AL 4004</b>	



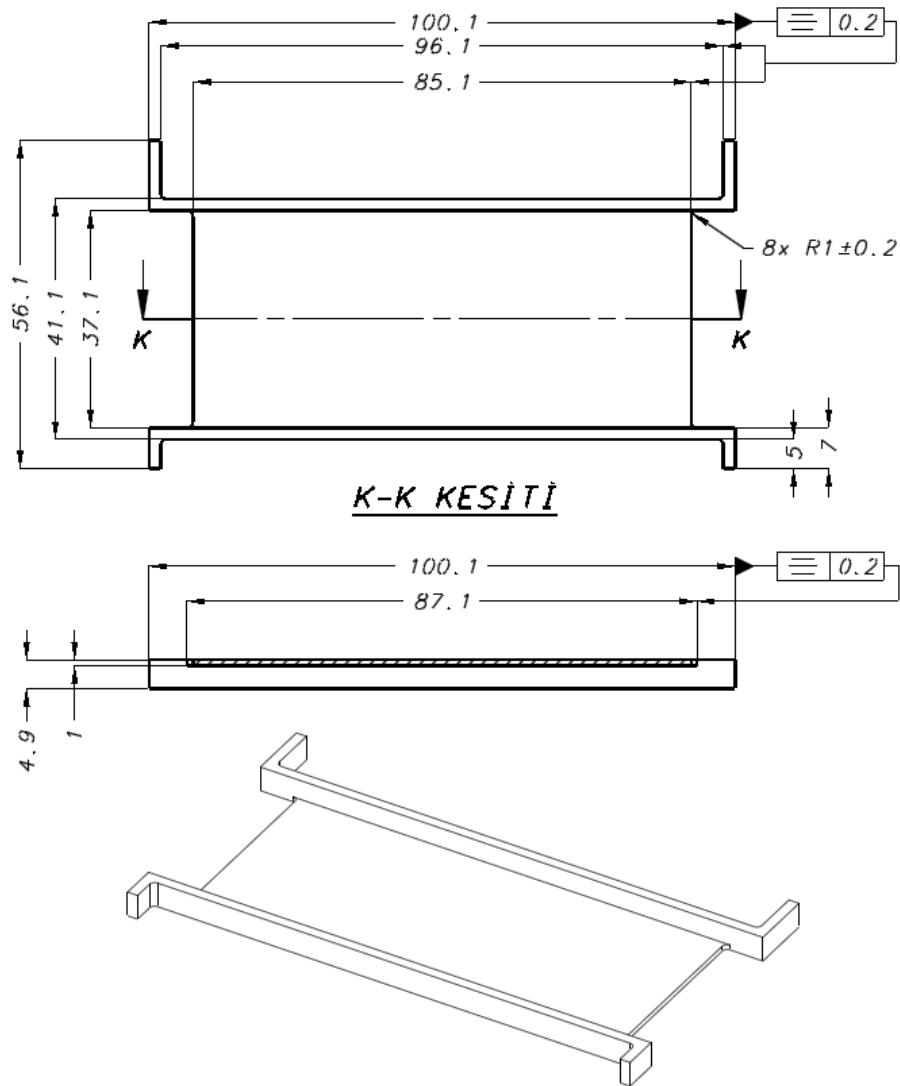
**M DETAYI**  
ÖLÇEK 5:1



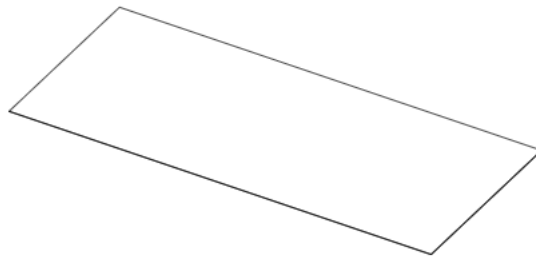
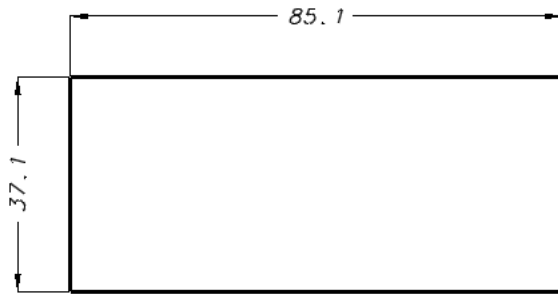
<b>3</b>		<b>FIN AIR SIDE</b>			
Part number		Part description			
Scale	Unit	General Roughness	Tolerances unless otherwise stated	Material	Burrfree
1:1	mm	3.2 $\mu\text{m}$ ✓	$\pm 0.1 \text{ mm} / \pm 30'$	AL 3003-O	



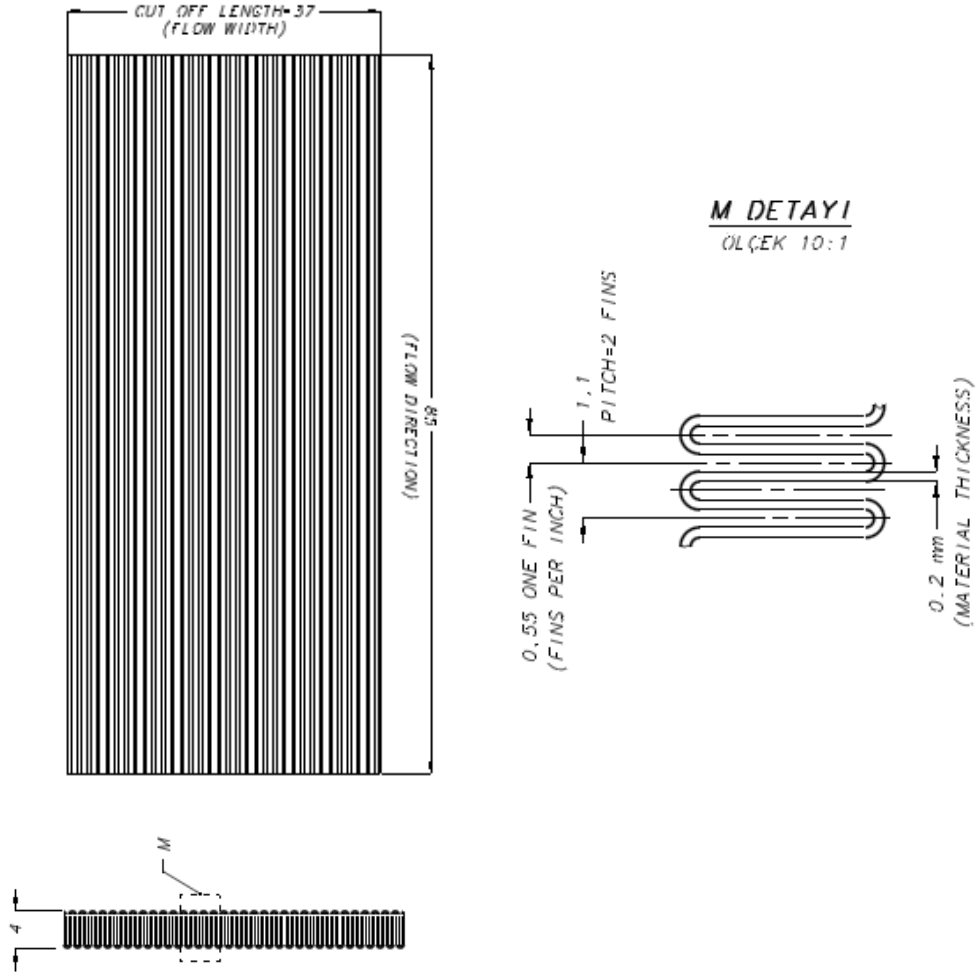
<b>4</b>		<b>FOIL AIR-WATER SIDE</b>			
<i>Part number</i>		<i>Part description</i>			
<i>Scale</i>	<i>Unit</i>	<i>General Roughness</i>	<i>Tolerances unless otherwise stated</i>	<i>Material</i>	<i>Burrfree</i>
<b>1:1</b>	<b>mm</b>	<b>3.2 μm</b> ✓	<b>± 0.1 mm / ± 30'</b>	<b>AL 4004</b>	☐ ⊕



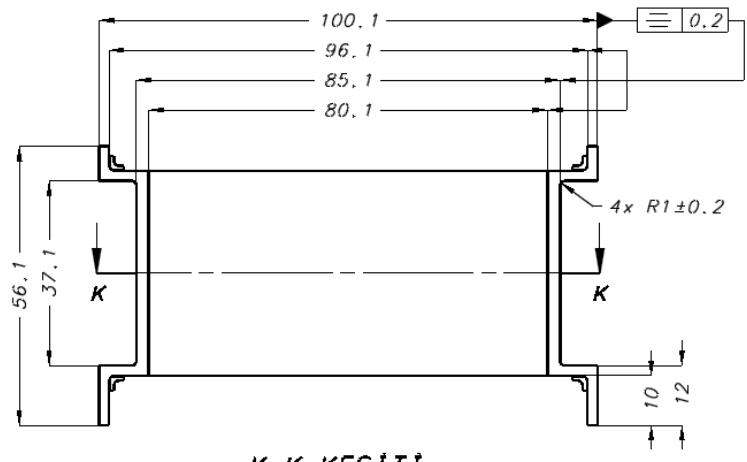
5		WATER BASE PLATE			
Part number		Part description			
Scale	Unit	General Roughness	Tolerances unless otherwise stated	Material	Burrfree
1:1	mm	3.2 $\mu\text{m}$ ✓	$\pm 0.1 \text{ mm} / \pm 30'$	AL 6061-T6	☐ ⊕



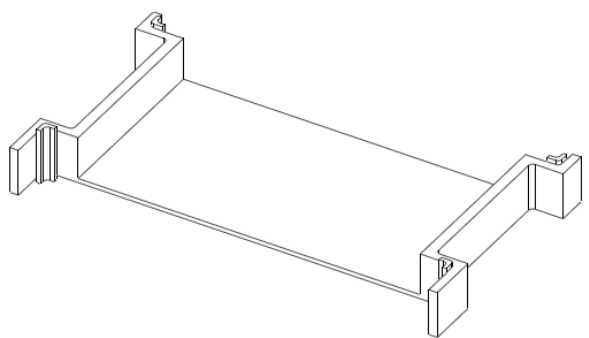
<b>6</b>		<b>FOIL WATER SIDE</b>			
<i>Part number</i>		<i>Part description</i>			
<i>Scale</i>	<i>Unit</i>	<i>General Roughness</i>	<i>Tolerances unless otherwise stated</i>	<i>Material</i>	<i>Burrfree</i>
<b>1:1</b>	<b>mm</b>	<b>3.2 μm</b> ✓	<b>± 0.1 mm / ± 30'</b>	<b>AL 4004</b>	☐ ⊕



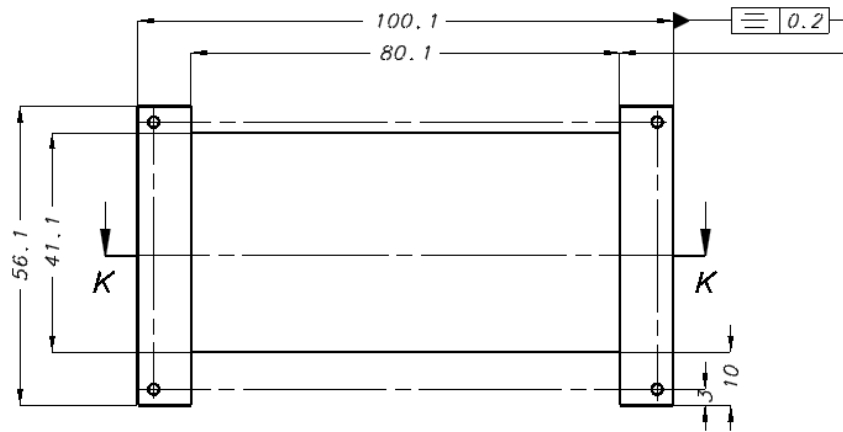
<b>7</b>		<b>FIN WATER SIDE</b>			
<i>Part number</i>		<i>Part description</i>			
<i>Scale</i>	<i>Unit</i>	<i>General Roughness</i>	<i>Tolerances unless otherwise stated</i>	<i>Material</i>	<i>Burrfree</i>
<b>1:1</b>	<b>mm</b>	<b>3.2 µm</b> ✓	<b>± 0.1 mm / ± 30'</b>	<b>AL 3003-O</b>	



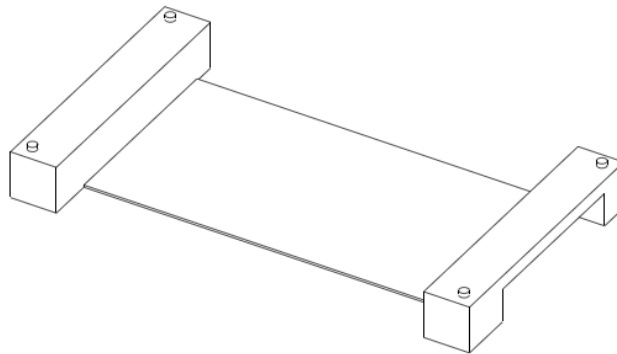
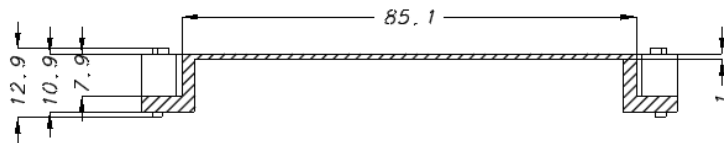
**K-K KESITI**



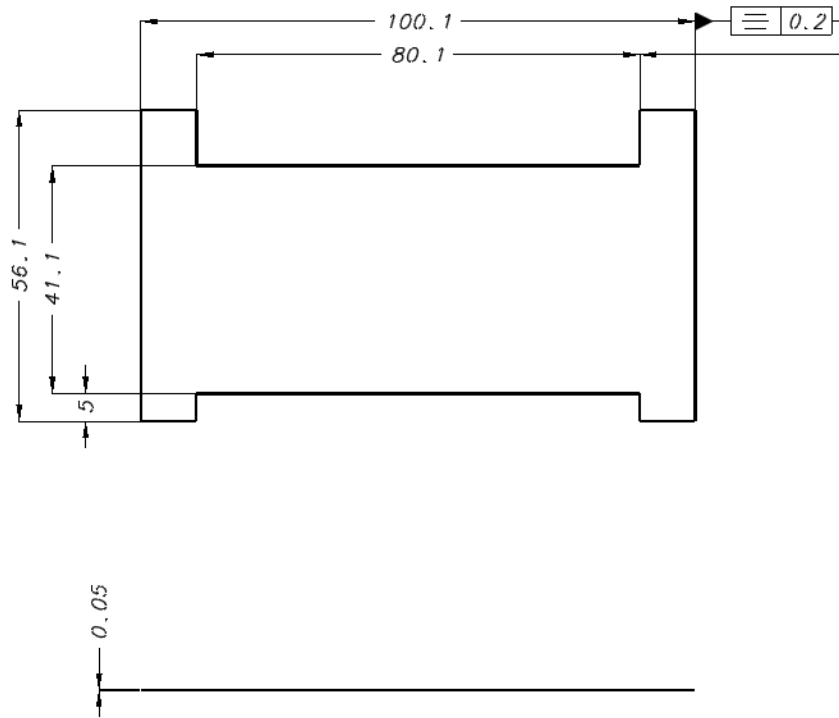
<b>8</b>		<b>AIR BASE PLATE</b>			
<i>Part number</i>		<i>Part description</i>			
<i>Scale</i>	<i>Unit</i>	<i>General Roughness</i>	<i>Tolerances unless otherwise stated</i>	<i>Material</i>	<i>Burrfree</i>
<b>1:1</b>	<b>mm</b>	<b>3.2 μm ✓</b>	<b>± 0.1 mm / ± 30'</b>	<b>AL 6061-T6</b>	



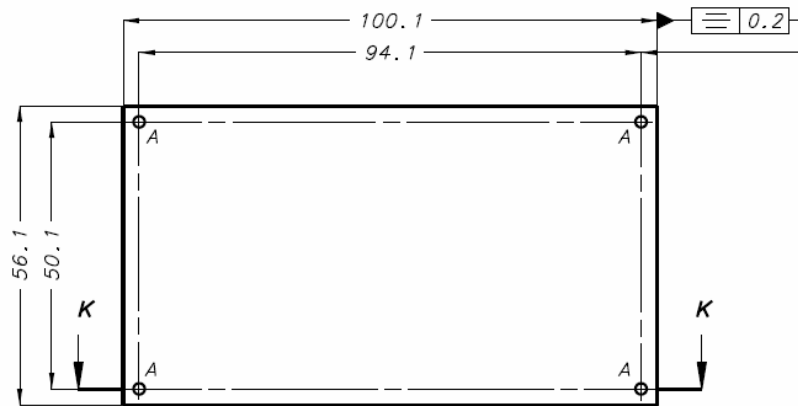
***K-K KESITI***



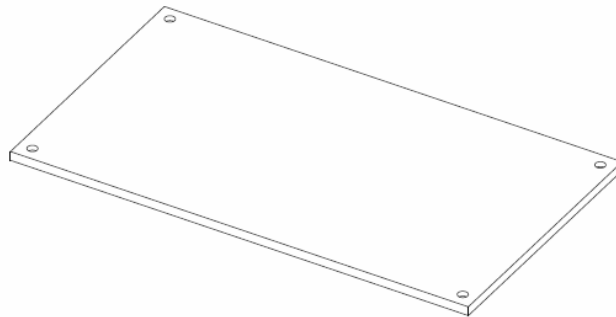
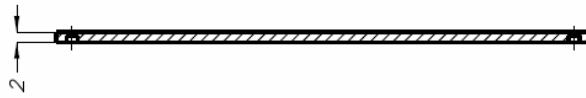
<b>9</b>		<b>TOP AIR PLATE</b>			
<i>Part number</i>		<i>Part description</i>			
<i>Scale</i>	<i>Unit</i>	<i>General Roughness</i>	<i>Tolerances unless otherwise stated</i>	<i>Material</i>	<i>Burrfree</i>
<b>1:1</b>	<b>mm</b>	<b>3.2 <math>\mu\text{m}</math> ✓</b>	<b><math>\pm 0.1 \text{ mm} / \pm 30'</math></b>	<b>AL 6061-T6</b>	



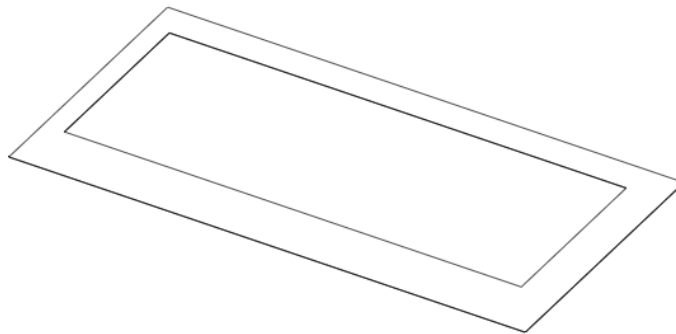
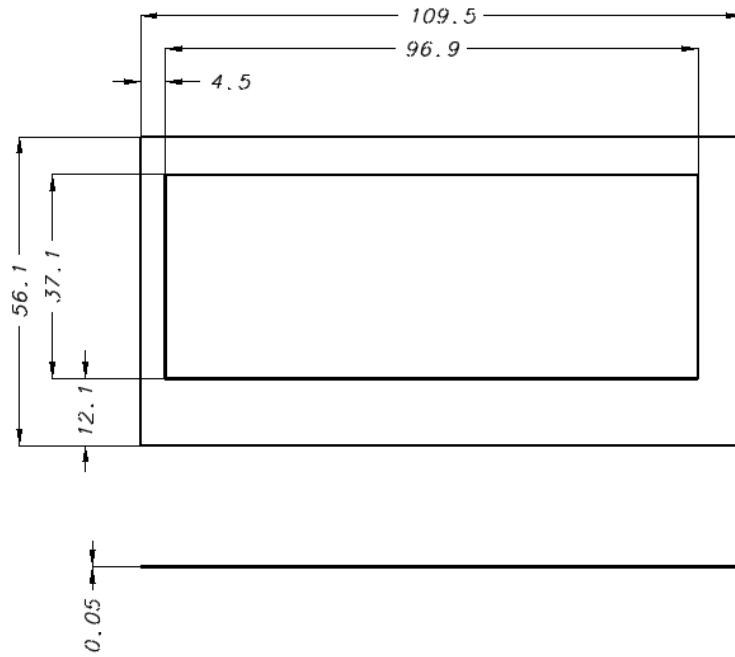
<b>10</b>		<b>FOIL TOP PLATE SIDE</b>			
<i>Part number</i>		<i>Part description</i>			
<i>Scale</i>	<i>Unit</i>	<i>General Roughness</i>	<i>Tolerances unless otherwise stated</i>	<i>Material</i>	<i>Burrfree</i>
<b>1:1</b>	<b>mm</b>	<b>3.2 μm</b> ✓	<b>± 0.1 mm / ± 30'</b>	<b>AL 4004</b>	



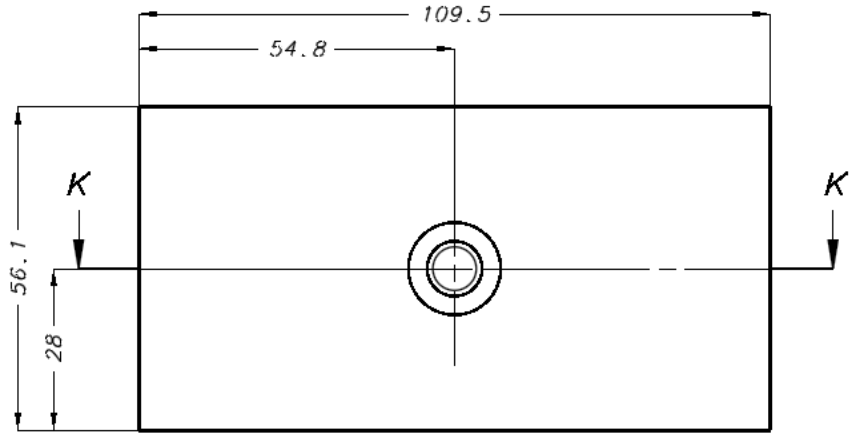
**K-K KESITI**



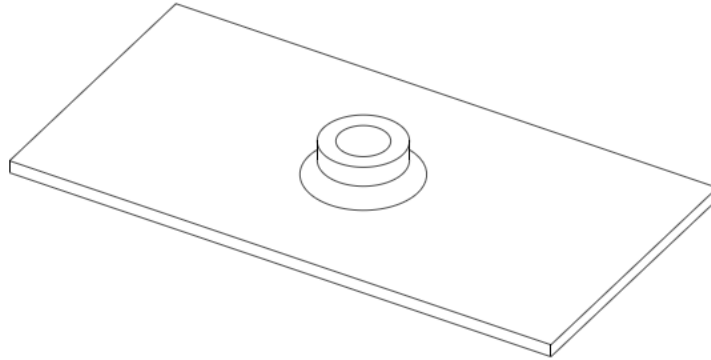
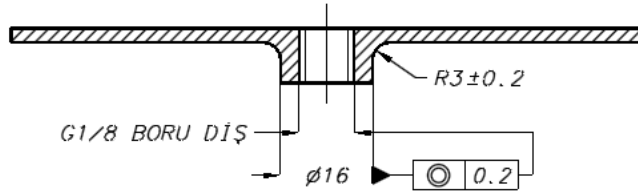
<b>11</b>		<b>TOP PLATE</b>			
<i>Part number</i>		<i>Part description</i>			
<i>Scale</i>	<i>Unit</i>	<i>General Roughness</i>	<i>Tolerances unless otherwise stated</i>	<i>Material</i>	<i>Burrfree</i>
<b>1:1</b>	<b>mm</b>	<b>3.2 μm</b> ✓	<b>± 0.1 mm / ± 30'</b>	<b>AL 6061-T6</b>	



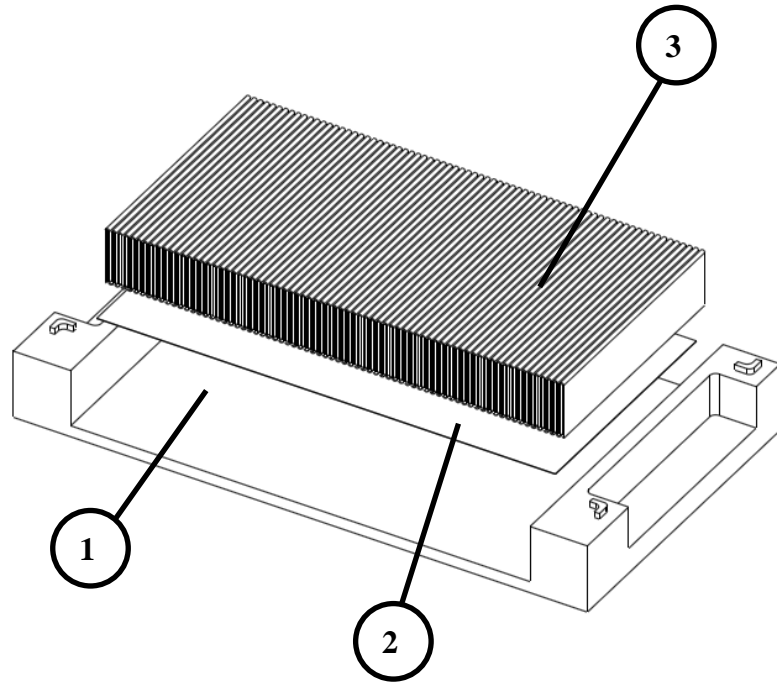
<b>12</b>		<b>FOIL SIDE</b>			
<i>Part number</i>		<i>Part description</i>			
<i>Scale</i>	<i>Unit</i>	<i>General Roughness</i>	<i>Tolerances unless otherwise stated</i>	<i>Material</i>	<i>Burrfree</i>
<b>1:1</b>	<b>mm</b>	<b>3.2 μm ✓</b>	<b>± 0.1 mm / ± 30 '</b>	<b>AL 4004</b>	



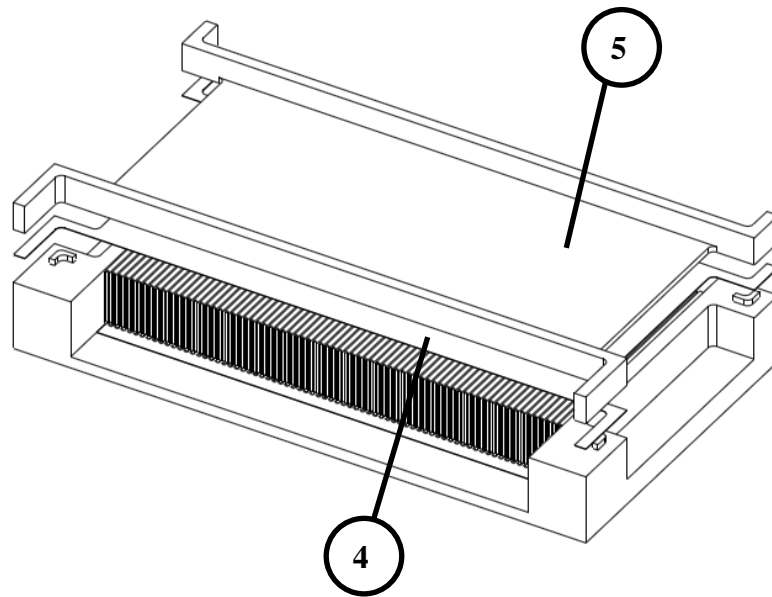
**K-K KESİTİ**



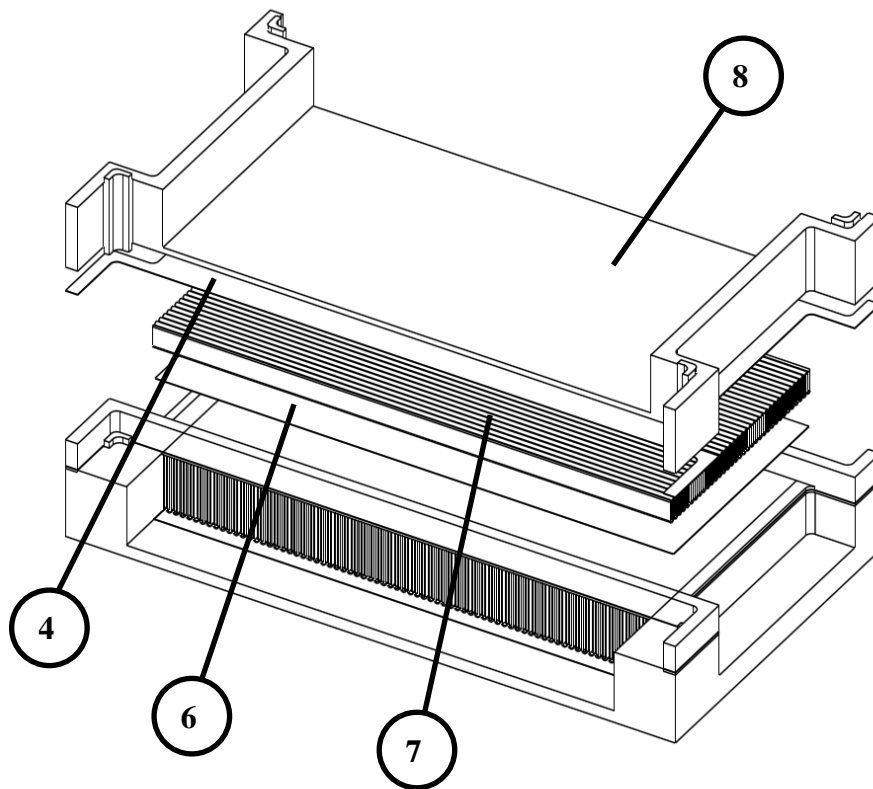
<b>13</b>		<b>SIDE PLATE</b>			
<i>Part number</i>		<i>Part description</i>			
<i>Scale</i>	<i>Unit</i>	<i>General Roughness</i>	<i>Tolerances unless otherwise stated</i>	<i>Material</i>	<i>Burrfree</i>
<b>1:1</b>	<b>mm</b>	<b>3.2 μm ✓</b>	<b>± 0.1 mm / ± 30'</b>	<b>AL 6061-T6</b>	



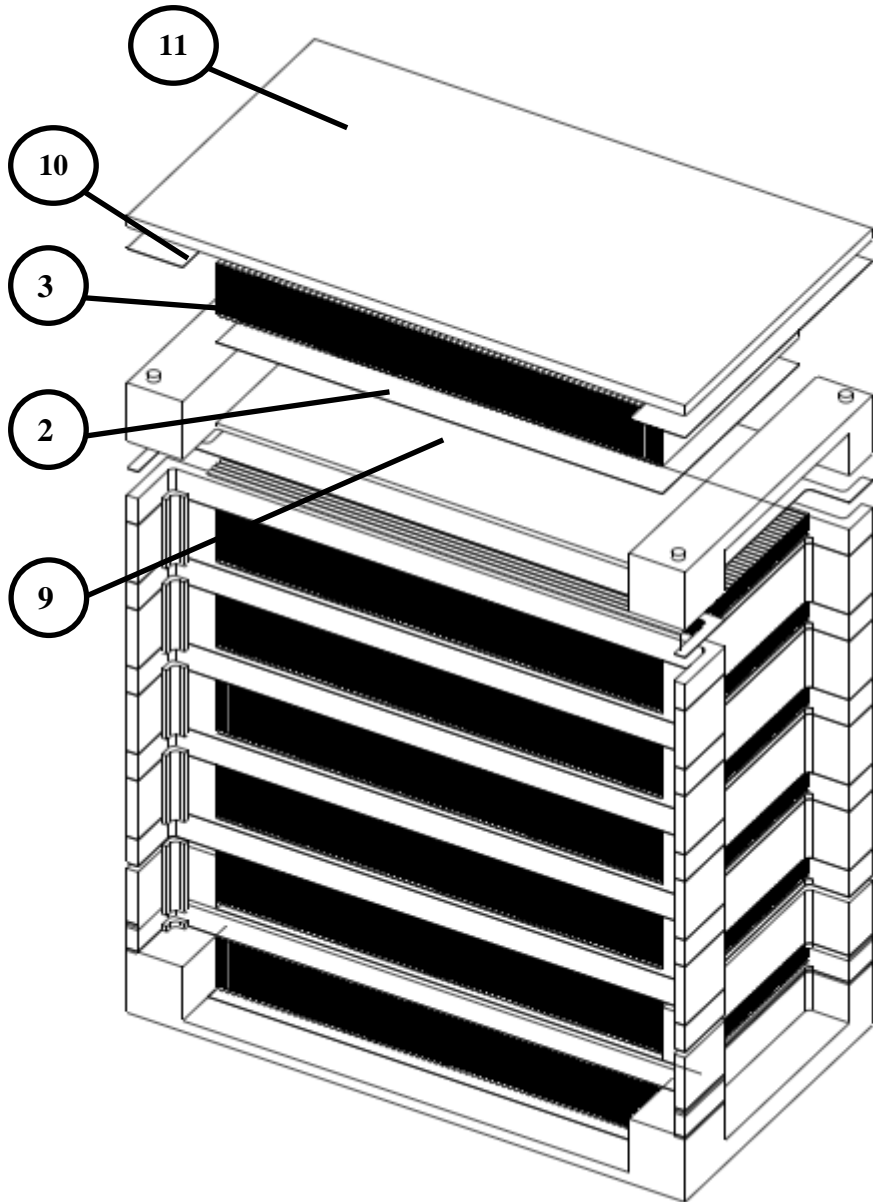
<b>Step 1</b>		<b>ASSEMBLY</b>			
<i>Part number</i>		<i>Part description</i>			
<i>Scale</i>	<i>Unit</i>	<i>General Roughness</i>	<i>Tolerances unless otherwise stated</i>	<i>Material</i>	<i>Burrfree</i>
∴	mm	μm	± .. mm / ± ..'	....	



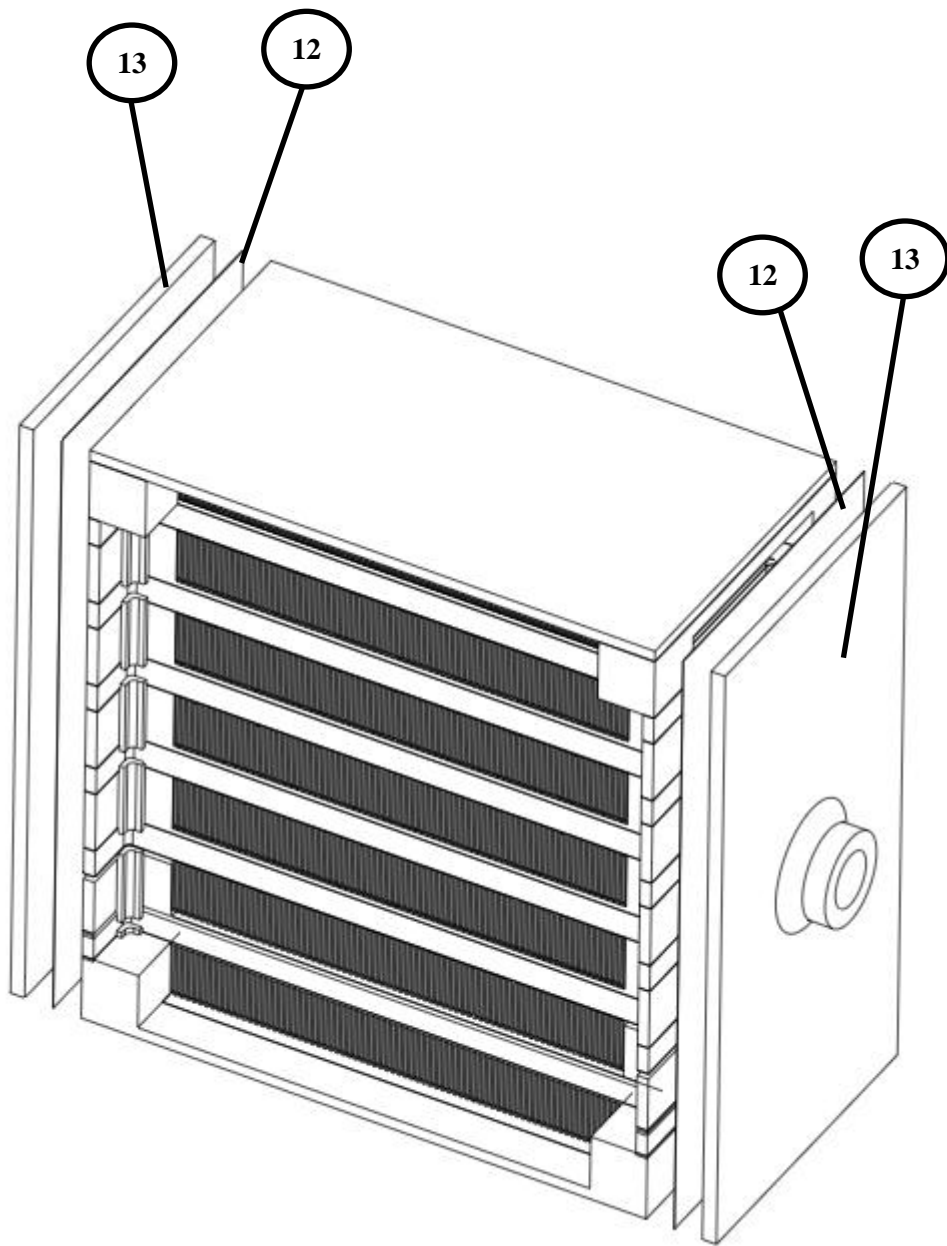
<b>Step 2</b>		<b>ASSEMBLY</b>			
<i>Part number</i>		<i>Part description</i>			
<i>Scale</i>	<i>Unit</i>	<i>General Roughness</i>	<i>Tolerances unless otherwise stated</i>	<i>Material</i>	<i>Burrfree</i>
∴	mm	μm	± .. mm / ± ..'	....	



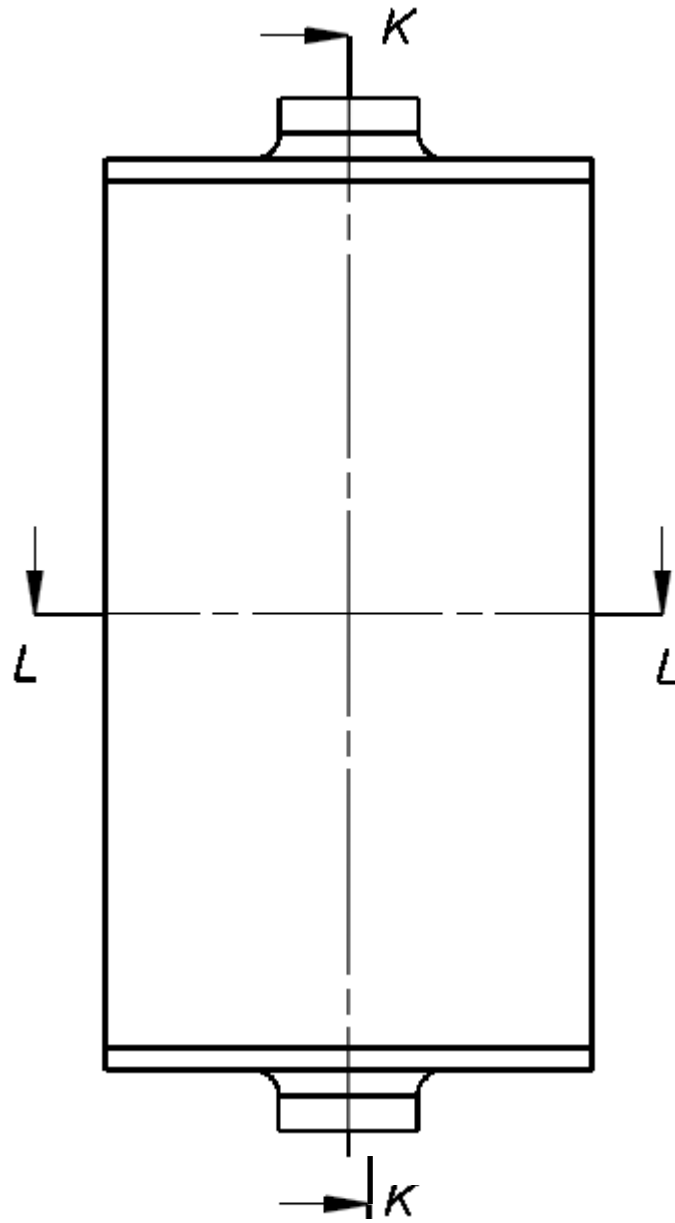
<b>Step 3</b>		<b>ASSEMBLY</b>			
<i>Part number</i>		<i>Part description</i>			
<i>Scale</i>	<i>Unit</i>	<i>General Roughness</i>	<i>Tolerances unless otherwise stated</i>	<i>Material</i>	<i>Burrfree</i>
∴	mm	µm	± .. mm / ± ..'	....	



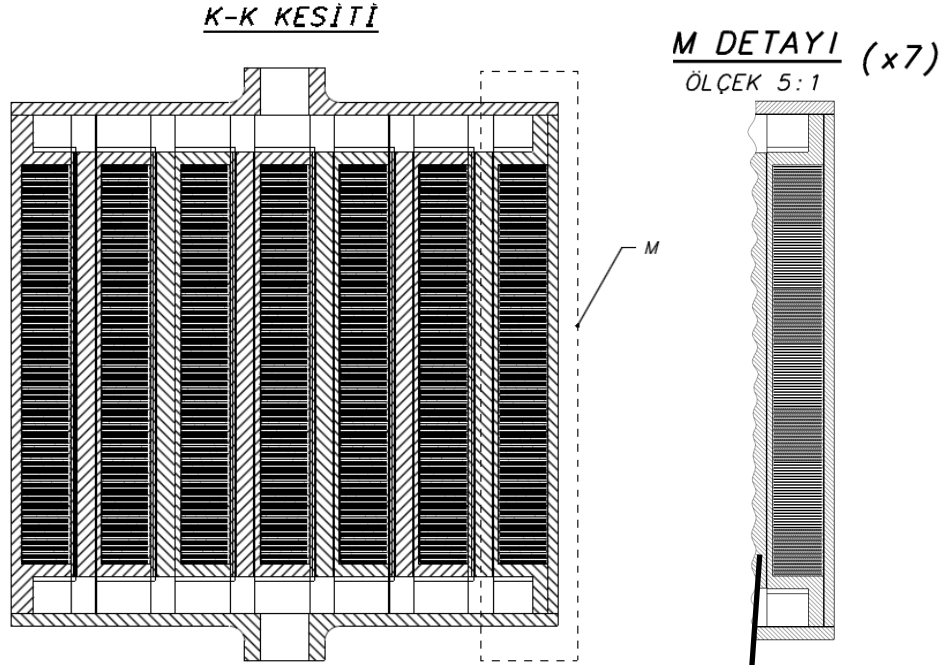
<b>Step 4</b>		<b>ASSEMBLY</b>			
<i>Part number</i>		<i>Part description</i>			
<i>Scale</i>	<i>Unit</i>	<i>General Roughness</i>	<i>Tolerances unless otherwise stated</i>	<i>Material</i>	<i>Burrfree</i>
∴	mm	µm	± .. mm / ± ..'	....	



<b>Step 5</b>		<b>ASSEMBLY</b>			
<i>Part number</i>		<i>Part description</i>			
<i>Scale</i>	<i>Unit</i>	<i>General Roughness</i>	<i>Tolerances unless otherwise stated</i>	<i>Material</i>	<i>Burrfree</i>
∴	mm	µm	± .. mm / ± .. '	....	



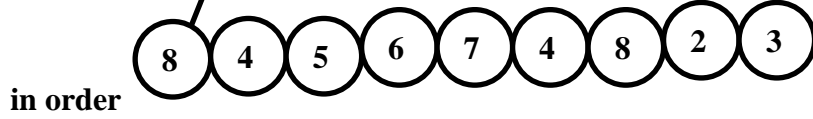
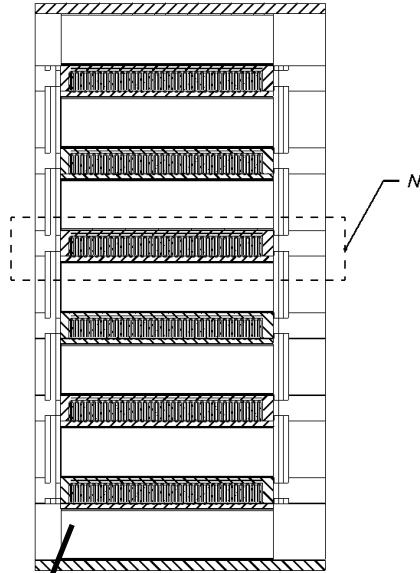
<b>MICROCHANNEL HEAT EXCHANGER</b>					
<i>Part number</i>		<i>Part description</i>			
<i>Scale</i>	<i>Unit</i>	<i>General Roughness</i>	<i>Tolerances unless otherwise stated</i>	<i>Material</i>	<i>Burrfree</i>
∴	mm	μm	± .. mm / ± ..'	....	



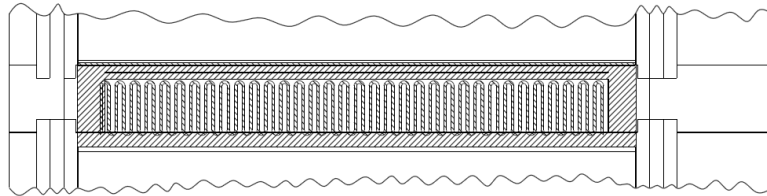
**in order**

		<b>MICROCHANNEL HEAT EXCHANGER</b>			
<i>Part number</i>		<i>Part description</i>			
<i>Scale</i>	<i>Unit</i>	<i>General Roughness</i>	<i>Tolerances unless otherwise stated</i>	<i>Material</i>	<i>Burrfree</i>
∴	<b>mm</b>	<b>µm</b>	$\pm .. \text{ mm} / \pm .. '$	....	☐ ⊕

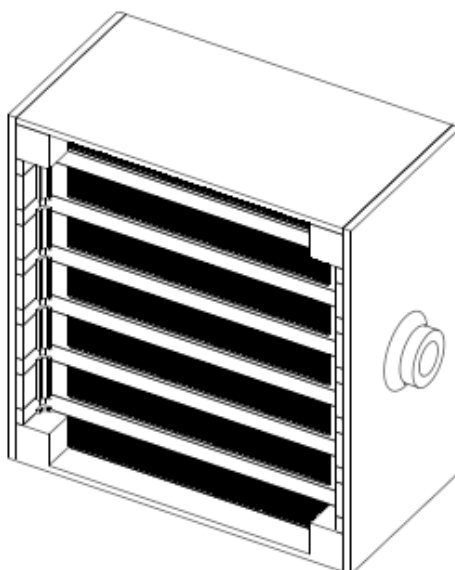
**L-L KESİTİ**



**N DETAYI** (x6)  
OLÇEK 5:1



<b>MICROCHANNEL HEAT EXCHANGER</b>					
<i>Part number</i>		<i>Part description</i>			
<i>Scale</i>	<i>Unit</i>	<i>General Roughness</i>	<i>Tolerances unless otherwise stated</i>	<i>Material</i>	<i>Burrfree</i>
∴	mm	µm	± .. mm / ± .. '	....	



<b>13</b>	SIDE PLATE	2
<b>12</b>	FOIL SIDE	2
<b>11</b>	TOP PLATE	1
<b>10</b>	FOIL TOP PLATE SIDE	1
<b>9</b>	TOP AIR PLATE	1
<b>8</b>	AIR BASE PLATE	5
<b>7</b>	FIN WATER SIDE	6
<b>6</b>	FOIL WATER SIDE	6
<b>5</b>	WATER BASE PLATE	6
<b>4</b>	FOIL AIR-WATER SIDE	12
<b>3</b>	FIN AIR SIDE	7
<b>2</b>	FOIL BASE PLATE SIDE	7
<b>1</b>	BASE PLATE	1
<i>Part Number</i>	<i>Part Description</i>	<i>Quantity</i>

<b>MICROCHANNEL HEAT EXCHANGER</b>					
<i>Part number</i>		<i>Part description</i>			
<i>Scale</i>	<i>Unit</i>	<i>General Roughness</i>	<i>Tolerances unless otherwise stated</i>	<i>Material</i>	<i>Burrfree</i>
∴	mm	µm	± .. mm / ± .. '	....	

## APPENDIX D

### TEST COMPONENTS

#### D1. Data Logger

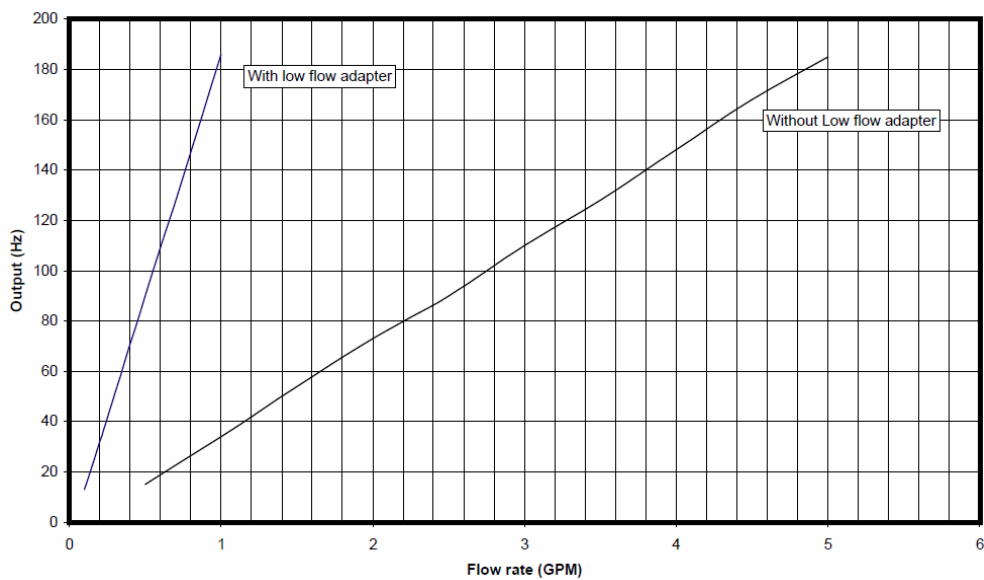
<b>Description</b>	:	AGILENT HP 34970A Data Logger
<b>Manufacturer</b>	:	Agilent Technologies
<b>Scan Count</b>	:	1 to 50,000 or continuous
<b>Scan Interval</b>	:	0-99 hours; 1ms step size
<b>Power Supply</b>	:	100V/ 120V/ 220V/ 240V $\pm$ 10%
<b>Power Consumption</b>	:	12 W
<b>Operating Environment</b>	:	Full accuracy for 0 °C to 55 °C Full accuracy to 80% RH at 40 °C
<b>Storage Environment</b>	:	-40 °C to 70 °C
<b>Weight</b>	:	3.6 kg



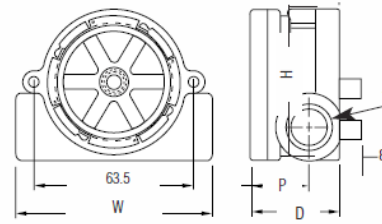
Figure D.1: The data logger

## D2. Flowmeter

<b>Description</b>	:	Rotorflow Indicator ad Output
<b>Manufacturer</b>	:	Gems Sensors Inc.
<b>Maximum Operating Pressure</b>	:	14 bar
<b>Maximum Operating</b>	:	100° C
<b>Electronics</b>	:	65 ° C Ambient
<b>Speed</b>	:	18400 RPM
<b>Maximum Viscosity</b>	:	45 cSt
<b>Input Power</b>	:	4.5 to 24 VDC
<b>Frequency Output Range</b>	:	25 Hz (Low Flow) to 225 Hz (High Flow)
<b>Maximum Current Source</b>	:	70 mA
<b>Electrical termination</b>	:	AWG 22 PVC-Jacketed Cable, Length 60 cm Colour Code: Red= +VDC Black= Ground, White=Signal Output



**Figure D.2:** The flowmeter output & flow rate graph



T	W	H	D	P
1/4	77	60	35	20

**Figure D.3:** The flowmeter dimensions

### D3. Temperature / Pressure Transducer

<b>Description</b>	:	Miniature, rugged temperature/pressure transducer
<b>Manufacturer</b>	:	Kulite Semiconductor Products Inc
<b>Pressure Range</b>	:	0-3.5 Bar absolute
<b>Material</b>	:	Aluminum body, platinum sensor material
<b>Color</b>	:	Gray

#### Physical Characteristics:

<b>Electrical Connection</b>	:	6 Conductor 26 AWG Viton Cable Without Shielding 1 Meter Long
<b>Weight</b>	:	15 Grams (Max.) excluding cable
<b>Sensing Principle</b>	:	Fully Active Four Arm Wheatstone Bridge Dielectrically Isolated Silicon on Silicon Patented Leadless Technology
<b>Mounting Torque</b>	:	6 Nm $\pm$ 1 Nm

#### Environmental Characteristics:

<b>Operating Temperature Range</b>	:	-65° F to +350° F ( -55° C to +175° C )
<b>Compensated Temperature Range</b>	:	+80° F to +180° F (+25° C to +80° C ) Any 100° F Range Within The Operating Range on Request
<b>Thermal Zero Shift</b>	:	$\pm$ 1% FS/100° F (55° C) (Typ.) ( $\pm$ 2 % FS/100° F For 25 PSI Range)
<b>Thermal Sensitivity Shift</b>	:	$\pm$ 1% FS/100° F (55° C) (Typ.) ( $\pm$ 2 % FS/100° F For 25 PSI Range)
<b>Linear Vibration</b>	:	100 g Peak, Sine up to 5000 Hz
<b>Humidity</b>	:	100% Relative Humidity
<b>Mechanical Shock</b>	:	20,000g 100 $\mu$ sec





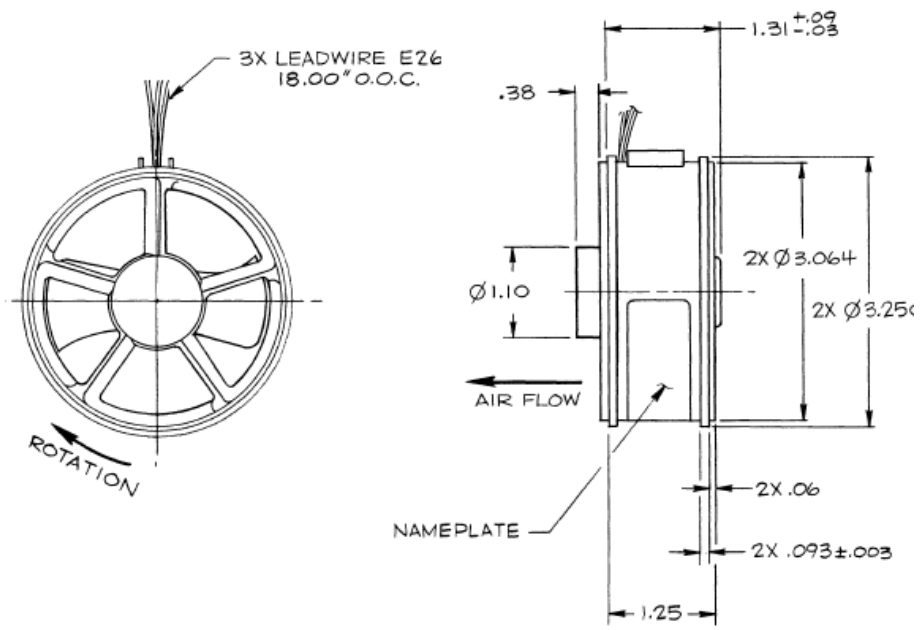
**Figure D.5:** The temperature / pressure transducer

#### D4. Axial Fan

<b>Description</b>	:	Tube axial fans, with electronically commutated DC motor are integrated axial flow air moving devices in which the motor is cast inside the impeller to achieve the smallest possible axial dimension.
<b>Manufacturer</b>	:	Amatek Aerospace & Defense Inc.
<b>Max. Air flow (free air)</b>	:	119 CFM
<b>Nominal Voltage</b>	:	26 VDC
<b>Power Input</b>	:	1.2 Amp x 26 Volt = 31.2 Watt
<b>Speed</b>	:	18400 RPM
<b>Max. Ambient Temp.</b>	:	+100° C
<b>Min. Ambient Temp.</b>	:	-54° C
<b>Acoustic levels</b>	:	as low as 55 dBA
<b>Mass</b>	:	186 g
<b>Materials</b>	:	All aluminum components are finished with a chemical conversion coating per MIL-C-5541, top coat of lusterless black enamel, color #37038, per Federal Standard 595 conforming to TT-E-489 Type B. The shaft and hardware are of corrosion-resistant stainless steel. The impeller runs on two high-precision, double-shielded, stainless



**Figure D.6:** The fan dimensions [inch]



NAMEPLATE MOTOR DATA (NOM)

VOLTS ——— 26VDC  
 AMPS ——— 1.2  
 RPM ——— 18,400

WIRING DIAGRAM

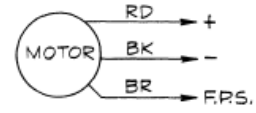


**Figure D.7:** Detailed dimensions of the fan

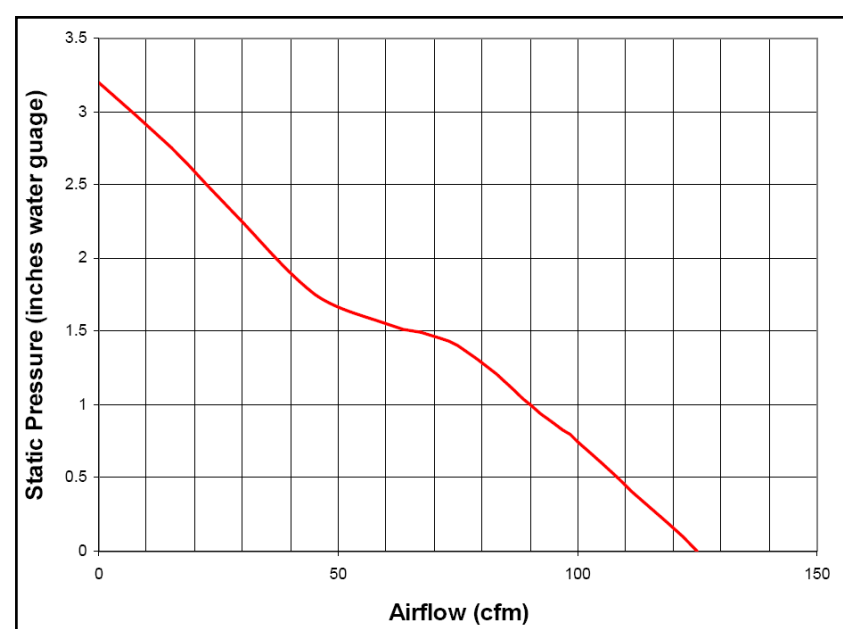


**Figure D.8:** The performance curve of the fan

## D5. Pump

<b>Manufacturer</b>	:	Gems Sensors Inc.
<b>Type</b>	:	GB P25
<b>Displacement</b>	:	0.58 ml/rev
<b>Maximum Flow (4 Pole Speed)</b>	:	850 ml/mn 1450 RPM (50 Hz)
<b>Maximum flow (2 Pole Speed)</b>	:	1660 ml/mn 2850 RPM (50 Hz)
<b>Maximum Differential Pressure</b>	:	8.7 Bar
<b>Maximum System Pressure</b>	:	21 Bar
<b>NIPR (Absolute)</b>	:	180 mBar
<b>Wet Lift (Typical)</b>	:	51 cm H <sub>2</sub> O (1450 RPM)
<b>Viscosity Range</b>	:	0.2 to 1500 cp
<b>Maximum Speed</b>	:	10000 RPM
<b>Rotation (Facing Motor Shaft)</b>	:	CW
<b>Weight (Pump head)</b>	:	0.34 kg
<b>Ports</b>	:	1/8-27 (F) NPT Side Ports
<b>Driven Magnet</b>	:	Ferrite

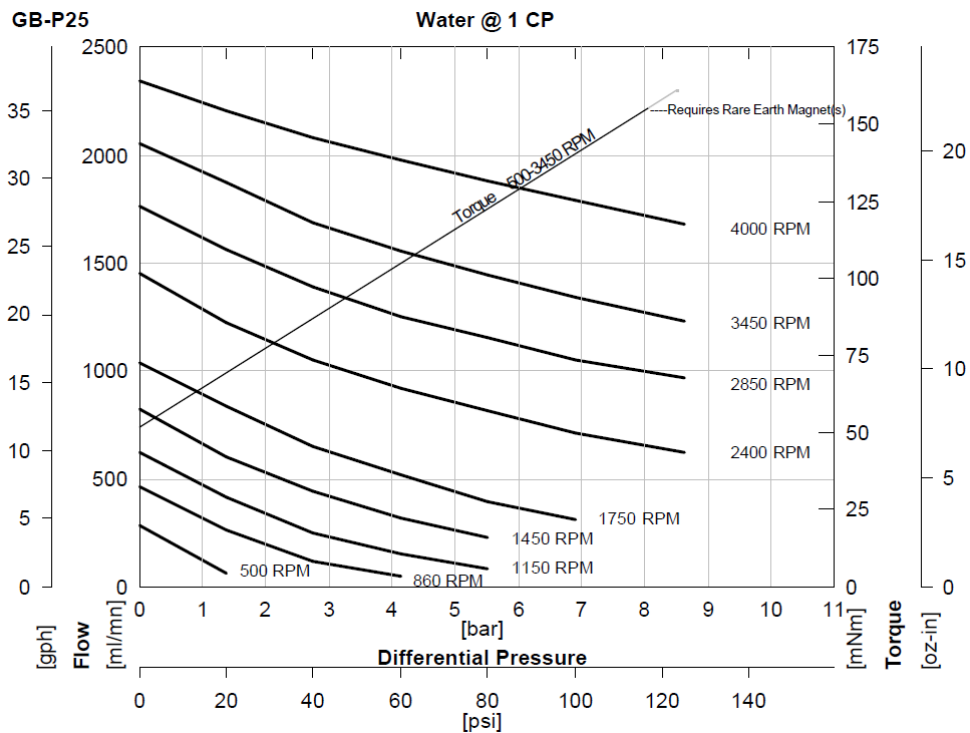


**Figure D.9:** Performance curve of the pump

## D6. Expansion Unit

<b>Description</b>	:	Edge Welded Bellow
<b>Manufacturer</b>	:	Bellows Tech. LLC
<b>Materials</b>	:	Flanges 316L SS ; Bellows Core: AM350
<b>Spring Constant</b>	:	0.95 N/mm
<b>Volume Change Per Stroke</b>	:	1.522 in <sup>3</sup>
<b>Extended Length</b>	:	1.549 in
<b>Compressed Stroke</b>	:	0.309 in
<b>Operating Stroke</b>	:	1.24 in

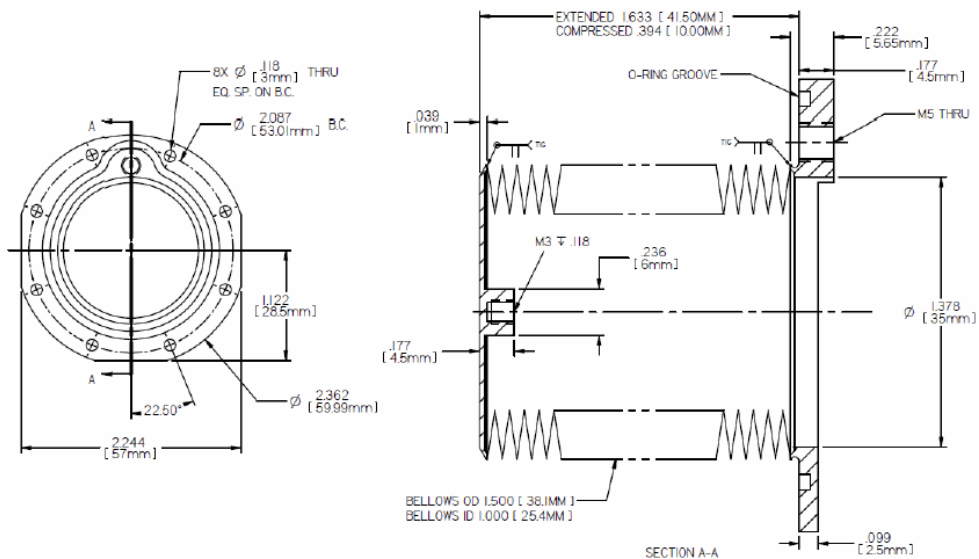


**Figure D.10:** Detailed drawings of the expansion unit

## D7. Heating Tank

<b>Description</b>	:	Heating Tank
<b>Material</b>	:	AL 5083
<b>Dimensions</b>	:	249x249x215 mm (LxWxH)
<b>Inside Volume</b>	:	approximately 8 lt
<b>Number of Heaters</b>	:	6
<b>Heaters Output</b>	:	200 W per heaters
<b>Number of expansion</b>	:	Max. 4

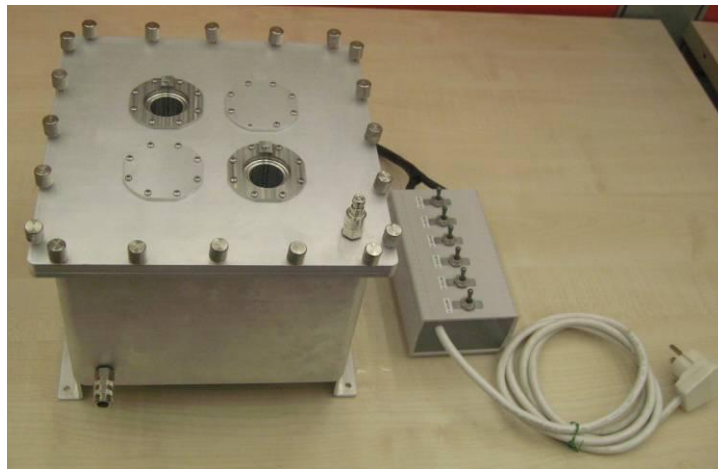


**Figure D.11:** Isometric view of the heating tank



**Figure D.12:** Top view of the heating tank



**Figure D.13:** Bottom side view of the heating tank

## D8. Air Velocity Meter

<b>Description</b>	:	Air Velocity Meter
<b>Manufacturer</b>	:	Airflow Instruments
<b>Velocity Range</b>	:	0.25 to 30 m/s
<b>Velocity Accuracy</b>	:	$\pm 1.0\%$ of reading
<b>Temperature Range</b>	:	0 to 60 °C
<b>Temperature</b>	:	$\pm 0.5$ °C
<b>Instrument Operating Conditions</b>	:	Altitude up to 4000 meters
	:	Relative humidity up to 80%
	:	Pollution degree 1 in accordance with IEC 664
	:	Transient over voltage category II
<b>Logging Interval</b>	:	1 second to 1 hour
<b>Dimensions</b>	:	8.4x17.8x4.4 cm
<b>Weight</b>	:	0.27 kg



**Figure D.14:** Air velocity meter

## APPENDIX E

### MATERIAL PROPERTIES

**Table E.1:** Air properties at atmospheric pressure [38]

<b>T</b> [ C ]	<b><math>\rho</math></b> [kg/m <sup>3</sup> ]	<b><math>c_p</math></b> [J/kg·K]	<b><math>\mu \cdot 10^5</math></b> [kg/m·s]	<b><math>\nu \cdot 10^6</math></b> [m <sup>2</sup> /s]	<b>k</b> [W/m·K]	<b><math>\alpha \cdot 10^6</math></b> [m <sup>2</sup> /s]	<b>Pr</b>
0	1.2930	1005	1.72	13.30	0.0242	18.7	0.711
20	1.2045	1005	1.82	15.11	0.0257	21.4	0.713
40	1.1267	1009	1.91	16.97	0.0271	23.9	0.711
60	1.0595	1009	2.00	18.90	0.0285	26.7	0.709
80	0.9908	1009	2.10	20.94	0.0299	29.6	0.708
100	0.9458	1013	2.18	23.06	0.0314	32.8	0.704

**Table E.2:** Calculated air properties at atmospheric pressure for each experimental average temperatures of air

<b>T</b> [ C]	<b><math>\rho</math></b> [kg/m <sup>3</sup> ]	<b><math>c_p</math></b> [J/kg·K]	<b><math>\mu \cdot 10^5</math></b> [kg/m·s]	<b><math>\nu \cdot 10^6</math></b> [m <sup>2</sup> /s]	<b>k</b> [W/m·K]	<b><math>\alpha \cdot 10^6</math></b> [m <sup>2</sup> /s]	<b>Pr</b>
34.2	1.1493	1008	1.88	16.43	0.0267	23.2	0.712
35.6	1.1438	1008	1.89	16.56	0.0268	23.4	0.711
36.1	1.1419	1008	1.89	16.61	0.0268	23.4	0.711
36.6	1.1399	1008	1.89	16.65	0.0269	23.5	0.711
36.7	1.1395	1008	1.90	16.66	0.0269	23.5	0.711
38.7	1.1318	1009	1.90	16.85	0.0270	23.7	0.711
39.8	1.1275	1009	1.91	16.95	0.0271	23.9	0.711
40.1	1.1264	1009	1.91	16.98	0.0271	23.9	0.711
40.2	1.1260	1009	1.91	16.99	0.0271	23.9	0.711
40.3	1.1257	1009	1.91	17.00	0.0271	23.9	0.711
40.4	1.1254	1009	1.91	17.01	0.0271	24.0	0.711
40.6	1.1247	1009	1.91	17.03	0.0271	24.0	0.711
41.0	1.1233	1009	1.91	17.07	0.0272	24.0	0.711
41.5	1.1217	1009	1.92	17.11	0.0272	24.1	0.711
41.8	1.1207	1009	1.92	17.14	0.0272	24.2	0.711
42.0	1.1200	1009	1.92	17.16	0.0272	24.2	0.711
42.5	1.1183	1009	1.92	17.21	0.0273	24.3	0.711
43.2	1.1159	1009	1.92	17.28	0.0273	24.3	0.711
43.4	1.1153	1009	1.93	17.30	0.0273	24.4	0.711
43.7	1.1143	1009	1.93	17.33	0.0274	24.4	0.711
44.8	1.1109	1009	1.93	17.42	0.0274	24.6	0.711
44.7	1.1106	1009	1.93	17.43	0.0274	24.6	0.711
45.3	1.1089	1009	1.93	17.48	0.0275	24.6	0.710
46.6	1.1045	1009	1.94	17.61	0.0276	24.8	0.710
47.1	1.1028	1009	1.94	17.66	0.0276	24.9	0.710
47.5	1.1015	1009	1.94	17.69	0.0276	25.0	0.710
49.5	1.0948	1009	1.95	17.89	0.0278	25.2	0.710
50.7	1.0907	1009	1.96	18.00	0.0278	25.4	0.710
51.3	1.0887	1009	1.96	18.06	0.0279	25.5	0.710
52.0	1.0864	1009	1.96	18.13	0.0279	25.6	0.710

**Table E.3:** Water (saturated) thermal properties [38]

<b>T</b> [ C]	<b>P</b> [kg/m <sup>3</sup> ]	<b>k</b> [W/m·C]	<b>c<sub>p</sub></b> [J/kg·C]	<b>μ</b> [kg/m·s]	<b>Pr</b>
0.0	999.8	0.566	4225	0.00179	12,9900
4.44	999.8	0.575	4208	0.00155	11,2047
10.0	999.2	0.585	4195	0.00131	9,2465
15.56	998.6	0.595	4186	0.00112	7,8825
21.11	997.4	0.604	4179	0.00098	6,7591
26.67	995.8	0.614	4179	0.00086	5,8584
32.22	994.9	0.623	4174	0.000765	5,1571
37.78	993.0	0.630	4174	0.000682	4,5344
43.33	990.6	0.637	4174	0.000616	4,0446
48.89	988.8	0.644	4174	0.000562	3,6020
54.44	985.7	0.649	4179	0.000513	3,2801
60.0	983.3	0.654	4179	0.000471	2,9799
65.55	980.3	0.659	4183	0.000430	2,7172
71.11	977.3	0.665	4186	0.000401	2,4811
76.67	973.7	0.668	4191	0.000372	2,2958
82.22	970.2	0.673	4195	0.000347	2,1311
87.78	966.7	0.675	4199	0.000327	1,9995
93.33	963.2	0.678	4204	0.000306	1,8774
104.4	955.1	0.684	4216	0.000267	1,6541
115.6	946.7	0.685	4229	0.000244	1,4850
126.7	937.2	0.685	4250	0.000219	1,3420

**Table E.4:** Calculated water thermal properties for each experimental average temperature of water

<b>T</b> [ C]	<b>P</b> [kg/m <sup>3</sup> ]	<b>k</b> [W/m·C]	<b>c<sub>p</sub></b> [J/kg·C]	<b>μ</b> [kg/m·s]	<b>Pr</b>
54.35	985.8	0.649	4178.92	0.000514	3.285
54.50	985.7	0.649	4179.00	0.000512	3.277
54.55	985.7	0.649	4179.00	0.000512	3.274
54.75	985.6	0.649	4179.00	0.000510	3.263
57.80	984.2	0.652	4179.00	0.000487	3.101
59.10	983.7	0.653	4179.00	0.000478	3.029
60.45	983.1	0.654	4179.32	0.000468	2.956
61.45	982.5	0.655	4180.05	0.000460	2.902
61.75	982.4	0.656	4180.26	0.000458	2.885
61.80	982.3	0.656	4180.30	0.000458	2.883
62.05	982.2	0.656	4180.48	0.000456	2.871
62.25	982.1	0.656	4180.62	0.000454	2.862
63.10	981.6	0.657	4181.23	0.000448	2.825
64.30	981.0	0.658	4182.10	0.000439	2.772
64.65	980.8	0.658	4182.35	0.000437	2.757
65.00	980.6	0.659	4182.60	0.000434	2.741
67.70	979.1	0.661	4184.16	0.000419	2.624
68.05	979.0	0.662	4184.35	0.000417	2.610
69.70	978.1	0.663	4185.24	0.000408	2.540
69.85	978.0	0.664	4185.32	0.000408	2.534
71.65	977.0	0.665	4186.49	0.000398	2.458
72.55	976.4	0.666	4187.29	0.000393	2.428
73.00	976.1	0.666	4187.70	0.000391	2.413
73.55	975.7	0.666	4188.19	0.000388	2.396
73.70	975.6	0.666	4188.33	0.000387	2.391
74.70	975.0	0.667	4189.23	0.000382	2.359
75.65	974.4	0.667	4190.08	0.000377	2.328
75.85	974.2	0.668	4190.26	0.000376	2.322
80.10	971.5	0.671	4193.47	0.000357	2.193
82.00	970.3	0.673	4194.84	0.000348	2.140
83.60	969.3	0.673	4195.99	0.000342	2.100
85.05	968.4	0.674	4197.04	0.000335	2.065

**Table E.5:** Calculated water and air viscosity for each experimental  
at wall temperature

<b>Experiment</b>	<b>T [ C] Wall Temperature</b>	<b><math>\mu</math> [kg/m·s] Water Viscosity</b>	<b><math>\mu</math> [kg/m·s] Air Viscosity</b>
1	37.1	0.000692	0.000019
2	40.9	0.000645	0.000019
3	44.3	0.000607	0.000019
4	48.9	0.000562	0.000020
5	45.6	0.000594	0.000019
6	51.9	0.000535	0.000020
7	54.8	0.000510	0.000020
8	57.0	0.000494	0.000020
9	48.2	0.000569	0.000019
10	46.8	0.000582	0.000019
11	49.5	0.000557	0.000020
12	56.7	0.000496	0.000020
13	57.4	0.000491	0.000020
14	50.1	0.000551	0.000020
15	51.5	0.000539	0.000020
16	60.2	0.000470	0.000020
17	62.6	0.000452	0.000020
18	64.6	0.000437	0.000020
19	65.9	0.000428	0.000020
20	65.8	0.000429	0.000020
21	69.6	0.000409	0.000020
22	70.9	0.000402	0.000021
23	71.7	0.000398	0.000021
24	71.9	0.000397	0.000021
25	77.8	0.000367	0.000021
26	79.5	0.000359	0.000021
27	80.3	0.000356	0.000021
28	81.1	0.000352	0.000021
29	66.1	0.000427	0.000020
30	64.9	0.000435	0.000020
31	67.1	0.000422	0.000020
32	68.2	0.000416	0.000020

## Aluminum 6061-T6 [44]

### Component Elements

Aluminum. Al	95.8 - 98.6 %
Chromium. Cr	0.040 - 0.35 %
Copper. Cu	0.15 - 0.40 %
Iron. Fe	0.70 %
Magnesium. Mg	0.80 - 1.20 %
Manganese. Mn	0.15 %
Other. each	0.050 %
Other. total	0.15 %
Silicon. Si	0.40 - 0.80 %
Titanium. Ti	0.15 %
Zinc. Zn	0.25 %

### Properties

Density	:2.70 kg/m <sup>3</sup>
Specific Heat Capacity	:896 J/kg·K
Thermal Conductivity	:167 W/m·K
Melting Point	
Solidus	:582 °C
Liquidus	:651.7 °C
Modulus of Elasticity	:68.9 GPa
Poisson's Ratio	:0.330
Tensile Strength. Ultimate	:310 MPa
Tensile Strength. Yield	:276 MPa
Hardness. Brinell	:95

## Aluminum 3003-O [44]

### Component Elements

Aluminum. Al	96.7-99 %
Copper. Cu	0.050 - 0.20 %
Iron. Fe	0.70 %
Manganese. Mn	1.0-1.50 %
Other. each	0.050 %
Other. total	0.15 %
Silicon. Si	0.60 %
Zinc. Zn	0.10 %

### Properties

Density	:2.73 kg/m <sup>3</sup>
Specific Heat Capacity	:893 J/kg·K
Thermal Conductivity	:193 W/m·K
Melting Point	
Solidus	:643 °C
Liquidus	:654 °C
Modulus of Elasticity	:68.9 GPa
Poisson's Ratio	:0.330
Tensile Strength. Ultimate	:110 MPa
Tensile Strength. Yield	:41.4 MPa
Hardness. Brinell	:28